Architecture and mineralization of developing jaw bone and their mechanical consequences

Mulder, L.

Publication date
2007

Document Version
Final published version

ARCHITECTURE AND MINERALIZATION OF DEVELOPING JAW BONE AND THEIR MECHANICAL CONSEQUENCES

L. Mulder

ARCHITECTURE AND MINERALIZATION OF DEVELOPING JAW BONE AND THEIR MECHANICAL CONSEQUENCES

ACADEMISCH PROEFSCHRIFT

ter verkrijging van de graad van doctor
aan de Universiteit van Amsterdam
op gezag van de Rector Magnificus
prof.mr. P.F. van der Heijden
ten overstaan van een door het college voor promoties ingestelde
commissie, in het openbaar te verdedigen in de Aula der Universiteit
op dinsdag 27 februari 2007, te 14.00 uur

door Lars Mulder

geboren te Oss

Promotiecommissie

Promotor:

prof.dr. T.M.G.J. van Eijden

Copromotor:

dr.ir. J.H. Koolstra

Overige leden:

prof.dr. V. Everts
prof.dr.ir. J.M.J. den Toonder
prof.dr. J. Klein Nulend
prof.dr. P.F. van der Stelt
dr.ir. B. van Rietbergen
prof.dr. W.A. Weijs

Faculteit der Tandheelkunde

The printing of this thesis was financially supported by:
Scanco Medical AG., Bassersdorf, Switzerland

SCANCOMEDICAL

This thesis was the result of a PhD program attended at the Interuniversity Research School of Dentistry (IOT). The study described in this thesis was performed at the department of Functional Anatomy of the Academic Centre for Dentistry Amsterdam (ACTA).

Aan Mariëlle

&

aan mijn ouders en mijn zusje

CONTENTS

This thesis is based on the following publications:

- Mulder L, Koolstra JH, van Eijden TMGJ (2004). Accuracy of microCT in the quantitative determination of the degree and distribution of mineralization in developing bone.
  Acta Radiol 45: 769-777.
  (Chapter 2)

- Mulder L, Koolstra JH, van Eijden TMGJ (2006). Accuracy of microCT in the quantitative determination of the degree and distribution of mineralization in developing bone.
  Acta Radiol 47: 882-883.
  (Chapter 2)

- Mulder L, Koolstra JH, Weijs WA, van Eijden TMGJ (2005). Architecture and mineralization of developing trabecular bone in the pig mandibular condyle.
  Anat Rec A Discov Mol Cell Evol Biol 285: 659-667.
  (Chapter 3)

- Mulder L, Koolstra JH, de Jonge HW, van Eijden TMGJ (2006). Architecture and mineralization of developing cortical and trabecular bone of the mandible.
  Anat Embryol 211: 71-78.
  (Chapter 4)

- Mulder L, van Groningen LB, Potgieser YA, Koolstra JH, van Eijden TMGJ (2006). Regional differences in architecture and mineralization of developing mandibular bone.
  Anat Rec A Discov Mol Cell Evol Biol 288: 954-961.
  (Chapter 5)

- Mulder L, van Ruijven LJ, Koolstra JH, van Eijden TMGJ (2006). Biomechanical consequences of developmental changes in trabecular architecture and mineralization of the pig mandibular condyle.
  J Biomech. In press.
  (Chapter 6)

- Mulder L, van Ruijven LJ, Koolstra JH, van Eijden TMGJ (2006). The influence of mineralization on intratrabecular stress and strain distribution in developing trabecular bone.
  Submitted for publication.
  (Chapter 7)

- Mulder L, Koolstra JH, den Toonder JMJ, van Eijden TMGJ (2006). Relationship between tissue stiffness and degree of mineralization of developing trabecular bone.
  Submitted for publication.
  (Chapter 8)

- Mulder L, Koolstra JH, den Toonder JMJ, van Eijden TMGJ (2006). Intratrabecular distribution of tissue stiffness in developing trabecular bone.
  J Struct Biol. Conditionally accepted for publication.
  (Chapter 9)

GENERAL INTRODUCTION

The mandible or lower jaw bone is part of the masticatory system and is important in functional daily behavior such as mastication, biting, clenching, and talking. During these behaviors it is subjected to forces exerted by contracting muscles of mastication and by reaction forces present at the jaw joint (or temporomandibular joint) and the teeth. Loads on the teeth and from muscular contractions are transmitted through the mandible to the mandibular condyle, and via the jaw joint to the skull. Besides its function as a fulcrum, the jaw joint also acts as guidance for jaw movement. The condyle translates and rotates along the articular surface of the temporal bone of the skull. Consequently, the bone of the mandible and its condyle are subjected to loads with various directions and magnitudes.

Mandibular bone is comprised of different types, i.e. compact and trabecular bone. Compact bone has a low porosity and forms the bony shell of the mandible. Trabecular or cancellous bone has a high porosity and is found within the cortical shell, for example under the articulating surface of the condyle and in the alveolar process which supports the teeth. Trabecular bone has an open structure formed by interconnected trabeculae which may have various shapes (plate-like to rod-like).

Since the nineteenth century, a close relationship between the architecture of trabecular bone and the governing loading patterns has been suspected (Wolff, 1892). The orientation of trabecular elements has been shown to align according to the stress trajectories that arise from specific loading directions. Furthermore, increased magnitude of loading will evoke an increase in bone density (amount of bone tissue in a specific bone volume). The adaptation has the consequence that the mechanical properties of the bone structure, such as its stiffness and strength, are optimized for the demanded loading configuration. This implies that there is a relationship between bone architecture and its mechanical properties.

Numerous studies have been performed in which multiple architectural (morphological) properties of trabecular bone were quantified using different techniques in order to relate them independently to the mechanical properties of the bone structure.

Mechanical properties are important characteristics of bones as they are, for example, a measure of their capability to resist deformation and thus of fracture risk. It has been shown that variation in the apparent mechanical properties can be explained mostly by the amount of bone present and related variables like the thickness and number of trabecular elements (e.g. Borah et al., 2000; Nafei et al., 2000b), the amount of connections between trabecular elements (Kinney and Ladd, 1998), their specific orientation (Odgaard et al., 1997; Kabel et al., 1999b), and the governing shape of the trabeculae (van Ruijven et al., 2005; Stauber et al., 2006). Throughout this thesis the word "apparent" will be applied to describe the properties of the whole trabecular structure as opposed to "tissue" level properties, which are the properties of the calcified tissue that makes up the bone.

Besides the apparent properties of bone, also these tissue level properties have been shown to be of significant importance (Turner et al., 1990; Borah et al., 2000; Müller, 2003; Follet et al., 2004). The bone tissue is comprised of calcium and phosphate containing salts of which hydroxyapatite is the most abundant form. The density of the calcium and phosphate ions is a determinant of tissue properties like the degree and distribution of mineralization. Due to variation in the location where the mineralization takes place throughout the bone tissue and variation in the state in which the mineralization process is, the degree of mineralization is distributed inhomogeneously over the bone tissue. It is, for instance, known that bone growth and replacement (modeling and remodeling) take place on the trabecular surface. Corresponding differences in mineralization between the surface and core of trabecular elements have been demonstrated (Paschalis et al., 1997).

However, the impact that the degree of mineralization of bone tissue and its intratrabecular distribution has on the apparent mechanical properties (e.g. apparent stiffness) as well as on the tissue mechanical properties (e.g. intratrabecular distribution of stress and strain) has been widely neglected, but has been shown to be of significant importance (van der Linden et al., 2001; Bourne and van der Meulen, 2004; van Ruijven et al., 2006). It is known that an increase in the degree of mineralization brings about an increase in tissue stiffness (Choi et al., 1990; Currey, 1999). Furthermore, the changes that the degree and distribution of mineralization undergo during development, due to continuous modeling and remodeling, and how this affects the changes in bone mechanical properties remain unidentified.

This thesis is therefore aimed at providing a more complete characterization of the prenatal development of compact and predominantly of trabecular bone in terms of its architecture, and its degree and distribution of mineralization. Knowledge regarding the early

development of bone is important and will augment the understanding of normal bone development and delivers baseline data to which deviations may be compared. For instance, bone diseases such as osteoporosis and the influences of pathogenic drugs or noxious environmental conditions can be traced back to the fetal development of bones (Cooper et al., 2002; Javaid and Cooper, 2002). Furthermore, as initial bone regeneration closely resembles fetal bone formation (Ferguson et al., 1999), it may be possible to shed light on the mechanisms involved in fracture healing or bone formation during surgical distraction methods.

Furthermore, the influence that developmental changes in architectural and mineralization parameters have on the bone mechanical properties at both the apparent and tissue level has been quantified and is described in this thesis. Both architectural and mineralization parameters have been shown to be of significant predictive value for the mechanical properties of bone (Currey, 1984; Turner et al., 1990; Borah et al., 2000; Ciarelli et al., 2003; Müller, 2003; Follet et al., 2004).

It has been shown that the coupling between architecture and mechanical loading also applies to the mandibular condyle. It has been demonstrated that the trabecular structure of the condyle consists mostly out of parallel plates which are oriented in the sagittal plane, perpendicular to the condylar axis. Regional differences in bone density, as associated with the thickness and amount of trabecular elements, reflect the ability of the trabecular structure to sustain multiple load directions (human: Giesen and van Eijden, 2000; pig: Teng and Herring, 1995). In succession to this, mechanical properties of the trabecular structure of the condyle have been quantified and found to exhibit similar directional dependencies as the structure did, thus establishing the predictive value of the bone structure for the mechanical qualities of the condylar bone compartment (human: Giesen et al., 2001; 2003; van Ruijven et al., 2003; van Eijden et al., 2006; pig: Teng and Herring, 1996).

It is thus known what the general build up of the bone structure of the mandibular condyle is. However, it is unknown how the architecture, the degree and distribution of mineralization, and the mineral composition of this structure are established during fetal development. There are a number of signs that even during early development prerequisites for morphogenesis guided by mechanical loading are present. It has been shown, for example, that fetuses demonstrate considerable movement *in utero* among which jaw opening, yawning, sucking, and swallowing reflexes were abundantly observed (Scott, 1951; de Vries et al., 1985). Involuntary contractions by developing masticatory muscles begin to exert small

but significant intermittent forces on the skeletal rudiments. These forces have been shown to modulate the development of the bone to which they are attached (Humphrey, 1968; Spyropoulos, 1977; Goret-Nicaise, 1981; Burger et al., 1991; Carter and Orr, 1992). Consequently, it can be assumed that if bone development is guided by mechanical loading, a proper mechanical environment is present at that stage.

Therefore, research described in this thesis (chapters 3-5) is focused on describing the early mandibular development and how this is reflected in architectural and mineralization changes. As no distinction has ever been made between mandibular compact and trabecular bone development, the differences between their developmental pathways are subject of the investigation reported here. This was performed by analyzing bone architecture in multiple regions within the mandibular condyle and corpus with micro-computed tomography (microCT). MicroCT was applied in these studies for the first time to assess changes in the degree and three-dimensional distribution of mineralization of the various mandibular regions. Adding mineralization information to the general knowledge of bone development will augment the understanding of the bone's apparent and tissue mechanical properties. Therefore, the dependency of both apparent and tissue mechanical properties on architectural and/or mineralization changes during development has been elucidated (chapters 6-9). Mutual relationships between architecture, mineralization, and mechanical properties are assessed using techniques such as microCT, finite element (FE) modeling, and nanoindentation. New approaches with these techniques were applied and they were used in a combined way for the first time. Knowledge about the relationships between architecture, degree and distribution of mineralization, and mechanical properties are critically important to understand the biomechanical behavior of bone in general and the mandible in particular (van Eijden, 2000). In this thesis pig mandibles were the material of choice, because human fetal material is scarce and the pig is a widely used model for studying bone and bone development.

Fetal development of the mandible

The mandible is among the first bones in the body to ossify during fetal development (Hodges, 1953), thus providing the opportunity to study the development of the mandibular bone at early fetal stages. The developing mandible is formed both by the endochondral and intramembranous ossification process. Regardless of its origin, all bone develops from an initial open structure into either a dense compact or more open trabecular structure (Cadet et al., 2003).

Endochondral ossification gives rise to the condyle and can be found on small focal points throughout the mandible, e.g. in the symphysis, coronoid process and ramus (Fig. 1). During endochondral bone formation, hypertrophic chondrocytes (cartilage cells) in a cartilage anlage eventually mineralize their surrounding matrix, and undergo apoptosis. On the degraded mineralized cartilaginous matrix osteoblasts (bone-forming cells) form the primary spongiosa, the precursor of trabecular bone (Hall, 1988; Wong and Carter, 1990; Buckwalter, 1995). Intramembranous ossification is responsible for the development of the corpus and ramus of the mandible. These are formed without an intermediate cartilage structure and bone formation occurs in mesenchyme (Opperman, 2000).

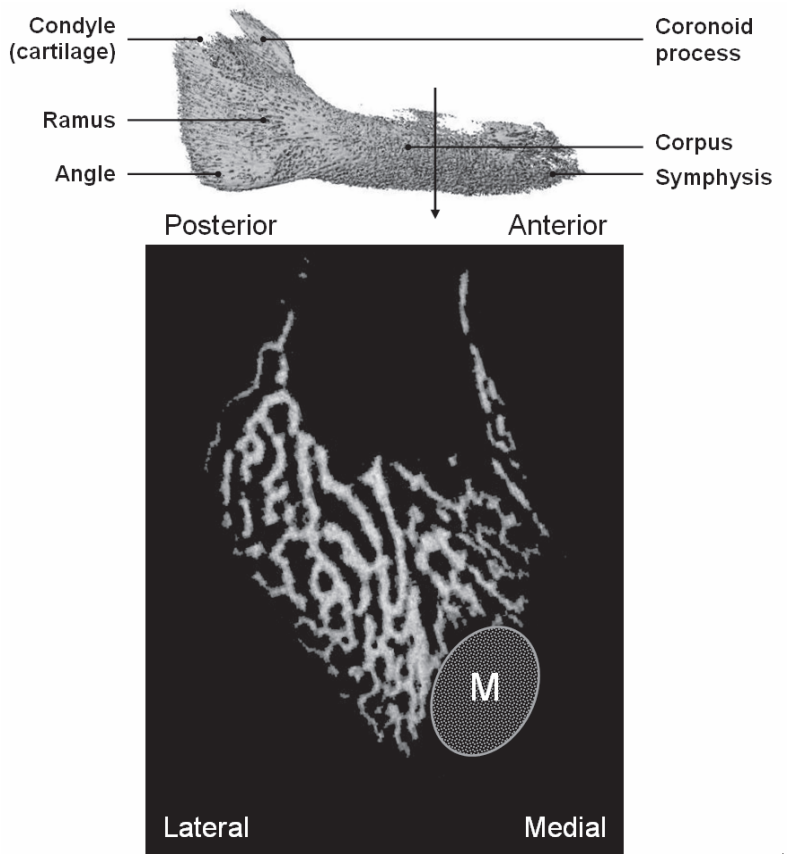

Figure 1. Top: Lateral view of a microCT reconstruction of a fetal mandible of a pig with a gestational age of approximately 60 days. The arrow indicates the location of the frontal cross-section depicted below. Bottom: Frontal cross-section through the corpus mandibulae. M: Meckel's cartilage, illustrated at the location where it presumably runs.

During both endochondral and intramembranous ossification, osteoblasts deposit calcium and phosphate ions in the osteoid (unmineralized) tissue, which is then organized into bone (Boskey, 1992; 1996; Landis, 1995). The most abundant species of calcium phosphate mineral in bone is a poorly-crystallized, carbonate-containing, highly disordered hydroxyapatite ($Ca_{10}(PO_4)_6(OH)_2$). However, the mineral is initially deposited as an amorphous calcium phosphate, which proceeds through transient intermediates as octacalcium phosphate (Driessens, 1986; Glimcher, 1987; Boskey, 2002; Crane et al., 2006). As the growth of mineral crystals continues, their amount increases, and the species of calcium phosphate mineral changes towards hydroxyapatite, the degree of mineralization of bone increases equivalently.

The embryonic origin of the mandibular mesenchymal cells, which will form the cartilage, bone, connective tissue, and dentine of the mandible, lies in the neural crest. The cells contribute to the formation of the first branchial arch, often called the mandibular arch, in which the mandible develops. The future mandible emerges as a process filled with a homogeneous mass of mesenchyme covered by epithelium. After penetration of nerves and blood vessels in the mandibular process, mesenchyme starts to differentiate into cartilage, ultimately destined to become Meckel's cartilage (Hall, 1982; 1987).

Meckel's cartilage ranges from the symphysis, where, as in many mammal species, the two sides may fuse (Friant, 1968), to the future middle ear where it contributes to the formation of two middle ear bones (malleus and incus). It has been proposed that Meckel's cartilage is an ephemeral element which disappears during fetal life after having only played a transitory supporting role (Orliaguet et al., 1994) and is the anchoring point of the primordia of the masticatory muscles, which will later be transferred to the mandible (Frommer and Margolies, 1971; Goret-Nicaise, 1982; Doskocil, 1989; Orliaguet et al., 1994).

The bone structure of the mandible is formed on the lateral side of Meckel's cartilage (Fig. 1) and first appears on the site of the future mental foramen (Radlanski et al., 2003). This primary growth center has the form of a plate, made up out of trabeculae, and spreads out in anterior, posterior, and upward direction. Mandibular bone formation follows the changing curved outline of Meckel's cartilage. As the bone grows further in superior and inferior direction, it bends around Meckel's cartilage to form a trough, but never covers the lingual aspect of Meckel's cartilage, except in the anterior region. As soon as the bone supersedes the superior level of Meckel's cartilage, the bony plate starts to develop into a double plate (a 'Y' shape), with the most lateral one representing the buccal side and the medial one representing the lingual side of the future mandible (Goret-Nicaise and Dhem,

1984; Azeredo et al., 1996). Thus, a bony gutter is formed to embed the inferior alveolar nerve and its accompanying vessels (Low, 1909) and later on in the development to form the alveolar process, which will hold the teeth. It is believed that the dental lamina, from which the teeth primordia evolve and grow into the alveolar process, plays a co-organizing role in guiding the bone formation in this region (Atchley and Hall, 1991; Mérida-Velasco et al., 1993).

Eventually, the bone develops also in posterior direction to contribute to the formation of the ramus and coronoid process, without the participation of Meckel's cartilage (Wissmer, 1927). The development of the mandibular condyle, however, commences later. Its first appearance is as a mesenchymal condensation (blastema) formed around the posterior end of the trabeculae of the ramus (Lee et al., 2001) as this structure grows towards the region of the future jaw joint. The blastema is preceded by the development of the masticatory muscles (Perry et al., 1985). This blastema of the condyle subsequently produces cartilaginous tissue, which will cause endochondral growth of the condyle. The fully formed cartilage anlage of the condyle consists roughly of four layers, namely a layer of flat undifferentiated cells at the future articular surface. Below that, an intermediate zone of proliferating cartilage cells. Below that, a layer of haphazardly arranged hypertrophic cartilage cells and finally, an erosive zone, where the cartilage is replaced by bone tissue (Christensen, 1975; Ben-Ami et al., 1992). In the pig, the cartilage is present from the superior side of the condyle all the way to the angle of the mandible (Wissmer, 1927). Concomitant with the onset of jaw movement and vascular penetration of the cartilage, the condylar blastema begins to ossify endochondrally (Baume, 1962; Perry et al., 1985; Berraquero et al., 1995). Ossification takes place at the inferior side of the cartilage and along its periphery, with the exception of the superior and posterior borders (Christensen, 1975). On these borders, articular cartilage is present, which is often designated as the fifth cartilage layer of the condyle with collagen fibers running parallel to the articulating surface.

Thus, quite a lot is known about the fetal development of the mandible and the mandibular condyle in particular and it has been shown that the developing mandible is a suitable model for other developing bones. However, the research that has been performed was all focused on the macroscopic appearance of the structures like bone and especially cartilage formation and their abnormalities during development. Studies on this subject have described mostly qualitative observations and did not treat the quantitative description of the developing bone structure in terms of its architecture, its degree and distribution of mineralization, and its

mineral composition. Moreover, the influence that changes in these parameters have on apparent and tissue level mechanical properties has not been investigated yet.

Micro-computed tomography (microCT)

The architecture and degree of mineralization of bone can be studied using X-rays. The X-ray-material interaction causes X-ray attenuation and is established predominantly by two effects, namely photoelectric absorption and Compton scattering. The attenuation of X-rays is dependent on the size of the object, its density, and its composition (atomic number of the atoms comprising the object), and the initial intensity of the X-ray beam. The attenuation property of a certain material is expressed as its linear attenuation coefficient. Computed tomography (CT) allows for the determination of the 3D distribution of attenuation coefficients of the analyzed object. The process of CT image reconstruction produces a map of X-ray attenuation coefficients in a cross-section of the object, which can be used to determine the density at any point (pixel) in the image (McCullough, 1975; Rüegsegger et al., 1976; Cann, 1988). These two-dimensional data can later be collected and stacked and represented in a three-dimensional image built up out of volume elements (voxels).

A microCT scanner is essentially equal to diagnostic CT scanners (Hounsfield, 1973; 1977; Kalender, 2006) that are found in hospitals with the major difference that a microCT scanner allows for higher resolution imaging, thus providing the opportunity to visualize and quantify the smallest anatomic features of bone (Feldkamp et al., 1989; Rüegsegger et al., 1996). On the other hand, microCT settings are specifically focused on bone and the X-ray dose that arises with the scan energies used and the prolonged exposure times are too high to be able to allow for *in vivo* scanning. Since ten years, microCT has been established as an accurate and powerful tool for determining three-dimensional architectural parameters of both compact and trabecular bone in a wide variety of species of all ages (Müller et al., 1996; Rüegsegger et al., 1996; Uchiyama et al., 1997; Laib et al., 1998; Müller et al., 1998).

Architecture

In a microCT reconstruction of bone, specific volumes of interest may be selected and three-dimensional representations of its structure can be constructed. For the determination of architectural characteristics, bone in the volume of interest has to be discriminated from the background. To this end a specific threshold is chosen based on attenuation coefficient differences between the bone and background. In a segmented image, every voxel with an attenuation coefficient below the threshold (presumably representing soft tissue or

background) is made transparent and voxels above the threshold (representing bone) are made opaque. In this manner a binary reconstruction is formed of, for example, the three-dimensional trabecular structure (Fig. 2A).

Using this reconstruction, several important parameters, able to describe the architecture of trabecular bone, can be determined quantitatively (Laib et al., 2000). The amount of bone in a selected volume of interest is assessed by calculating the ratio between the amount of bone in the volume (BV) and the total volume (TV) of the volume of interest and is expressed as the bone volume fraction (BV/TV). The mean trabecular number (Tb.N), mean trabecular thickness (Tb.Th), and mean trabecular separation (Tb.Sp) are calculated using a direct technique based on distance transformation of the reconstruction. This method estimates a volume-based local thickness by fitting maximal spheres to every point in the structure. From the mean diameters of these spheres, an estimation of mean trabecular thickness and thickness distribution can be obtained. The same holds true for trabecular separation, where the spheres are fitted in the background data. The trabecular number is the inverse of the mean spacing between the mid axes of the trabecular elements (Hildebrand and Rüegsegger, 1997a). Such techniques do not rely on an assumed model type (e.g. parallel plate model) and are therefore not biased by eventual deviations of the actual structures from this model (Hildebrand et al., 1999). The number of connections between the trabecular elements can be expressed by the connectivity density (Conn.D), which is calculated using the Euler method (Odgaard and Gundersen, 1993).

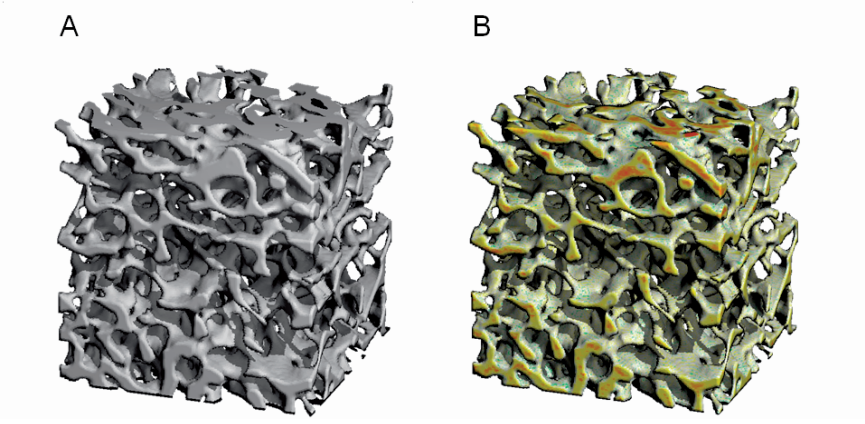

Figure 2. A: Three-dimensional reconstruction of a volume of interest selected in the trabecular bone of the mandibular condyle of a newborn pig. The image is binary, which is used to calculate the architectural parameters of the structure. B: The same piece of trabecular bone with the attenuation values of the bone tissue depicted in a color scale. From this reconstruction the average degree of mineralization and its distribution can be determined.

Based on the assumption that a trabecular structure is composed of plate-like and rod-like trabeculae, the bone structure can be characterized by its structure model index (SMI). This parameter is based on a differential analysis (behavior of the bone surface (degree of convexity) due to an artificial increased bone volume) of the bone surface. For an ideal plate and rod structure the SMI value is 0 and 3, respectively (Hildebrand and Rüegsegger, 1997b). This method is based on the plate model, making it unreliable when the trabecular structure is more rod-like in nature. However, a new method, which is also based on distance transformation, was developed recently and provides an unbiased and independent manner of determining the amount of rod-like and plate-like trabecular elements in the trabecular structure (van Ruijven et al., 2005).

To determine the direction and anisotropy of the trabecular structure, a mean intercept length (MIL) tensor can be calculated (Harrigan and Mann, 1984). The eigenvectors of this tensor align with the principal directions of the trabecular structure. The eigenvalues of this tensor (H_1, H_2, and H_3) express the prevalence of the bone material in the corresponding directions. They are sorted such that $H_1 > H_2 > H_3$. The degrees of anisotropy (DA) are defined by H_1/H_3, H_1/H_2, and H_2/H_3.

Degree and distribution of mineralization

Estimations of the density distributions within the object can be visualized and quantified. To obtain an approximation of the object density one needs to have a basic knowledge about the tissue composition. In case of bone, which is predominantly composed of hydroxyapatite mineral salt, a calibration series containing various concentrations of hydroxyapatite or dipotassium hydrogen phosphate (K_2HPO_4) is scanned. The attenuation values are in this way coupled to a hydroxyapatite concentration. Then the attenuation characteristic of the bone under investigation can be compared to this calibration curve and estimations for bone hydroxyapatite density can be made.

In this thesis, the assessment of the degree and distribution of mineralization in bone with microCT is described for the first time. Ideally, the attenuation value of each voxel would be an accurate reflection of the true density and composition of the corresponding point in the investigated object. However, unambiguous quantification of various mineralization properties is not straightforward owing to the polychromatic character of the X-ray beam in commercially available microCT systems. The disadvantage of such a polychromatic beam (the X-ray contains a broad spectrum of energies) is that the energy spectrum changes as it passes through an attenuating object (Brooks and di Chiro, 1976). In a scan, a homogeneous

specimen will give the impression that it contains various degrees of material density. This is known as the beam hardening effect. Beam hardening, moreover, leads to a non-linear relationship between the attenuation coefficient and the material density (see chapter 2 for a more specific explanation). The microCT system used in this thesis (µCT 40, Scanco Medical AG., Bassersdorf, Switzerland) is equipped with a beam hardening correction algorithm, which reduces the non-linearity of the relationship by fitting it with polynomials (Hammersberg and Mångård, 1998). In addition, to reduce the beam hardening effect, an aluminum filter is applied to remove the radiation with the lowest energy.

In order to be able to assess the degree of mineralization with microCT a different thresholding scheme of the same volume of interest as described above was adopted. In stead of making every bone-containing voxel opaque, creating a binary reconstruction, they retain their attenuation coefficient, which is represented by a grey or color value (Fig. 2B). By comparing the average attenuation value in a bone specimen to reference measurements of series of K_2HPO_4 solutions with different concentrations (chapters 2-5) or hydroxyapatite standards (chapters 6-9) the degree of mineralization can be determined. Here it is important to recognize the difference between two mineralization parameters. The first is generally indicated as the bone mineral density (BMD) and is determined as the mass of the mineralized (bone) tissue (mg) relative to the total volume (cm^3) of the selected volume of interest. This variable is therefore both dependent on the amount of bone present in the volume of interest (BV/TV) and on the average degree of mineralization of the bone tissue (DMB), which is the second mineralization parameter and is the variable of choice in this thesis. The degree of mineralization is expressed as the mass of mineralized tissue (mg) relative to its volume (cm^3) in a volume of interest after thresholding has been performed.

Besides the average degree of mineralization of a bone structure also its three-dimensional distribution over the trabecular elements is important in that it provides insight into the formation, growth, and remodeling state of the bone. In addition, local variation in the degree of mineralization can be expected to correlate with local variation in tissue stiffness. In this thesis, the distribution of mineralization is characterized in two ways. The first is the determination of the frequency distribution of the degree of mineralization. Hereby, the frequency of every attenuation value and thus every degree of mineralization that is present in the voxels is recorded and herewith the variation in mineralization may be determined and statistical comparison to other bones or regions within the same bone can be achieved.

Frequency distributions, however, do not hold information about the intratrabecular distribution of the degree of mineralization. By distinguishing the course of the degree of

mineralization from the trabecular surfaces to their cores one is able to gain a better comprehension of the way that trabecular elements are formed and how the remodeling process progresses. In this thesis the intratrabecular distribution of mineralization was determined by applying a custom-built algorithm in which layers of bone-containing voxels are consecutively peeled from the trabecular surface. Bone-containing voxels were identified as surface voxels when minimally one of its six sides bordered on voxels that were identified as background. The average degree of mineralization of the layer that was peeled off was determined. Subsequently, the voxels that were peeled off were replaced by background voxels, containing the value zero. In this way, consecutive layers were characterized until all bone-containing voxels were usurped.

A complicated issue is the fact that microCT reconstructions are discrete (built up out of voxels), where the real bone is continuous. This becomes relevant at the boundary between bone and background. Discrete voxels at this boundary will be partially filled. Their attenuation value (grey values/degree of mineralization) is based partly on bone tissue and partly on background, whether it is soft tissue, bone marrow or the fluid in which the sample was scanned. Therefore, this phenomenon is called partial volume effect. It makes thresholding more complicated, because the discrimination is complicated due to the fact that thresholding is based upon the difference between bone and background attenuation. The choice of threshold influences the values of the architectural and mineralization parameters (Ding et al. 1999). Especially for bone specimens with a low bone volume fraction, incorrect adjustment of the threshold leads to inaccurate measurements (Hara et al., 2002). Therefore, in this study the threshold was determined using an adaptive method, in which the 3D grey value reconstruction of a volume of interest was segmented at multiple levels. The threshold, where the bone volume fraction changed the least, was chosen as the threshold to separate bone from background in the specific volume of interest after being checked visually (Ding et al., 1999). It was assured that the threshold corresponded to the minimum between the background and bone tissue peak in the grey value-histogram. By repeating every scan projection four times and averaging these, the signal-to-noise ratio was improved substantially.

Although this procedure greatly facilitated the determination of the suitable threshold, partial volume effects are inevitable and will bias also the assessment of the degree of mineralization. In order to minimize the bias, the outermost voxel layer characterized as bone was omitted in the calculation of the average degree of mineralization and in the construction of frequency distributions. This of course has its downsides when small trabecular dimensions

are involved and removing the surface layer of voxels will clearly reduce the representativeness of the reconstruction of the real trabecular elements.

Finite element (FE) modeling

Determination of the mechanical properties of trabecular bone has been performed using physical tests, including compression, tension, shearing, indentation, and bending testing. However, physical mechanical tests require meticulous preparation of samples and bring about edge effects, which can seriously impair the results and significance of these tests (Linde, 1994). Physical mechanical testing is often difficult or impossible to perform when specimens are too small to allow for adequate sample preparation, as is the case for developing bones. Finite element (FE) models have been applied to simulate and replace physical mechanical tests. Over the past couple of years finite element analysis based on microCT reconstructions has become a powerful tool to determine the apparent mechanical properties of selected trabecular bone volumes (van Rietbergen et al., 1995; van Ruijven et al., 2003; van Eijden et al., 2004) or even large bone parts (Pistoia et al., 2002; van Rietbergen et al., 2003; Homminga et al., 2004; van Verhulp et al., 2005; van Ruijven et al., 2006). FE analysis allows for fast and realistic simulations of multiple uniaxial testing procedures, yielding the relevant components of the apparent stiffness matrix, when cubic models of trabecular bone are used (van Rietbergen et al., 1995). This matrix contains the stiffness of the trabecular structure, i.e. its resistance against deformation should it be loaded in different directions.

To create a finite element mesh of the trabecular bone of interest, the voxels in the three-dimensional microCT reconstruction are converted directly into cubic eight-node brick elements. The apparent mechanical properties of the FE models are estimated using an element-by-element FE-solver (van Rietbergen et al., 1995). Six uniaxial mechanical tests (three compression and three shear tests) can be simulated by applying a uniform displacement at the surfaces of the specimen cubes. Each simulated test yields a part of the apparent stiffness matrix of the specimen.

In FE modeling the elements in the FE mesh of trabecular bone are attributed with an elastic modulus (equal to stiffness), which should represent the mechanical properties of the bone at the tissue level and is indicated as the tissue stiffness. Typically, it has been assumed to be homogeneous, isotropic, and linearly elastic (Kabel et al., 1999a; Ulrich et al., 1999). The tissue stiffness, however, has been found to be proportional to the degree of mineralization (Choi et al., 1990; Currey, 1999), which is naturally not distributed

homogeneously over the bone tissue due to continuous modeling and remodeling processes taking place on the trabecular surface. In this thesis the influence of the incorporation of the degree and distribution of mineralization into FE models on both the apparent mechanical properties of the trabecular structure (stiffness) and the intratrabecular distribution of stress (internal forces/pressure) and strain (deformation) has been investigated. Moreover, thus far intratrabecular distribution of stress and strain and the influence of the degree and distribution of mineralization hereupon, have never been quantified.

The apparent mechanical properties of bone are important markers for bone quality and may be used as predictors for fracture risk in patients. Insight into the influence of changes in the degree and distribution of mineralization hereupon are important in that they represent a more true-to-life representation of the bone behavior during mechanical loading. Quantitative knowledge about the three-dimensional intratrabecular tissue stress and strain distributions provides information on the nature of trabecular deformation during loading. This may additionally give insight into micro-crack initiation and propagation behavior, which is considered to be influenced considerably by heterogeneity in bone mineralization (Ciarelli et al., 2003). It may, furthermore, provide information about stimuli that are the basis for modeling and remodeling of bone tissue. Finally, knowledge regarding the changes in mechanical properties during fetal bone modeling and remodeling will augment the understanding of the mechanical consequences of normal bone development.

Nanoindentation

The finite element simulations that are described above, characterize the mechanical properties of trabecular bone on the apparent level as well as its intratrabecular stress and strain distributions. In the present thesis, implementation of the tissue stiffness in the FE models relative to the degree of mineralization was performed according to a relationship between the two variables acquired from the literature (Currey, 1999). Although based on tests with specimens from a variety of species and many different anatomical locations, this relationship only considered cortical bone samples and the applied analysis methods are unlike the ones applied in this thesis. Therefore, in this thesis, the relationship between degree of mineralization and tissue stiffness was investigated empirically for fetal and newborn trabecular bone specimens of the domestic pig mandibular condyle. Besides this, intratrabecular distribution of tissue stiffness was explored by taking into consideration multiple locations spanning the width of trabecular elements and it was scrutinized if the intratrabecular profile of tissue stiffness was according to the intratrabecular distribution of

the degree of mineralization. Therefore, the degree of mineralization was examined at the same location where the tissue stiffness was determined. In order to investigate the tissue stiffness, nanoindentation was applied.

Nanoindentation, which evolved from the classical Vickers microhardness test, has proven to be a powerful technique for characterizing the mechanical properties of material at the tissue level, such as thin films on dissimilar substrates (Malzbender et al., 2002; Bushby et al., 2004). In this method the depth of indentation is reduced to submicron range and it allows for estimation of the tissue stiffness, expressed as an elastic modulus, under specific assumptions and careful calibration (Zysset et al., 1999). The theoretical basis of this technique relies on the Boussinesq solution of indentation of an elastic material with a rigid indenter (Sneddon, 1965). In the present thesis, application of this solution to the initial unloading step in an indentation test with a deformable pyramidal Berkovich tip was established by the well-documented method of Oliver and Pharr (1992). They devised a relationship between the stiffness and Poisson's ratio of the indenter and the stiffness and Poisson's ratio of the bone tissue under consideration. Over the past 10 years, nanoindentation has been used frequently to assess the bone tissue stiffness. It was found to vary greatly between different species, individuals (Zysset et al., 1998), anatomical locations (Rho et al., 2001; Hengsberger et al., 2005), bone structural units (Rho et al., 1997; Roy et al., 1999; Xu et al., 2003), and direction of testing (longitudinal vs. transverse) (Swadener et al., 2001; Fan et al., 2002).

Specimens need to be dehydrated in graded ethanol solutions (70-100%) and embedded in polymethylmethacrylate (PMMA) prior to nanoindentation. The embedded bones are sectioned using a microtome exposing the bone structure at the surface. The exposed surface is then polished with successively finer grades of abrasive paper. The effects of the dehydration steps, embedding, and polishing procedures on the tissue stiffness have to be taken into consideration (Donnelly et al., 2006).

In the present study, indentations were performed in an array across the width of the trabecular elements. Indentations close to the edge of trabecular elements, however, need to be interpreted with care, as the influence of the embedding medium in the vicinity of the bone-PMMA boundary has an unknown influence on the determined tissue stiffness. Generally, as a rule-of-thumb, the indentation depth should be less than one tenth of the thickness of the underlying trabecular bone in order to measure the properties of the bone tissue without significant interference of the embedding medium (Malzbender et al., 2002).

After nanoindentation, the specimens were scanned using microCT. Volumes of interest were defined, each containing the location of a single indent and the degree of mineralization of the bone tissue in this volume of interest was determined. Combining these two methods for the first time allowed for the determination of the relationship between tissue stiffness and location corresponding degree of mineralization. Understanding the intratrabecular tissue stiffness and degree of mineralization variation and their mutual relationship is important for the comprehension of the mechanical behavior of bone at both the apparent and tissue level (Turner et al., 1990; van der Linden et al, 2001; Bourne and van der Meulen, 2004; Follet et al., 2004; van Ruijven et al., 2006). Furthermore, quantification of bone tissue properties is prerequisite to characterizing the mechanical environment in which bone cells reside (Jee, 2001) and may be of value for the etiology of bone tissue micro-damage and may provide insights into modeling and remodeling processes that take place.

Aims of the thesis

The studies described in this thesis aimed at providing a more complete description of the fetal development of the compact and trabecular bone of the mandible and its condyle. To achieve this, changes in the architecture and the degree and distribution of mineralization during development were examined. In addition, the consequences of these changes for the mechanical properties at both the apparent and tissue level were investigated. Throughout this thesis, pig specimens were used. New applications of existing methods were conceived, for example, the determination of the degree and distribution of mineralization with microCT, its incorporation in three-dimensional finite element models and the coupling of results obtained by microCT and nanoindentation.

X-rays are attenuated by material. The density of the material and its composition are the predominant factors that determine the amount of attenuation. Three-dimensional X-ray techniques may therefore be used to obtain knowledge about the spatial distribution of the material density. MicroCT has never been applied before to examine degree and distribution of mineralization of bone. The goal of chapter 2 was therefore, to assess the accuracy of microCT in the determination of the degree of mineralization and the influence of beam hardening hereupon. This was performed by comparing attenuation values of known concentrations of salt solutions measured with microCT to theoretically determined values. MicroCT applicability was shown by characterizing the degree of mineralization of various parts of the mandible from pigs of different developmental ages.

The mandibular condyle is an important load-bearing part of the jaw joint and is loaded recurrently during fetal development. The trabecular structure in the mandibular condyle is said to be a reflection of the governing stress trajectories. It has a rapid formation of trabecular elements and would provide a suitable model for developing trabecular bone. The purpose of the study described in chapter 3 was to simultaneously examine developmental alterations in the trabecular architecture, the average degree of mineralization, and its intratrabecular distribution. A series of pigs of chronological developmental age were studied by microCT.

It is known that both compact and trabecular bone develop from an initial open structure. The developing bone of the shell of the corpus of the mandible is destined to develop into compact bone, while the bone within the condyle develops into trabecular bone. Thus far, it is unknown how the two bone types arise in terms of architecture and mineralization, which is essential in understanding differences between normal trabecular and cortical bone development. In chapter 4, the developmental pathways of both bone types are determined by investigating mandibles from pigs of different developmental ages with microCT.

Earlier studies have shown that the condyle grows mainly in a superoposterior direction and that the ossification of the corpus commences from the mandibular primary growth center in an anterior, posterior, and lateral direction. The main goal of chapter 5 was to examine if these known growth courses are reflected in architectural and mineralization parameters of the two structures. Therefore, a detailed regional analysis was performed by selecting multiple volumes of interest in both condyle and corpus. Architecture and mineralization were quantified using microCT. Furthermore, mineral composition was assessed by spectrophotometry, in order to provide information about developmental changes in the type of mineral present in developing bone tissue. A fetal and newborn group of pig specimens were compared.

In chapter 6, finite element models of the trabecular bone in the developing mandibular condyle were created to simulate physical compression and shear testing and thereby to estimate the mechanical properties on the apparent level. Thus far, the influence of the degree of mineralization and its heterogeneous distribution on these properties has been neglected. In the present study, models were created by transforming three-dimensional microCT reconstructions directly into finite element meshes. Three conditions were explored. In the first type, the elements of the model contained a tissue stiffness that was scaled to the local distribution of mineralization. In addition, models with homogeneous tissue stiffness

were constructed to study the separate influence of architecture and degree of mineralization on the apparent mechanical properties. The influence of development was examined by comparing a fetal and newborn group of pig specimens.

Besides apparent level stiffness of trabecular bone, intratrabecular distributions of stress and strain parameters are important. Thus far, the influence of the heterogeneous distribution of mineralization hereupon has been neglected. Insight into these distributions provides information on the nature of trabecular deformation during loading. It may additionally provide knowledge on trabecular micro-damage initiation and propagation. Chapter 7 describes a finite element investigation in which these distributions were determined and also how they depend on the incorporation of tissue stiffness when it is scaled to the local distribution of mineralization and how they might change during development. The same groups of specimens as in the previous chapter were applied.

Understanding variation in intratrabecular tissue stiffness and degree of mineralization and their mutual relationship is important for the comprehension of the mechanical behavior of bone at both the tissue and apparent level. Additionally, in the finite element studies reported in this thesis, the tissue stiffness applied to the elements was scaled to the degree of mineralization using an already existing relationship from the literature. This relationship was, however, contrived from cortical bone specimens from a variety of animals from a postnatal stadium. Therefore, it is unknown if the same relationship holds for fetal and newborn samples. Chapter 8 deals with the determination of an empirical relation between tissue stiffness and degree of mineralization. To this end, nanoindentation and microCT experiments were combined to measure the tissue stiffness and location corresponding degree of mineralization, respectively. A fetal and newborn group of pig specimens were compared.

The investigation of the intratrabecular distribution of tissue stiffness is described in chapter 9. It is known that the degree of mineralization of trabecular elements varies due to continuous modeling and remodeling processes taking place on the trabecular surface. It is, however, unknown if the tissue stiffness is distributed according to the degree of mineralization and how it changes during development. To examine this, nanoindentation and microCT were applied in a joint fashion and location corresponding regions spanning the width of trabecular elements were investigated. The same groups of specimens as in the previous chapter were applied.

CHAPTER 2

ACCURACY OF MICROCT IN THE QUANTITATIVE DETERMINATION OF THE DEGREE AND DISTRIBUTION OF MINERALIZATION IN DEVELOPING BONE

Abstract

The purpose of the present study was to evaluate the accuracy and applicability of a commercially available microCT system for comparative measurements of the degree and distribution of mineralization of developing bone. Homogeneous K_2HPO_4 solutions with different concentrations (range: 0-800 mg/cm^3) were used to assess the accuracy of a microCT system, equipped with a polychromatic X-ray source. Both low (45 kV) and high (70 kV) tube peak voltages were explored. The resulting attenuation was compared with calculated theoretical attenuation values to estimate the accuracy. As an example of its applicability, the method was used to assess the changes in the degree of mineralization of various regions of the mandible from two pigs of different developmental age. On average, the estimated error of the measured linear attenuation was 10% or less. The accuracy was dependent on the average mineral concentration, the size of the sample, and the energy of the X-ray beam. The accuracy of the microCT system appeared sufficient to distinguish regional differences in the degree of mineralization within and between specimens of developing mandibular bone. Furthermore, the resolution of the system allowed identification of different degrees of mineralization within trabeculae. It was concluded that the accuracy of microCT with polychromatic radiation can be considered adequate for the assessment of the degree of mineralization of developing bone. Therefore, this method provides a three-dimensional means to simultaneously investigate the bone structure as well as the degree of mineralization during development in a non-destructive manner and with a high resolution.

Introduction

Together with architecture, bone mineralization has proven to be a key factor in the determination of the quality and mechanical properties of trabecular bone (Rho et al., 1995; Borah et al., 2000; Ding, 2000). Several techniques have been applied in order to quantify the structure and/or mineralization of bone during its development in fetuses and newborns. Among these techniques are, histology (Lee et al., 2001), dual energy X-ray absorptiometry (DXA, Braillon et al., 1992; Salle et al., 1992; Panattoni et al., 1995, 1999), quantitative computed tomography (QCT, Braillon et al., 1996), synchrotron radiation computed tomography (Nuzzo et al., 2003), and backscattered electron microscopy (BSE, Skedros et al., 1993; Roschger et al., 2001). The resolution of DXA and clinical QCT is insufficient to reveal the degree of mineralization at the trabecular level, whereas histology and BSE require destruction of the investigated object and can only visualize the object in two dimensions. Synchrotron radiation computed tomography, although its unbiased assessment of the degree of mineralization, its high resolution, and its non-destructive measurement, is very time consuming and has a limited availability. In the past few years, micro-computed tomography (microCT) has been used extensively to quantify the architectural properties of trabecular bone three-dimensionally (Rüegsegger et al., 1996). Bone volume fraction, trabecular number, thickness, and separation, and anisotropy, for example, have proven to be fundamental characteristics in describing the trabecular structure of bone (e.g. adult bone: Barbier et al., 1999; Giesen and van Eijden, 2000; Laib et al., 2000; postnatal development: Lerner and Kuhn, 1997; Tanck et al., 2001). However, thus far the possibilities for the application of microCT in the quantification of the degree of mineralization of bone have not been explored.

Unambiguous quantification of the degree of mineralization using microCT is not straightforward due to the polychromatic character of the X-ray beam in commercially available microCT systems. The disadvantage of such a polychromatic beam (the X-ray beam contains a broad spectrum of energies) is that low energy ("soft") radiation is more readily absorbed than high energy ("hard") radiation, which causes the energy spectrum of the beam to change as it passes through the investigated object (Brooks and di Chiro, 1976). When the beam has passed through the object, it contains a relative large portion of high energy ("hard") radiation, hence this effect is known as beam hardening. The high absorption of soft radiation at the outer region of an object gives the impression of a higher mineral

concentration in this portion in comparison with the internal region, where the remaining hard radiation is not so readily absorbed, causing an underestimation of the mineral concentration in this section of the object (Fig. 1A, B, C). Moreover, beam hardening leads to a non-linear relationship between the linear attenuation of radiation and the material density and object dimensions. The attenuation becomes more underestimated with increasing density and object size (Fig. 1D). As this effect is well known, a microCT apparatus is commonly equipped with a beam hardening correction algorithm, which reduces the non-linearity of the relationship by fitting it with polynomials (Hammersberg and Mångård, 1998).

The goal of this study was to evaluate the accuracy and applicability of a microCT system, equipped with a beam hardening correction algorithm, to quantify the degree of mineralization as well as its distribution in developing bone. As the beam hardening artifact becomes stronger when more radiation is absorbed, it is likely that these measurements are much less influenced by beam hardening than mature bone due to a relatively low degree of mineralization in developing bone. The developing mandible has been chosen to assess the applicability of the method in an environment with a non-homogeneous mineral density distribution. As this structure exhibits a complex timing of ossification, it can be expected that in each stage of development a wide range of mineralization densities will be present.

Material and methods

MicroCT

The degree of mineralization was analyzed with a high-resolution microCT system (µCT 40, Scanco Medical AG., Bassersdorf, Switzerland). This microCT system is based on an X-ray tube that produces a cone-shaped beam which is detected by a CCD detector (2048 x 64 elements; 2048 x 2048 pixels in image matrix). A detailed description of the system can be found elsewhere (Rüegsegger et al., 1996). Cross-sections were reconstructed using the Feldkamp algorithm (Feldkamp et al., 1989).

The analysis was performed at low (45 kV) and high (70 kV) peak voltages of the X-ray tube. Furthermore, a high current and a low current setting for each peak voltage were evaluated. The X-ray beam was prefiltered with an aluminum filter (0.5 mm) to remove the softest rays. Reduction of the effect of beam hardening was accomplished by applying a correction function to the detected X-ray radiation attenuation, which was developed by the

manufacturer. For imaging purposes each voxel was depicted with a grey value which was related to the linear attenuation. It was assumed that this attenuation was proportional to the degree of mineralization.

Reference measurements

The mineral hydroxyapatite ($Ca_{10}(PO_4)_6(OH_2)$) is the main constituent in calcified bone that causes X-ray attenuation. Therefore, the degree of mineralization is assumed to be equivalent with the concentration of hydroxyapatite. Due to solubility problems, it was impossible to obtain a homogeneous solution of this mineral for calibration purposes. As the easily in water soluble dipotassium hydrogen phosphate (K_2HPO_4, Merck, Darmstadt, Germany) displays the same absorption characteristics as hydroxyapatite over a wide range of energies (Nuzzo et al., 2002), it was utilized for the calibration of linear attenuation coefficients and determining the accuracy of the method.

The influence of the available beam hardening correction algorithm was illustrated by comparing the linear attenuation for a series of K_2HPO_4 reference solutions of different concentrations in a sample holder of 20 mm outer diameter (polyetherimide, wall thickness: 1.5 mm) with and without the implementation of the beam hardening correction algorithm. They were scanned using a low energy X-ray beam (45 kV, 177 μA combination). For each concentration, the average attenuation was calculated over a circular cylinder in the center of the sample, with a diameter approximately three-quarters of the total inner diameter of the sample. Here the linear attenuation values are approximately constant.

Reference measurements were performed with cylindrical specimen holders with different outer diameters (12, 20, and 36 mm), filled with different solutions of K_2HPO_4 (0, 10, 50, 150, 250, 375, 500, and 800 mg/cm^3). Four energy-current settings were applied, namely low energy (45 kV with 88 μA and 177 μA) and high energy (70 kV with 57 μA and 114 μA). All the reference measurements were performed with application of the polynomial beam hardening correction algorithm. The average linear attenuation of a specific concentration of K_2HPO_4 was determined for the central cylindrical portion with a diameter of three-quarters of the inner diameter of the sample. For each specimen holder diameter - energy combination, a relationship between K_2HPO_4 concentration and linear attenuation was obtained. By fitting these curves with 2nd order polynomials, calibration curves for each specimen diameter - energy combination were established.

Accuracy

In order to assess the accuracy of the recorded linear attenuation, the measured relationship between attenuation and K_2HPO_4 concentration of the reference solutions was compared with the theoretical relationship. The calculation of the theoretical linear attenuation coefficients for a specific mixture is based on the concept of additivity. According to this concept, the mass attenuation coefficient for a mixture [$(\mu(E)/\rho)_{mixture}$] with atomic constituents i for a given energy can be determined according to:

$$\left(\frac{\mu(E)}{\rho}\right)_{mixture} = \sum_i w_i \cdot \left(\frac{\mu(E)}{\rho}\right)_i$$

where w_i is the fraction by weight of the ith atomic constituent. For each concentration of K_2HPO_4 in water, there are different ratios between the atoms in the mixture, which leads to different mass attenuation coefficients for the specific mixtures.

The mass attenuation coefficients of the different mixtures of K_2HPO_4 with water were obtained from the National Institute of Standards and Technology (NIST) databases (http://physics.nist.gov/PhysRefData) with the effective energy representing the total radiation spectrum. These effective energies were estimated by taking the average linear attenuation value in the center of a cross-section through a K_2HPO_4 solution. The energy corresponding to this attenuation value of this specific mixture was looked up in the NIST databases (Kumar et al., 2002) and treated as the effective energy. This was performed for every holder-diameter – K_2HPO_4 combination for both tube voltages separately. The obtained values showed very little variation and were 24 keV (± 0.8 keV) for the low tube voltage (45 kV) and 31 keV (± 1.2 keV) for the high tube voltage (70 kV). Linear attenuation coefficients ($\mu(E)$) were obtained by multiplying the mass attenuation coefficients with the density of the solution.

The accuracy of a measured linear attenuation value (of a specific K_2HPO_4 concentration) was quantified as the relative deviation from its theoretically determined value and was expressed as a percentage of the latter.

Developing mandibles

Two porcine mandibles (*Sus domesticus*) of different developmental age were used as an example of the progress of mineralization in the ossification process. One was from a female fetus (gestation age between 55-60 days and crown-rump length (CRL) of 124 mm). The

other was from a newborn female pig (CRL of 392 mm). The mandibles were removed by dissection and cut in half at the symphyseal region. They were stored in a 4% formaldehyde solution at ambient temperature. Prior to scanning, the hemimandibles (right side) were mounted in a cylindrical specimen holder and secured with synthetic foam. The holders were filled with water until the specimens were completely submerged.

The complete specimens were scanned with a 10 x 10 x 10 μm^3 and 30 x 30 x 30 μm^3 resolution for the fetal and newborn mandible, respectively. The hemimandible of the newborn pig was rescanned with a resolution of 10 x 10 x 10 μm^3 after it had been cut into a number of sections. The bone scans were performed with low energy (45 kV/24 keV).

In order to obtain a three-dimensional visualization of the mandibular bone, it was digitally separated from the background, soft tissues, and cartilage in the resulting attenuation maps by applying global thresholds (Dufresne, 1998). Every voxel below this attenuation threshold was made transparent, whereas the remaining voxels, belonging to bone, were made opaque. For the quantification of the degree of mineralization, the same global threshold was applied in the three-dimensional attenuation maps, to remove all soft tissue, while the attenuation values of all bony matter remained unaffected.

Several volumes of interest, approximately 1 by 1 by 0.5 mm^3 (resolution: 10 μm) in size, were defined to compare the regional degree of mineralization of both mandibular specimens. They were selected in the symphyseal region, mandibular corpus, mandibular ramus, mandibular angle, coronoid process, condylar neck, and condylar head (Fig. 4 and 5). The degree of mineralization was calculated as the average mineralization density of the bone within a volume of interest using the calibration lines obtained from the reference measurements. The accuracy of the measured degree of mineralization of the bone was calculated according to the accuracy of the reference measurements.

Results

Reference measurements

The cross-sectional images in Fig. 1A and B illustrate the influence of the beam hardening correction function in a 500 mg/cm^3 K_2HPO_4 solution. The characteristic cupping profile (Fig. 1A) with the relative high absorption of (soft) radiation at the edges and less absorption (hard

radiation) in the inner region was clearly reduced when beam hardening correction was used (Fig. 1B).

The line profiles through the cross-sectional images in Fig. 1A and B also show that the obtained attenuation varied throughout the entire specimen in contrast to its theoretical homogeneous mineral density indicated by the blue line in Fig. 1C. Therefore, in order to quantify the accuracy of the reference measurements, the average attenuation for a cylinder at the center of the sample with a diameter that was three-quarters of the total diameter was analyzed to avoid the worst cupping artifacts. The relationship between the average measured linear attenuation of the central cylinder and the K_2HPO_4 concentration appeared to be non-linear for the non-corrected scans (Fig. 1D). The obtained linear attenuation values were less than the theoretical ones and the difference between the two increased with the K_2HPO_4 concentration. The beam hardening correction algorithm however, improved the relationship between linear attenuation and K_2HPO_4 concentration considerably (Fig. 1D). Therefore, all subsequent reference and bone measurements were performed with implementation of this beam hardening correction algorithm.

The results of the reference measurements are depicted in Fig. 2. For small specimen diameters the resulting linear attenuation coefficients were larger than for larger specimens. Furthermore, for scans with low energy (45 kV/24 keV), the resulting linear attenuation coefficients were larger than for scans performed with high energy (70 kV/31 keV), which was consistent with theoretical linear attenuation values from the NIST database. The measured attenuation in the case of the lower concentrations of the K_2HPO_4 solutions lay above the theoretical values, whereas with higher concentrations, the linear attenuation coefficients lay beneath the theoretical value. The variation in current had a negligible influence on the measured attenuation values (data not shown).

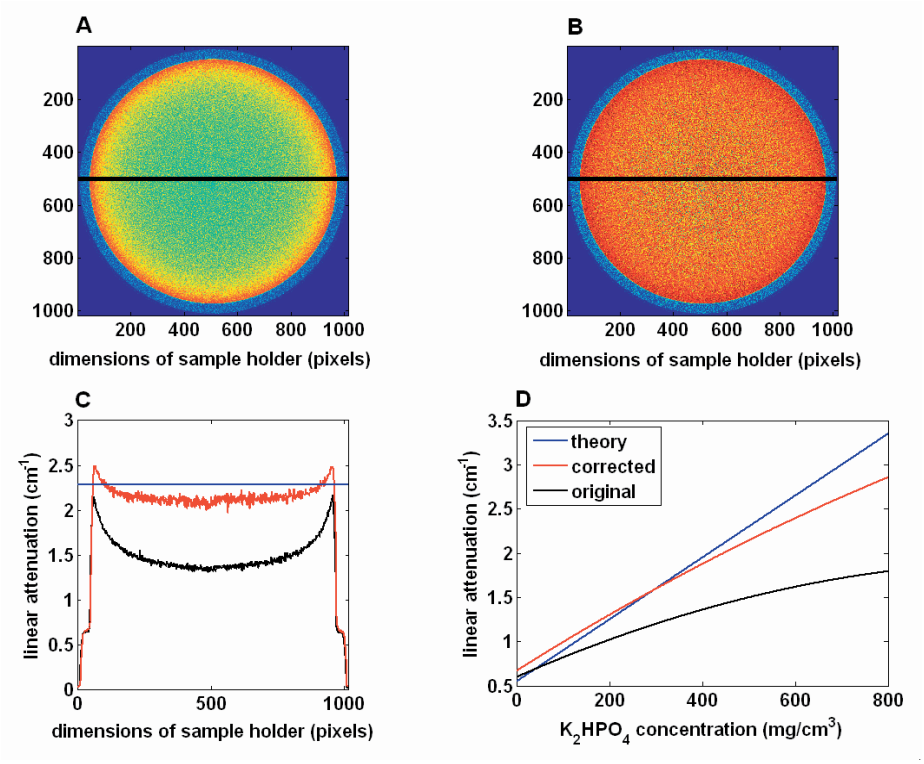

Figure 1. Influence of the beam hardening correction. A: Cross-section through a 20 mm sample holder filled with a homogeneous K_2HPO_4 solution of 500 mg/cm^3, scanned with low radiation energy (45 kV/24 keV), without implementation of the polynomial beam hardening correction algorithm. Light blue, the sample holder; red, high attenuation (edge); green, low attenuation (center). B: Same as Fig. 1A, but with implementation of the correction algorithm. Light blue, the sample holder; dark red, high attenuation (edge); orange, low attenuation (center). C: Line profiles through the cross-sections of Fig. 1A and B (black bars). Theoretical value is 2.28 cm^{-1} (blue line). Black curve, uncorrected profile; red curve, corrected profile. D: Attenuation curves for the range of concentrations (object densities) analyzed. Blue line, theoretical linear attenuation curve for the low energy setting (45 kV/24 keV); red line, the, for beam hardening corrected, measured calibration curve for a 20 mm specimen; black line, uncorrected linear attenuation curve for a 20 mm specimen.

Accuracy

In order to determine the accuracy of the measured mineralization density, the measured linear attenuation coefficients were compared with the theoretical ones for the concentration range in every energy – sample diameter combination. With the exception of the scans of the smallest samples with high energy settings, the average relative errors over the range of concentrations were around 10% or less (Fig. 3A). Furthermore, scans performed with low

energy settings deviated less from the theoretically determined linear attenuation values, than those performed with high energy, especially when smaller specimens were concerned.

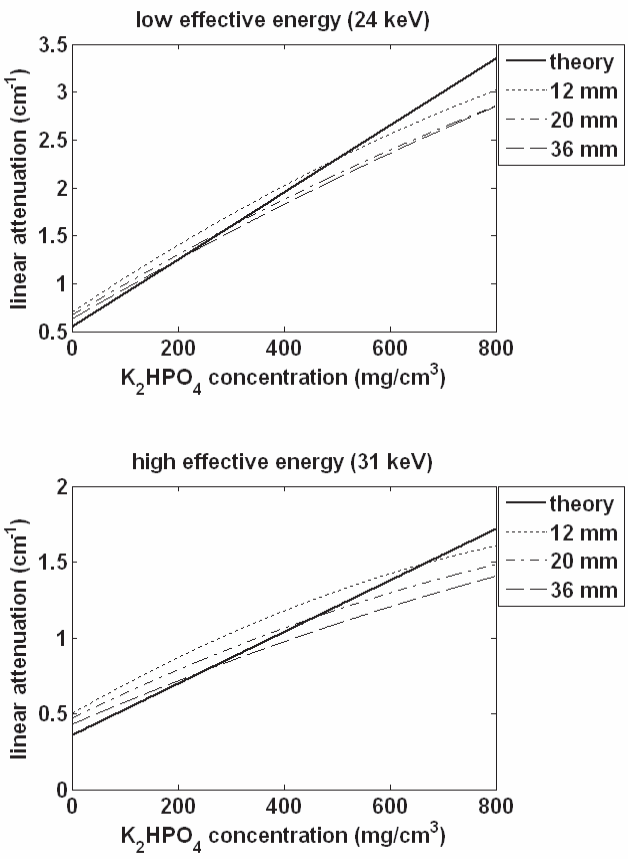

Figure 2. Calibration lines of different combinations of sample dimensions and energy settings for the relationship between sample concentration and the linear attenuation coefficient. Solid line: theoretical relationship; dotted line: specimen diameter 12 mm; dash-dotted line: specimen diameter 20 mm; dashed line: specimen diameter 36 mm.

An overview of the specific error as a function of the concentration is shown in Fig. 3B. This figure shows the average error, over the complete range of concentrations for a scan with a sample diameter of 20 mm, which were scanned using low energy (24 keV). The smallest errors occurred in the concentration region between 300 and 500 mg/cm^3. The

minimal error shifted to higher mineralization density values with decreasing specimen dimensions (data not shown). The resolution of the scan had no influence on the accuracy of the measured attenuation coefficients (data not shown).

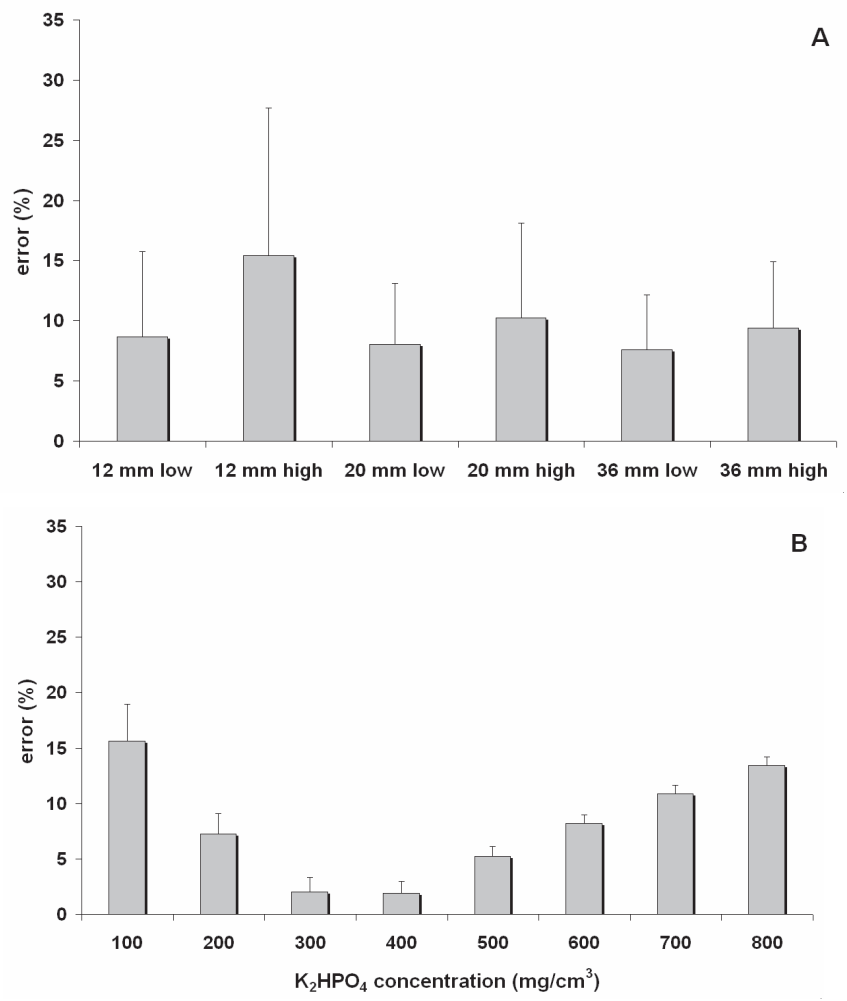

Figure 3. Average errors. A: The average error and standard deviation (n=8), over all concentrations, of the measured linear attenuation from the theoretical values. Bars are shown for every measured specimen size – energy combination. B: The error of the measured linear attenuation coefficients, averaged over bins of 100 mg/cm^3, for measurements made with a 20 mm specimen with low energy settings.

Developing mandibles

Comparison of the reconstructions of the two mandibular specimens revealed considerable morphological differences between the two developmental stages (Fig. 4 and Fig. 5). The mandible of the fetal pig showed no solid cortical bone, in contrast to the mandible of the newborn. In the newborn mandible the bone in the coronoid and condylar processes and the symphyseal region was clearly visible.

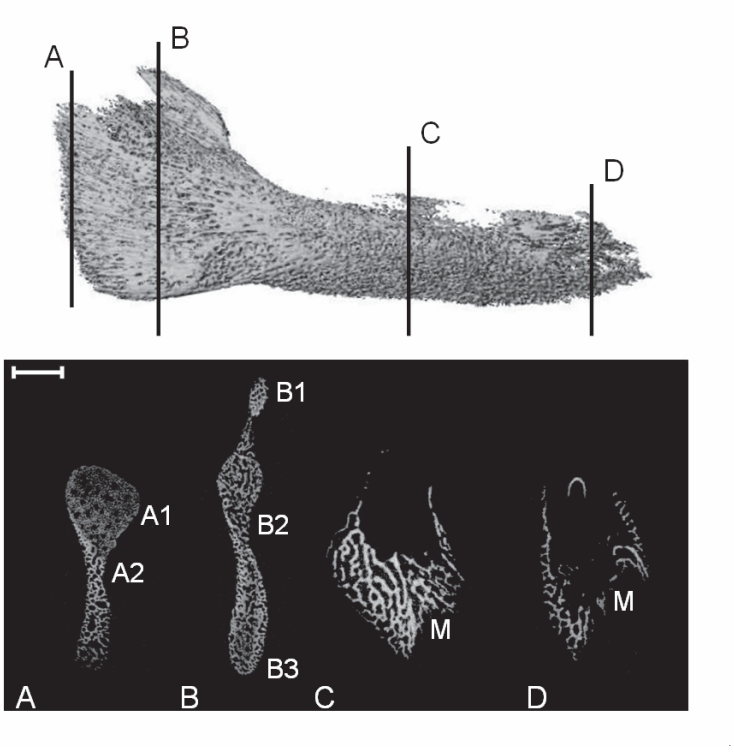

Figure 4. Top: Three-dimensional reconstruction of the mandible of the fetal specimen. Lines represent the location of the cross-sections depicted below. A1: Condylar head; A2: Condylar neck; B1: Coronoid process; B2: Ramus; B3: Angle. Mandibular corpus and symphysis are depicted in cross-section C and D respectively. M: Groove where Meckel's cartilage presumably runs. In cross-section D, the tooth germ of the first incisor is just discernable. Bar, 1 mm.

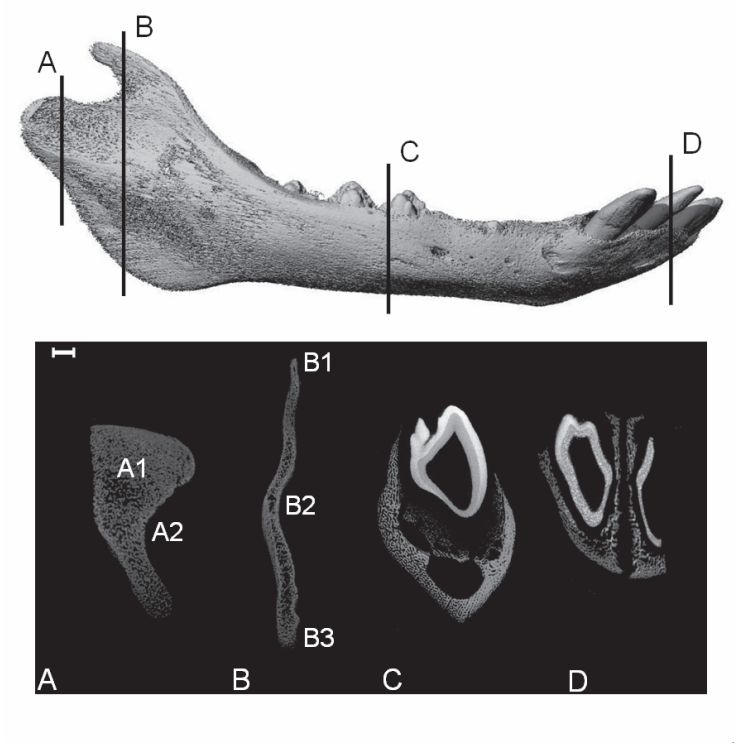

Figure 5. Top: Three-dimensional reconstruction of the mandible of the newborn specimen. Lines represent the location of the cross-sections depicted below. Note, for example, the changes in the cortical bone structure as compared to the fetal specimen. Coding as in Fig. 4. Bar, 1 mm.

The degree of mineralization appeared distinctly higher in all regions of the mandible of the newborn pig (Table 1). In both the fetal and newborn mandible a difference in the degree of mineralization between the different regions could be distinguished (Table 1). In both specimens, the corpus was the region which showed the highest degree of mineralization. The lowest degrees of mineralization were observed in the condylar head and the mandibular angle. Also, at the trabecular level, mineral density distribution differences within trabeculae were observed between the fetal and the newborn specimen (Fig. 6). The trabeculae showed a higher degree of mineralization in their centers than near the surfaces. Besides the overall thickening of the trabeculae, more regions of higher degrees of mineralization were recognized in the newborn specimen.

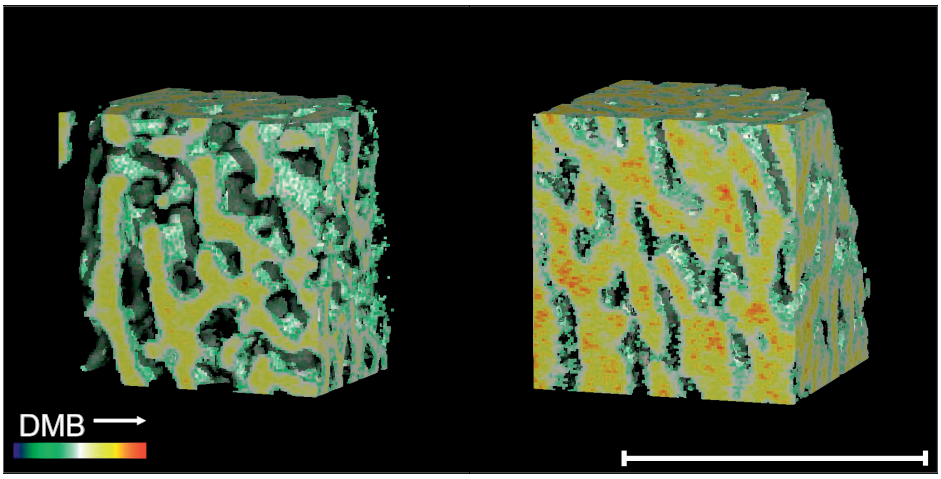

Figure 6. Three-dimensional, linear attenuation maps of two volumes of interest selected in the mandibular corpus of the fetal (left) and newborn specimen (right). Increasing degree of mineralization (DMB) from blue to red. An overall increase in trabecular thickness can be observed, as well as higher mineralization in the centers of the trabeculae of the newborn specimen. Bar, 1 mm.

Table 1. The degree of mineralization of different regions of fetal and newborn pig mandibles.

Region	Fetal degree of mineralization (mg/cm^3)	Estimated error* (mg/cm^3)	Newborn degree of mineralization (mg/cm^3)	Estimated error * (mg/cm^3)
Symphysis	382	16	751	61
Corpus	650	32	985	149
Angle	360	19	651	33
Ramus	586	16	803	79
Coronoid process	616	23	843	93
Condylar neck	550	9	642	30
Condylar head	279	24	580	15

* Estimated error of the degree of mineralization of bone was estimated according to the accuracy in the reference measurements.

Discussion

This study deals with the quantification of the degree of mineralization in developing bone using a commercially available microCT device, equipped with a polychromatic X-ray source. It was hypothesized that the measured attenuation profiles in developing bone were

accurate enough to make quantitative comparisons despite the beam hardening effect, which is a common artifact when using polychromatic X-ray sources.

It appeared that the absorption of X-rays by various solutions of K_2HPO_4 was considerably underestimated due to beam hardening. This could be largely corrected by applying the correction algorithm with which the microCT system was equipped. However, the remaining beam hardening effect still had some influence. Subsequent reference measurements, for instance, showed that the attenuation values in reference specimens with smaller diameters were higher than for larger specimens, although they were of the same concentration K_2HPO_4 (Fig. 2). This can be explained by the fact that the soft radiation was equally absorbed at the surfaces of both the small and large specimen. As the volume/surface ratio increases with the diameter, the attenuation was lower in a larger area. Averaging the attenuation over a cylindrical section in the center of a reference specimen thus led to a greater accuracy of the attenuation values in reference measurements with a larger diameter. The high attenuation values measured in small diameter tubes is probably due to an overcorrection of the beam hardening correction algorithm. The fact that the measured reference curves lay above the theoretical curve in all cases, when low K_2HPO_4 concentrations were concerned (Fig. 2), has to be attributed to the applied beam hardening correction function. Furthermore, the theoretical attenuation values were obtained by assuming the average effective energy as the representative of the polychromatic radiation spectrum.

As was mentioned above, the beam hardening correction function did not have a completely linearizing effect on the measured attenuation curve and deviations from the theoretical curve remained. Especially when higher bone mineral densities were concerned, these errors remained substantial. As the degree of mineralization in adult bone often exceeds 1250 mg/cm^3 (Maki et al., 2001), errors larger than 25% can be expected despite the application of the correction algorithm. Moreover, specimens with high mineralization densities may be impenetrable to low energy radiation and thus require high energy application, which in turn causes a further decrease in accuracy. For fetal bone specimens, however, the present correction function proved to be sufficient to obtain adequate results. Average deviation from the theoretical attenuation profile was below 10% for all sample dimensions and energy-current settings, with the exception of the high energy measurements of the smallest sample (Fig. 3A). Errors were even smaller in the density range between 300 and 500 mg/cm^3 (lower than 6%). This accuracy is comparable to that obtained with synchrotron radiation, which reaches an average deviation from theory of less than 6%

irrespective of the degree of mineralization (Nuzzo et al., 2003). Still, extrapolation of these results to measurements of the degree of mineralization of bone has to be performed with care. The present results were obtained with homogeneous solutions of K_2HPO_4. Bone, however, is a heterogeneous material and radiation absorption in specific parts of the bone may influence the absorption of radiation in an adjacent region of bone. Furthermore, the high degrees of mineralization of teeth that are present in the later developmental stages have an unknown influence on the measured degree of mineralization of adjacent bone and caused some streaking. Moreover, the presence of soft tissues could have influenced the attenuation of radiation. As this only has a minor contribution to the absorption of rays (approximately 7%), it was not elaborated in this study (Postnov et al., 2003).

A wide variety in degree of mineralization as expected in the developing mandible could indeed be retrieved from the attenuation maps obtained from the two porcine mandibles (Fig. 4 and 5, and Table 1). They reflect a normal mandibular development. At locations where the ossification process of the mandible starts (the corpus, Tomo et al., 1997), the obtained attenuation was relatively large, whereas at sites that ossify much later - for instance the symphysis and condylar head, which are both involved in endochondral ossification (Orliaguet et al., 1993; Lee et al., 2001) - it remained relatively low. Furthermore, the degree of mineralization at the mandibular angle was relatively low. This could be related to the backward growth of the ramus and angle, where new, not fully mineralized bone is constantly added to the posterior border. As this process continues after birth, the degree of mineralization in the mandibular angle of the newborn specimen was relatively low. Also, in all other regions the degree of mineralization had increased, but the relative small increase of the degree of mineralization of the condylar neck is presumably caused by the continuous upward growth of the condyle.

There were also differences observed in bone mineral distribution at the trabecular level. With age, the overall thickness of the trabeculae increased and higher degrees of mineralization were found in the centers of the trabeculae (Fig. 6). The observed lower mineral density at the surfaces of the trabeculae could be caused partially by a volume effect, i.e. voxels at the surfaces may be partly filled with bone. The computed degree of mineralization for such a voxel could therefore be reduced. This effect can only be present in a shell with a thickness of 10 μm (the resolution). As the trabeculae have a thickness of 70-100 μm, most of the observed mineralization differences have to be attributed to real differences. This suggests that new unmineralized bone tissue is laid down at the surfaces of

the trabeculae and progressively mineralizes leading to more mature and thus more mineralized tissue in their centers.

From this study it can be concluded that the applied microCT system is adequate to quantify the degree of mineralization in developing bone. Herewith, it provides a means to simultaneously investigate the three-dimensional structure and mineral density distribution of developing bone. It was proven adequate to assess the relative complex timing of the mineralization process present in the mandible in a non-destructive manner. The resolution is high enough to observe the architecture and the degree of mineralization on a trabecular level. In adult bone, beam hardening presumably disturbs the quantification of the degree of mineralization unacceptably, as errors larger than 25% can be expected[1].

The present method can provide a better understanding of the development of the relationship between the degree of mineralization and architectural parameters such as bone volume fraction, trabecular number, trabecular thickness, and anisotropy. The combined investigation of the degree of mineralization and the architecture could provide a better comprehension of the mechanical properties of trabecular bone. The use of this method might be applied in the future to other parts of the skeleton to enrich the basic embryological information. Furthermore, the method might be useful for the evaluation of the influence of genetic diseases, pathogenic drugs or other noxious environmental conditions, which could influence the fetal development of bone.

[1] Throughout this thesis, two different beam hardening correction algorithms were used. In chapters 2-5, the 'old' correction was used. In chapters 6-9, a new and improved one was applied, which corrects the beam hardening effect better at higher degrees of mineralization and will thus lead to lower uncertainties than in the earlier chapters at high degrees of mineralization.

CHAPTER 3

ARCHITECTURE AND MINERALIZATION OF DEVELOPING TRABECULAR BONE IN THE PIG MANDIBULAR CONDYLE

Abstract

Architecture and mineralization are important determinants of trabecular bone quality. To date, no quantitative information is available on changes in trabecular bone architecture and mineralization of newly formed bone during development. Three-dimensional architecture and mineralization of the trabecular bone in the mandibular condyle from six pigs of different developmental ages were investigated with microCT. Anteriorly in the condyle, a more advanced state of remodeling was observed than posteriorly, where more active growth takes place. Posteriorly, the bone volume fraction increased with age (R = 0.87; P < 0.05) by an increase in trabecular thickness (R = 0.88; P < 0.05), while the number of trabeculae declined (R = -0.86; P < 0.05). Anteriorly, despite an increase in trabecular thickness (R = 0.97; P < 0.001), there was no change in bone volume fraction due to a simultaneous decline in trabecular number (R = -0.84; P < 0.05) and increase in trabecular separation (R = 0.95; P < 0.01). Posteriorly, rods were remodeled into plates as expressed by the structure model index (R = -0.97; P < 0.001), whereas anteriorly, a plate-like structure was already present in early stages. The trabecular structure had a clear orientation throughout the developmental process. The degree of mineralization increased both anteriorly (R = 0.86; P < 0.05) and posteriorly (R = 0.89; P < 0.05). We suggest that the degree of mineralization does not depend on the bone volume, but on the thickness of the trabeculae as the mineralized centers of trabeculae were getting larger and more highly mineralized with age compared to their appositional layers. This indicates that besides apposition of new bone material on the surface of trabeculae, the mineralized tissue in their centers still changes and matures.

Introduction

The trabecular architecture of bone adapts to the mechanical circumstances to which it is subjected during function. Except for architecture, the mechanical properties of trabecular bone depend on the degree and distribution of mineralization (Turner et al., 1990; Borah et al., 2000; Müller, 2003; Follet et al., 2004). The plates and rods of adult trabecular bone are composed of packets of remodeled bone of different ages and thus different degrees of mineralization (Parfitt et al., 1983). It has also been shown that tissue mineralization varies spatially within trabeculae of adult bone (Paschalis et al., 1997) and fetal bone (Meneghini et al., 2003). Furthermore, these variations appeared to be consistent with the preexisting notions that formation of trabecular bone takes place on the surface of trabeculae, and that newly produced collagenous tissue becomes more mineralized and rigid with age (Ziv et al., 1996). So far, there is no quantitative information concerning the development of the architecture and mineralization properties of trabecular bone and both properties have not been interrelated.

After initial formation, the fetal trabecular bone structure is likely to adapt to the mechanical environment *in utero* by remodeling. Besides, also the mineralization of this structure will undergo changes. The supposedly rapidly developing structure of fetal trabecular bone and its mineralization would provide an interesting model to investigate the simultaneous changes of these two properties. The development of the trabecular architecture has been studied in the femur (Salle et al., 2002) and in the vertebra (Nuzzo et al., 2003). Both studies solely investigated the architecture of the trabecular bone and did not elaborate on the degree and distribution of mineralization. Thus far, no information is available on the degree and distribution of mineralization and its relation to the architecture of developing trabecular bone. Knowledge regarding the development of trabecular bone architecture and its relation to mineralization will augment the understanding of normal trabecular bone development and delivers baseline data to which deviations can be compared. For instance, bone diseases like osteoporosis and the influences of pathogenic drugs or noxious environmental conditions can be traced back to the fetal development of bones (Cooper et al., 2002; Javaid and Cooper, 2002). In addition, knowledge of the degree and distribution of mineralization will add to a more accurate estimation of the apparent mechanical properties of trabecular bone as investigated by, for example, finite element models (van der Linden et al., 2001; Bourne and van der Meulen, 2004).

In the present study, the method of micro-computed tomography (microCT) was applied to simultaneously investigate the architecture and mineralization of developing trabecular bone. Recently, microCT has been established as an accurate and powerful tool for determining three-dimensional architectural parameters of young and adult trabecular bone in a non-destructive manner (Müller et al., 1996; Rüegsegger et al., 1996; Uchiyama et al., 1997; Müller et al., 1998). It has been proved applicable to investigate the changes in trabecular architecture during aging and postnatal development (Barbier et al., 1999; Ding, 2000; Nafei et al., 2000b; Tanck et al., 2001; Wolschrijn and Weijs, 2004). In addition, it has been recently demonstrated that commercial microCT systems are not only capable of describing the architectural but also the physical properties of trabecular bone like the degree and distribution of mineralization (Mulder et al., 2004).

An interesting piece of bone that has a rapid formation of trabeculae and that would provide a suitable model for developing trabecular bone is the mandibular condyle (Teng and Herring, 1995; Giesen and van Eijden, 2000). Moreover, the mandibular condyle is subjected to mechanical usage *in utero*: fetal swallowing and yawning (de Vries et al., 1982). In this study, the trabecular bone of the mandibular condyle of developing pigs was analyzed. Although a lot is known about the structure of the trabecular bone in the juvenile and adult mandibular condyle, it is unclear how this specific structure develops during fetal life. Extensive research has been performed on the fetal development of the mandibular condyle. However, these studies focused mainly on the cartilage part (Durkin and Irving, 1973; Hall, 1987; Copray et al., 1988; Ben-Ami et al., 1992; Shibata et al., 1996). The underlying endochondrally developing trabecular bone has received little attention.

Material and methods

Samples

The mandibular condyles from six pigs (standard Dutch commercial hybrid race) of different developmental ages were used in this study. The fetuses had an estimated age of 65-70, 70-75, 82-87, and 95-100 days of gestation and were obtained from slaughtered sows in a commercial slaughterhouse. Fetal age was determined from the mean weight of the litter, using growth curves (Evans and Sack, 1973). A newborn (112-115 days post conception) and a two weeks old (130 days post conception) piglet were obtained from the experimental farm

of the Faculty of Veterinary Medicine in Utrecht, the Netherlands, and were euthanized by an intravenous overdose of ketamine (Narcetan) after premedication. The specimens were obtained from other experiments that were approved by the Committee for Animal Experimentation of the Faculty of Veterinary Medicine, Utrecht, the Netherlands. They were stored at -20°C prior to assessment.

The mandibles were prepared by dissection from the heads and cut in half at the symphyseal region. No attempt was made at removing all the soft tissue. The condyles of the three oldest specimens had to be separated from the mandibular ramus in order to be able to analyze all specimens with the same resolution, which is limited by the diameter of the microCT specimen holders.

MicroCT

Three-dimensional reconstructions of the trabecular bone of the specimens were obtained by using a high resolution microCT system (μCT 40, Scanco Medical AG., Bassersdorf, Switzerland). The condyles were mounted in cylindrical specimen holders (polyetherimide, 20 mm outer diameter, wall thickness: 1.5 mm) and secured with synthetic foam. The specimens were completely submerged in 70% ethanol. The scans yielded an isotropic spatial resolution of 10 μm. A 45 kV peak voltage X-ray beam was used, which corresponds to an effective energy of approximately 24 keV (Mulder et al., 2004). The microCT system was equipped with an aluminum filter and a correction algorithm, which reduced the beam hardening artifacts sufficiently to enable quantitative measurements of the degree and distribution of mineralization of developing bone (Mulder et al., 2004). The computed linear attenuation coefficient of the X-ray beam in each volume element (voxel) was stored in an attenuation map and represented by a grey value in the reconstruction. This attenuation coefficient can be considered to be proportional to the local degree of mineralization (Nuzzo et al., 2003).

Architecture

To determine the architecture of the bone specimens, volumes of interest (approximately 1 mm^3) were built up out of 10 x 10 x 10 μm^3 voxels and segmented using an adaptive threshold, which was visually checked. In a segmented image every voxel with a linear attenuation value below the threshold (assumingly representing soft tissue or background) was made transparent and voxels above this threshold (representing bone) were made opaque.

For a quantitative analysis of the architecture and the determination of the degree of mineralization, volumes of interest were chosen within four different regions of the condylar specimens to investigate the suspected heterogeneity. These regions were located anterosuperiorly, anteroinferiorly, posterosuperiorly, and posteroinferiorly (Fig. 1).

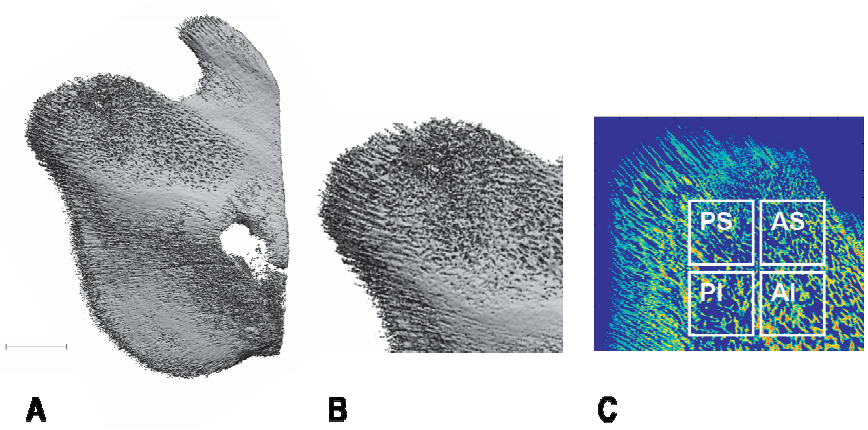

Figure 1. A: A segmented three-dimensional representation of the ramus of the mandible of the 2 weeks old piglet. Bar, 5.0 mm. Anterior is to the right, posterior to the left. B: Same as A only zoomed in on the condyle. C: Sagittal cross-section through the mandibular condyle. The regions that were investigated in this study were situated within the condyle in the anterosuperior (AS), anteroinferior (AI), posterosuperior (PS), and posteroinferior (PI) area. The degree of mineralization in C is represented by a colour-scale increasing from blue to red. Notice the absence of a solid cortex and the heavily oriented bony structure at the posterior and superior border, indicating an active growth of the structure in these directions.

To quantify the changes in architecture of the trabecular bone during development, several bone architectural parameters (BV/TV: bone volume fraction, Tb.N: trabecular number, Tb.Th: trabecular thickness, Tb.Sp: trabecular separation, Conn.D: connectivity density, SMI: structure model index, DA: degree of anisotropy) were calculated (Software Revision 3.2, Scanco Medical AG). The structure model index quantifies the characteristic shape of the trabecular bone in terms of plate-like and rod-like trabecular elements. For an ideal plate-like and rod-like structure this index is zero and three, respectively. The three principal directions of the trabecular structure were estimated by the mean intercept length (MIL) method and the degree of anisotropy was defined as the ratio between the maximal MIL and the minimal MIL (Hildebrand et al., 1999).

Degree and distribution of mineralization

The previously determined thresholds to separate bone from background were applied to the defined volumes of interest for the determination of the degree of mineralization. For this analysis, the voxels exceeding the threshold kept their original grey value. The outermost voxel layer characterized as bone was disregarded as this layer is likely to be corrupted by partial volume effects. The degree of mineralization was determined by comparing the average linear attenuation coefficient of the part of the reconstructed volume of interest which had been characterized as bone, with reference measurements of a series of solutions with different concentrations of the mineral K_2HPO_4 (Mulder et al., 2004). To investigate the degree of mineralization from the surface of the trabeculae to their centers, a specifically designed algorithm was used. Briefly, layers of bone-containing voxels were consecutively "peeled" from the surface of the reconstructed bone structure containing all the trabeculae. After a layer had been peeled off, its average degree of mineralization was calculated using the method mentioned.

Statistics

Linear regression analysis was applied to assess changes in architectural parameters and mineralization with age for the different volumes of interest using SPSS (11.5.1 software SPSS Inc.). A test for the equality of two dependent correlations was applied. This was done in order to examine the equality between the correlation coefficients of a certain parameter with developmental age for the anterior and posterior regions. The correlation between the two regions was taken into account (Steiger, 1980). This is because the two investigated regions were taken from the same mandibular condyle and therefore should be treated as dependent samples. A p-value of less than 0.05 was considered statistically significant.

Results

The reconstructed images of the specimens clearly showed the orientation of the condylar development, as it grows in a backward and slightly upward direction (Fig. 1). Distinctly orientated bony spiculae could be observed at locations of rapid growth at the posterior and superior border of the condyle. More anteriorly in the condyle, these spiculae were less apparent and integrated with the trabecular structure. No solid cortex had been formed in any

of the analyzed specimens. The cartilage covering the posterosuperior border of the actively growing mandible is not visible in these reconstructions. As no statistical differences between inferior and superior regions were found, both anterior and posterior regions were combined to investigate anteroposterior differences.

Architecture

An overview of the development of the trabecular structure in the condyle can be found in Fig. 2, where trabecular bone of the posterior region of the mandibular condyle is compared for different ages. The figure illustrates that during development there is an increase in the amount of bone and trabecular thickness and also a marked development of anisotropy of the trabeculae.

Quantitative changes in trabecular structure have been summarized in Fig. 3. The amount of bone, expressed by the bone volume fraction (BV/TV), significantly increased with age in the posterior region ($R = 0.87$; $P < 0.05$). The increase in bone volume fraction in the posterior region could be attributed to an increase in trabecular thickness (Tb.Th) ($R = 0.88$; $P < 0.05$), which outweighed a simultaneous decrease in trabecular number (Tb.N) ($R = -0.86$; $P < 0.05$). No significant changes were found for trabecular separation (Tb.Sp) in the posterior region.

In the anterior region, the bone volume fraction did not change; a decrease in trabecular number ($R = -0.84$; $P < 0.05$) and an increase in trabecular separation ($R = 0.95$; $P < 0.01$) were compensated by an increase in thickness ($R = 0.97$; $P < 0.001$) of the trabeculae. The posterior region displayed a decrease in the structure model index (SMI) ($R = -0.97$; $P < 0.001$), indicating a change from rods to plates. Anteriorly, the trabeculae had a plate-like structure which remained unchanged during the investigated ages. The connectivity density (Conn.D) decreased significantly in the anterior region ($R = -0.92$; $P < 0.01$) as well as the posterior region ($R = -0.95$; $P < 0.01$). No changes in the degree of anisotropy (DA) with age were found in the anterior region, whereas in the posterior region, the trabeculae became increasingly more orientated with age ($R = 0.92$; $P < 0.01$). Investigation of differences between correlation coefficients of the anterior and posterior region for each individual parameter yielded significant results for the bone volume fraction, trabecular separation, structure model index and degree of anisotropy. This means that there is a difference between these regions in the way that these parameters relate to age.

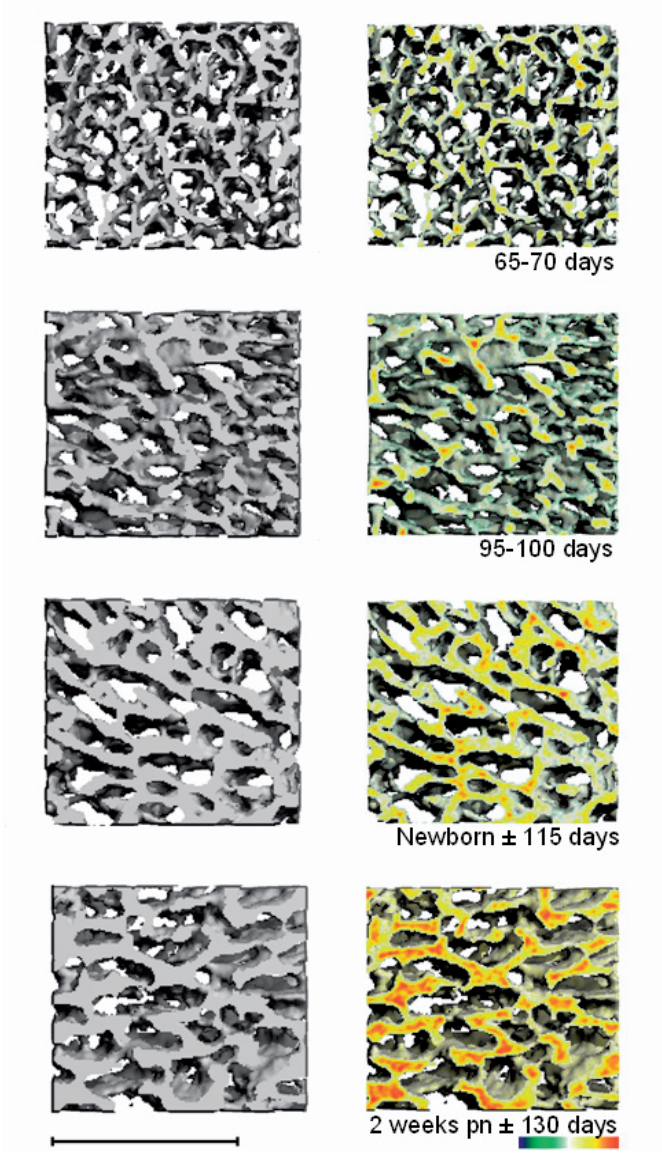

Figure 2. Left: A series of segmented cubes from the posterior part of the mandibular condyle from the fetal pigs of 65-70 and 95-100 days of gestation and the newborn and two weeks old piglets to illustrate the development of the trabecular architecture with gestational age. An increased bone volume fraction, trabecular thickness, and anisotropy are evident. Right: The same four volumes of interest, but now the original attenuation coefficients of the trabecular bone are shown. An increase in the degree of mineralization can be qualitatively observed as well as a spatial inhomogeneous distribution of the mineralization with the centers of the trabeculae being more mineralized than their surfaces. Bar, 1.0 mm; color-scale: increasing degree of mineralization from blue to red.

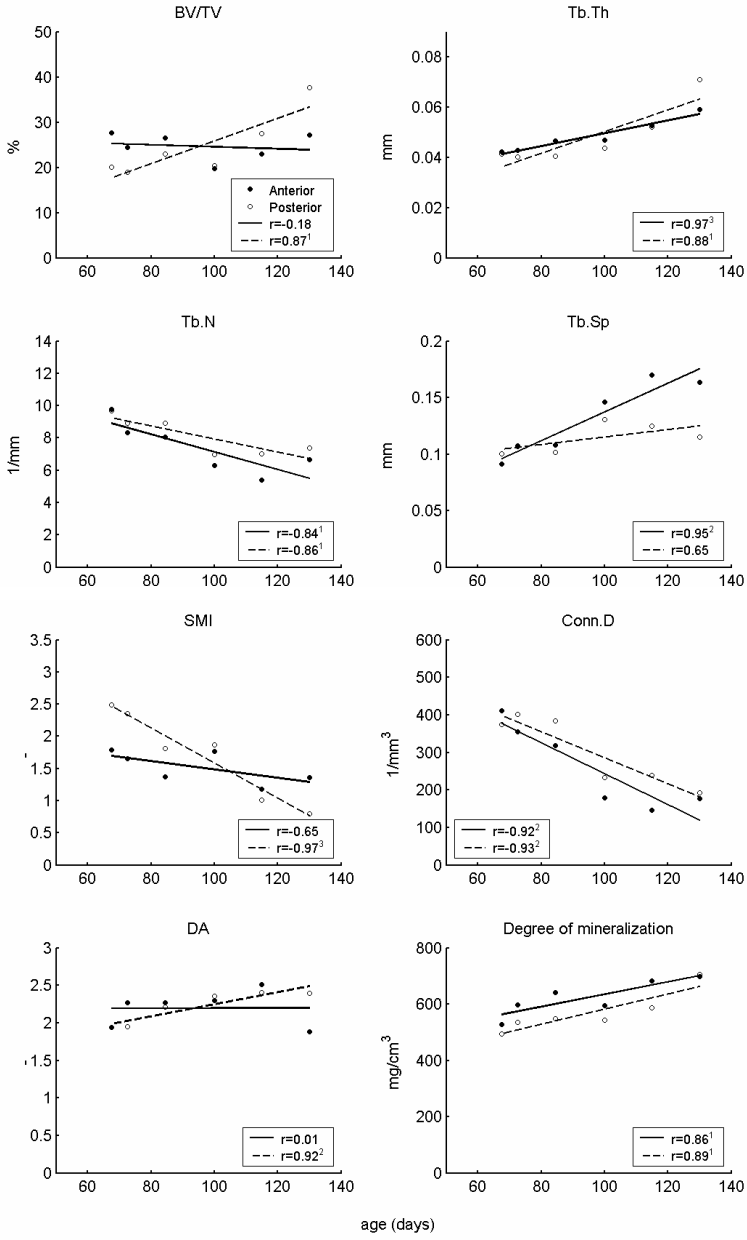

Figure 3. Results of all the investigated parameters plotted against gestational age. Closed circles: values for the anterior part of the mandibular condyle. Open circles: values for the posterior part of the mandibular condyle. BV/TV: bone volume fraction; Tb.Th: trabecular thickness; Tb.N: trabecular number; Tb.Sp: trabecular separation; SMI: structure model index; Conn.D: connectivity density; DA: degree of anisotropy. Solid line: linear regression line for anterior data points. Dashed line: linear regression line for posterior data points. The significance of the r-values of the regression is indicated as follows: [1] $P < 0.05$; [2] $P < 0.01$; [3] $P < 0.001$.

Degree and distribution of mineralization

Fig. 2 shows a clear increase in the degree of mineralization of trabeculae with age and a gradient of increasing mineralization from the surfaces towards the centers of the trabeculae. The degree of mineralization increased significantly with age (anterior $R = 0.86$; $P < 0.05$, posterior $R = 0.89$; $P < 0.05$) (Fig. 3). In the anterior region, the highest degrees of mineralization were observed. No significant differences were found in correlation coefficients between the anterior and posterior region, indicating that all regions mineralized at a similar rate. The three-dimensional distribution of attenuation values of reconstructed trabeculae revealed that mineralization was higher in the centers of the trabeculae than near their surfaces (Fig. 4).

Besides this, a steeper gradient in the degree of mineralization from the surface to the center was observed in the oldest specimen as compared to the youngest one. In the oldest specimen a relatively large "constant" region of highly mineralized bone in the centers of the trabeculae was present, which could also be confirmed in the two-dimensional cross-section through a section of trabecular bone (Fig. 4). The degree of mineralization of the outermost layers of trabeculae was nearly equal in the anterior and posterior regions of all examined ages.

Discussion

To our knowledge, this is the first quantitative descriptive study of the concurrent changes in trabecular bone architecture and mineralization of newly formed bone during development. The data were obtained quickly, accurately, and in a non-destructive manner using a commercially available desktop microCT system. The resolution was sufficiently high to analyze the early development of trabecular bone. Fetal pigs of gestational age 65-70 days and older were chosen for this study as younger specimens did not have clearly discernable trabecular bone in the condylar head in the microCT reconstructions. It must be mentioned that only six specimens were used. However, the strong correlations found in this study justify this choice and rule out any coincidence based on inter-individual variation.

It was shown that there is a considerable difference between anterior and posterior regions within the developing condyle. The posterior region exhibited an increasing bone volume fraction and every sign of an actively developing region. The anterior region on the

other hand showed a more advanced state of remodeling with no increase in bone volume fraction. The increase in bone volume fraction in the posterior region with age can be attributed to an increase in trabecular thickness and an unchanged trabecular separation despite a decline in trabecular number. A decline in structure model index in the posterior region indicated an ongoing change from rod-like trabeculae to a more plate-like shape. Along with complete disappearance of rod-like trabeculae, merging of two or more rods into plates is a likely cause for the decline in trabecular number, which in turn supposedly caused the observed decrease in connectivity density. A fall in trabecular number and rise in thickness was also observed anteriorly. As simultaneously the trabecular separation increased, the bone volume fraction remained unchanged. The decline in trabecular number was in this case likely to be caused by removal of complete trabecular elements as no change in structure model index was observed. It did, however, cause a decrease in connectivity density (Fig. 3). The anteroposterior differences could be largely explained by the fact that the trabecular bone had been formed earlier anteriorly than posteriorly and thus that remodeling had been going on for a longer period of time anteriorly.

The values for the architectural parameters of the trabecular bone in the pig mandibular condyle corroborate more with those of the developing human femur than those of the developing human vertebra. Bone volume fraction and trabecular thickness and separation in the present study (BV/TV: 20-38%, Tb.Th: 35-80 μm, and Tb.Sp: 80-180 μm) were low compared to values found for the vertebra (BV/TV: 30-54%, Tb.Th: 84-118 μm, and Tb.Sp: 155-321 μm) (Nuzzo et al., 2003), but in agreement with values for the femur (BV/TV: 24-34%, Tb.Th: 71-98 μm) (Salle et al., 2002). This indicates that the development of the condyle resembles the development of the trabecular bone in long bones. It should be mentioned, however, that the age-range chosen in this study resembled that of the femur study closer than that of the vertebra study.

Comparison with results of the mandibular condyle of juvenile pigs suggests that the trabecular bone in the condyle remains subject to extensive modeling and remodeling during further postnatal development. This is probably due to continuous changes in mechanical usage of the temporomandibular joint after birth (Langenbach and van Eijden, 2001). After birth, trabecular thickness and trabecular separation increase up to 180 μm and 280 μm, respectively, while trabecular number decreases to 2.9 mm^{-1} (Teng and Herring, 1995). The net result is that the bone volume fraction does not change after birth. The fetal (and older) specimens illustrated that the trabecular bone in the fetal condyle is already strongly oriented

as the obtained degrees of anisotropy were generally above 2.0. It has been suggested (Teng and Herring, 1995) that the orientation of the trabeculae in the posterosuperior direction is simply a reflection of the growth pattern in juvenile pigs. This might also be a likely explanation for the strongly oriented trabecular structure in the mandibular condyles investigated in this study. However, besides the fact that the trabecular orientation might be a reflection of a growth pattern, it has also been demonstrated that mechanical loading of bone during development (Goret-Nicaise, 1981; Burger et al., 1991) might be a determinant of the morphology of the developing trabecular bone.

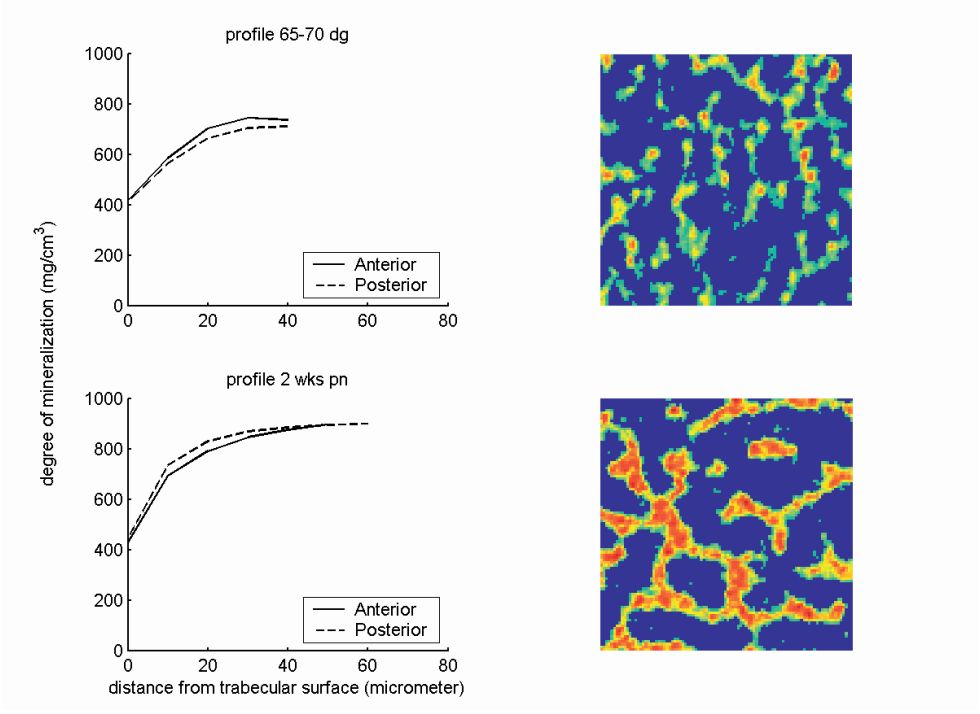

Figure 4. Left: "Peeling" results for the 65-70 days of gestation pig (top) and the 2 weeks postnatal pig (bottom) as a function of the distance from the trabecular surface with zero being the surface. The bone structure in the mandibular condyle of the two weeks old pig had a higher degree of mineralization in the center of the trabeculae. More layers could be peeled off in this stage because of increased trabecular thickness. Right: Two-dimensional cross-section through a section of trabecular bone in the mandibular condyle of the pigs mentioned; top: 65-70 days of gestation; bottom: two weeks postnatal. Both images were composed using the same color-scale (not comparable with Fig. 2) to clarify the differences in mineralization.

We found that the degree of mineralization of fetal trabecular bone increases with gestational age, and that the highest values were found anteriorly (Fig. 3). It is noticeable that anteriorly, the increase in degree of mineralization during development was not accompanied by an increase in bone volume fraction. We suggest that the degree of mineralization does not depend on the bone volume, but on the thickness of the trabeculae as the highly mineralized centers of trabeculae are getting larger with age (Fig. 4). The fact that mineralization increases from the surface of the trabeculae towards their centers, indicates that bone remodeling in trabecular bone takes place at the surface of trabeculae. Therefore, the bone in the centers of trabeculae is older than that on the surface and consequently more highly and more maturely mineralized. The observed distribution of mineralization in individual trabeculae is consistent with observations in the condyles of the distal femur of mature rabbits (Morgan et al., 2002; Bourne and van der Meulen, 2004), obtained with a similar peeling algorithm. We also found that the bone in the centers of the trabeculae became more highly mineralized with age, while the appositional layers had the same degree of mineralization throughout the age range studied. This indicates that besides apposition of new bone material on the surface of trabeculae, the mineralized tissue in their centers still changes and matures (Fig. 4). The net result of this process is an increasing degree of mineralization of the entire trabecular structure. It should be realized that the estimated degree of mineralization would be underrated by partial volume effects if the most superficial layers were taken into account while determining the average degree of mineralization of the structure. As trabecular elements of various thicknesses exist within one volume of interest not all trabecular elements are peeled at the same rate. For instance, when a thin trabecular element is completely peeled, a thicker trabecular element is still in the process. Therefore, the distance from the trabecular surface in Figure 4 should be considered as the average distance from the trabecular surface for the volume of interest.

In conclusion, investigating the changes in the trabecular bone of the developing mandibular condyle with microCT revealed regional differences concerning the trabecular architecture. The degree and distribution of mineralization on the other hand seemed to be quite independent of location and did not coincide with bone volume (anteriorly), but more with the trabecular thickness. A gradient in the degree of mineralization was observed between the centers of individual trabeculae and their outer surfaces, indicating bone growth by apposition. With age, the centers became more highly mineralized and larger and thus clearly suggesting a relationship between trabecular thickness and degree of mineralization.

CHAPTER 4

ARCHITECTURE AND MINERALIZATION OF DEVELOPING CORTICAL AND TRABECULAR BONE OF THE MANDIBLE

Abstract

Ossification of the presumptive trabecular bone in the mandibular condyle and presumptive compact cortical bone in the mandibular corpus of the pig mandible was investigated during development using micro-computed tomography (microCT). Both three-dimensional architecture and mineralization characteristics were assessed from ten pigs of different developmental ages. In the condyle, increases in trabecular thickness and separation and a decrease in trabecular number led to an unchanged bone volume fraction. A conversion from rod-like into plate-like trabeculae was observed. Bone volume and trabecular thickness were always higher in the corpus, where an increase in bone volume fraction was caused by an increase in trabecular thickness and a decrease in separation. A transition from a plate-like structure into a more compact structure took place. Average degree of mineralization in condyle and corpus increased with age. In the corpus the degrees of mineralization were higher than in the condyle. The differences between condyle and corpus and changes with age could be explained by differences in distribution of mineralization within trabecular elements. Generally, degrees of mineralization increased from the surface towards the centers of trabecular elements, indicating growth of trabecular elements by surface apposition of new mineral.

Introduction

Ossification of bone during prenatal development comprises two different mechanisms. Chondral ossification is a process in which an initial mesenchymal condensation converts into bone through an embryonic cartilage intermediate. During desmal ossification the mesenchyme is transformed directly into bone. Both processes are present in the developing mandible, chondral ossification giving rise to the condyle and symphyseal region of the mandible, and desmal ossification being responsible for the development of the corpus. Regardless of its origin, all bone develops from an initial open structure into either a dense compact (cortical) bone structure or a trabecular bone structure (Leeson and Leeson, 1970; Cadet et al., 2003). It is presumed that the regulation mechanisms of trabecular and compact bone development are similar (Tanck et al., 2004).

The mandible is among the first bones in the body to ossify during fetal development (Hodges, 1953), thus providing the opportunity to study the development of the bone at early fetal stages. The gross development of bony regions of the mandible during fetal life has been subject to investigation (Goret-Nicaise and Dhem, 1984; Lee et al., 2001; Radlanski et al., 2003). These studies, however, have described mostly qualitative observations and did not treat the quantitative description of the developing bone structure in terms of architecture and mineralization. Moreover, they have not differentiated between the compact and trabecular bone structure. Therefore, the resemblance of their developmental pathways remains unknown and is thus the subject of this study. Knowledge of the development of these early bone structures and their similarities and differences augments the basic understanding of normal compact and trabecular bone formation.

Recently, microCT has been established as an accurate and powerful tool to determine three-dimensional architectural parameters of young and adult trabecular bone in a non-destructive manner (Rüegsegger et al., 1996; Müller et al., 1998). It has been proven applicable to investigate the changes in trabecular architecture during postnatal development and aging (Ding, 2000; Nafei et al., 2000b; Tanck et al., 2001). Furthermore, it has been recently demonstrated that commercial microCT systems are not only capable of describing the architectural, but also the physical properties of bone like the degree and distribution of mineralization down to the level of individual trabeculae (Mulder et al., 2004; 2005). Therefore, in the present study, microCT was used to analyze mandibles from ten pig specimens of different developmental ages. It was applied to investigate the architectural and

mineralization properties of developing trabecular (condyle) and cortical bone (corpus) concurrently.

Material and methods

Samples

The mandibles from ten pigs (standard Dutch commercial hybrid race) of different developmental ages were used in this study. Included were eight fetuses with an estimated age of 40-45, 45-50, 50-55, 55-60, 65-70, 70-75, 82-87, and 95-100 days of gestation, obtained from sows in a commercial slaughterhouse. Fetal age was estimated from the mean weight of the litter, using growth curves (Evans and Sack, 1973). Furthermore, one newborn (112-115 days post conception) and one two weeks old (130 days post conception) piglet, obtained from the experimental farm of the Faculty of Veterinary Medicine in Utrecht, the Netherlands were used. They were euthanized by an intravenous overdose of ketamine (Narcetan) after premedication. The specimens were obtained from other experiments that were approved by the Committee for Animal Experimentation of the Faculty of Veterinary Medicine, Utrecht, the Netherlands. They were stored at -20°C prior to assessment.

The mandibles were harvested by dissection and cut in half at the symphyseal region. No attempt was made at removing all the soft tissue. Older specimens were divided into smaller sections in order to be able to analyze all specimens with the same resolution, which is limited by the diameter of the microCT specimen holders.

MicroCT

Three-dimensional, high resolution reconstructions of the bone of the specimens were obtained by using a microCT system (μCT 40, Scanco Medical AG., Bassersdorf, Switzerland). The hemi-mandibles were mounted in cylindrical specimen holders (polyetherimide, 20 mm outer diameter, wall thickness: 1.5 mm) and secured with synthetic foam. The mandibular specimens were completely submerged in 70% ethanol. The scans yielded an isotropic spatial resolution of 10 μm. A 45 kV peak voltage X-ray beam was used, which corresponds to an effective energy of approximately 24 keV. The microCT system was equipped with an aluminum filter and a correction algorithm, which reduced the beam hardening artifacts sufficiently to enable quantitative measurements of the degree and

distribution of mineralization of developing bone (Mulder et al., 2004). The computed linear attenuation coefficient in each volume element (voxel) was stored in an attenuation map and represented by a grey value in a three-dimensional reconstruction. This attenuation coefficient can be considered to be proportional to the local degree of mineralization (Nuzzo et al., 2002).

Architecture

The architecture and degree of mineralization of the bone specimens were determined in volumes of interest that were built up out of 10 x 10 x 10 μm^3 voxels and segmented using an adaptive threshold, which was visually checked. In a segmented reconstruction every voxel with a linear attenuation value below the threshold (assumingly representing soft tissue or background) was made transparent and voxels above this threshold (representing bone) were made opaque.

The volumes of interest were chosen at six different locations in the mandibular corpus; three regions, from anterior to posterior on the buccal side and three more on the lingual side. They were chosen in regions of presumptive cortical bone. In the condyle four volumes of interest were chosen that were located anteroinferiorly, anterosuperiorly, posteroinferiorly, and posterosuperiorly. The data from the selected regions of the corpus and condyle were averaged to obtain values representative for the entire corpus and condyle.

To quantify the changes in architecture of the bone during development, several bone architectural parameters (BV/TV: bone volume fraction, Tb.N: trabecular number, Tb.Th: trabecular thickness, Tb.Sp: trabecular separation, Conn.D: connectivity density, SMI: structure model index, DA: degree of anisotropy) were calculated (Software Revision 3.2, Scanco Medical AG).

Degree and distribution of mineralization

The degree of mineralization was estimated from the attenuation values in the portion of the reconstructed sample that was characterized as bone. The previously determined threshold to separate bone from background was applied. For this analysis, the voxels exceeding the threshold kept their original grey value. The outermost voxel layer characterized as bone was disregarded as this layer is likely to be corrupted by partial volume effects. The degree of mineralization was estimated by comparing the linear attenuation coefficient with reference measurements obtained from a series of solutions with different concentration of the mineral K_2HPO_4 (Mulder et al., 2004). The distribution of mineralization within the structural elements of the bone in the condyle and corpus was determined using a so-called peeling

algorithm (Mulder et al., 2005). By determining the degree of mineralization in voxel layers that were consecutively peeled from the surface of the reconstructed bone structure, a relationship between the degree of mineralization and the distance from the trabecular surface was established. The average degree of mineralization was estimated for the consecutive layers using the method mentioned.

Statistics

Regression analysis was applied by best fit of the obtained results for the architectural and mineralization parameters. This yielded for the condyle a linear regression and for the curvilinear results of the corpus a second-degree polynomial regression. Statistical analysis was performed in SPSS (11.5.1 software SPSS Inc.). A p-value of less than 0.05 was considered statistically significant.

Results

When assessing the gross anatomical changes that occurred during the development of the pig mandible (Fig. 1), it was calculated that the fetal pig mandible roughly increased 0.8 mm in length per day. During this growth a porous type of cortex developed in the area of the mandibular corpus. In other regions, for instance the condyle, the development of apparent cortical bone was not observed.

Architecture

During the development of the mandibular condyle, there was a marked increase in trabecular thickness and an increase in trabecular separation in case of the trabecular bone (Fig. 2). Also, in the mandibular corpus the presumptive cortical bone underwent trabecular thickening, which ultimately led to coalescence of trabecular elements into a highly porous compact-like bone (Fig. 2).

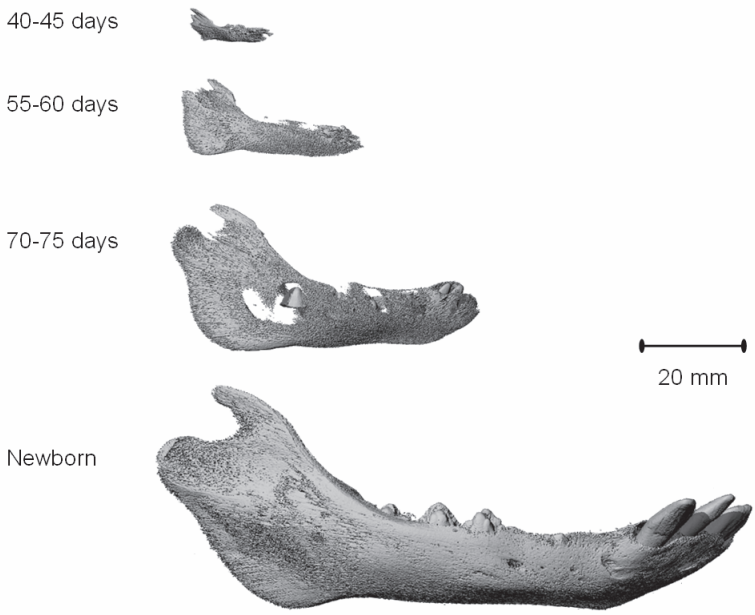

Figure 1. Three-dimensional reconstruction of the right mandible of pigs of different gestational ages. The specimens are 40-45, 55-60, 70-75 days of age, and a newborn (approximately 115 days) specimen. Note the absence of mineralized trabecular tissue in the mandibular condyle of the younger stages, which is thus not visible in these reconstructions.

Quantitative changes in the presumptive trabecular (condyle) and cortical bone (corpus) have been summarized in figure 3. The amount of trabecular bone in the mandibular condyle, expressed by the bone volume fraction (BV/TV), did not increase significantly over the investigated age range. On the other hand, there was a significant drop in trabecular number (Tb.N) (R = -0.86; $P < 0.05$) and a significant increase in trabecular thickness (Tb.Th) (R = 0.92; $P < 0.01$) and trabecular separation (Tb.Sp) (R = 0.90; $P < 0.05$).

A change from rod-like into plate-like trabeculae was expressed by a significant drop in the structure model index (SMI) during development (R = -0.92; $P < 0.01$). Furthermore, the number of connections (Conn.D) between trabecular elements in the condyle decreased significantly (R = -0.94; $P < 0.01$). The presumptive trabecular bone in the condyle was highly oriented with degrees of anisotropy (DA) generally above two, which did not change over the investigated age range.

As opposed to the presumptive trabecular bone in the condyle, the presumptive cortical bone in the corpus did show a significant increase in BV/TV ($R = 0.95$; $P < 0.001$). On the other hand, no changes were observed concerning Tb.N. There was, however, a significant increase in Tb.Th ($R = 0.97$; $P < 0.001$) and a decrease in Tb.Sp ($R = 0.92$; $P < 0.01$). The average trabecular thickness increased by 1.1 micrometer per day. The SMI showed a significant decrease ($R = 0.99$; $P < 0.001$) with developmental age with values reaching well below zero. In the early developmental stages more connections were established between trabecular elements. Later on in the development, Conn.D decreased again ($R = 0.91$, $P < 0.01$). Just like the presumptive trabecular bone of the condyle, the presumptive cortical bone of the corpus showed a high orientation throughout the developmental period examined, but no change in this orientation were observed.

Degree and distribution of mineralization

A clear increase in the degree of mineralization of the trabecular elements with age in the mandibular condyle was evident (Fig. 2). Furthermore, there was a marked gradient in mineralization, increasing from the surface of the trabecular elements towards their centers. The average degree of mineralization (DMB) of both the condyle and corpus increased significantly with developmental age (condyle: $R = 0.91$; $P < 0.05$; corpus: $R = 0.90$, $P < 0.01$) (Fig. 3; bottom right panel). In the developing corpus the degree of mineralization was higher than in the condyle.

In the trabecular elements the degree of mineralization increased from their surfaces towards their centers. This was the case for both the condyle and the corpus (Fig. 4). The degree of mineralization in the center of the trabecular elements of the corpus was higher than in the trabecular elements of the condyle. The degree of mineralization in the surface of the trabecular elements was similar in both regions. With increasing developmental age the gradient in the degree of mineralization in the condyle became steeper. Besides this, a relatively larger constant region of higher mineralized bone material was present in the centers of the trabecular elements of the condyle of older specimens.

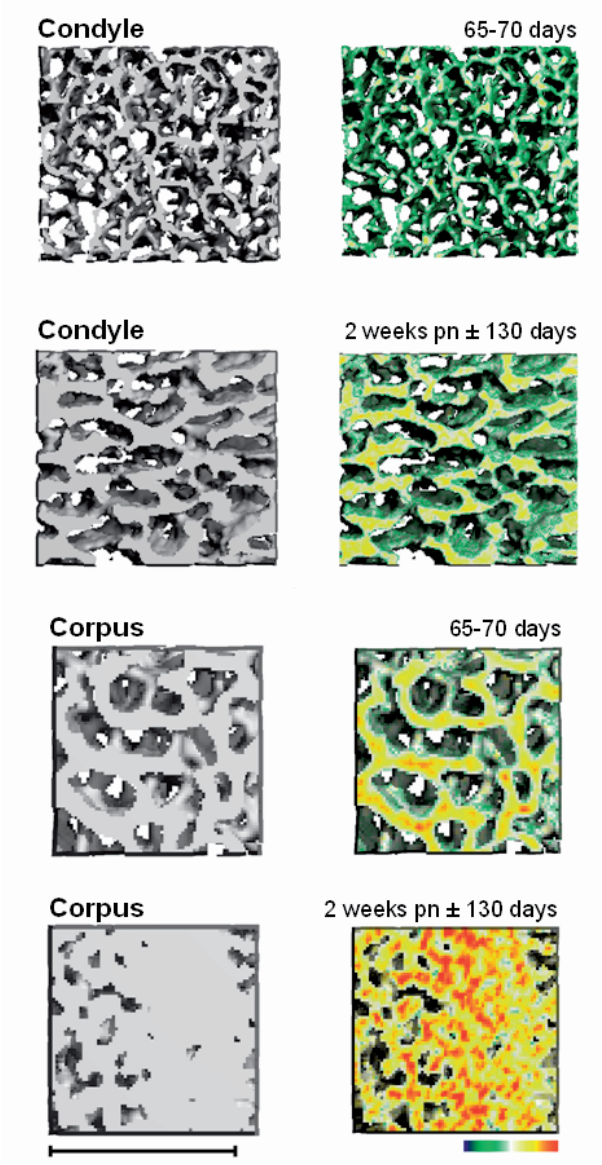

Figure 2. Left: A number of reconstructed volumes of interest from the corpus (middle region on buccal side) and condyle (posterior) from a 65-70 days old specimen and from a two week old specimen to illustrate qualitatively the development of the architecture with age. Increasing bone volume fraction could be clearly observed in both the corpus and condyle, although there was no significant increase in the condyle (Fig. 3). Note the coalesced trabecular elements in the corpus. Right: The same volumes of interest, but now the original attenuation coefficients of the trabecular elements are shown. An increase in the degree of mineralization could be qualitatively observed as well as a spatial inhomogeneous distribution of the mineralization with the centers of the trabecular elements being more mineralized than their surfaces. Bar: 1.0 mm. Color-scale: Increasing degree of mineralization from blue to red.

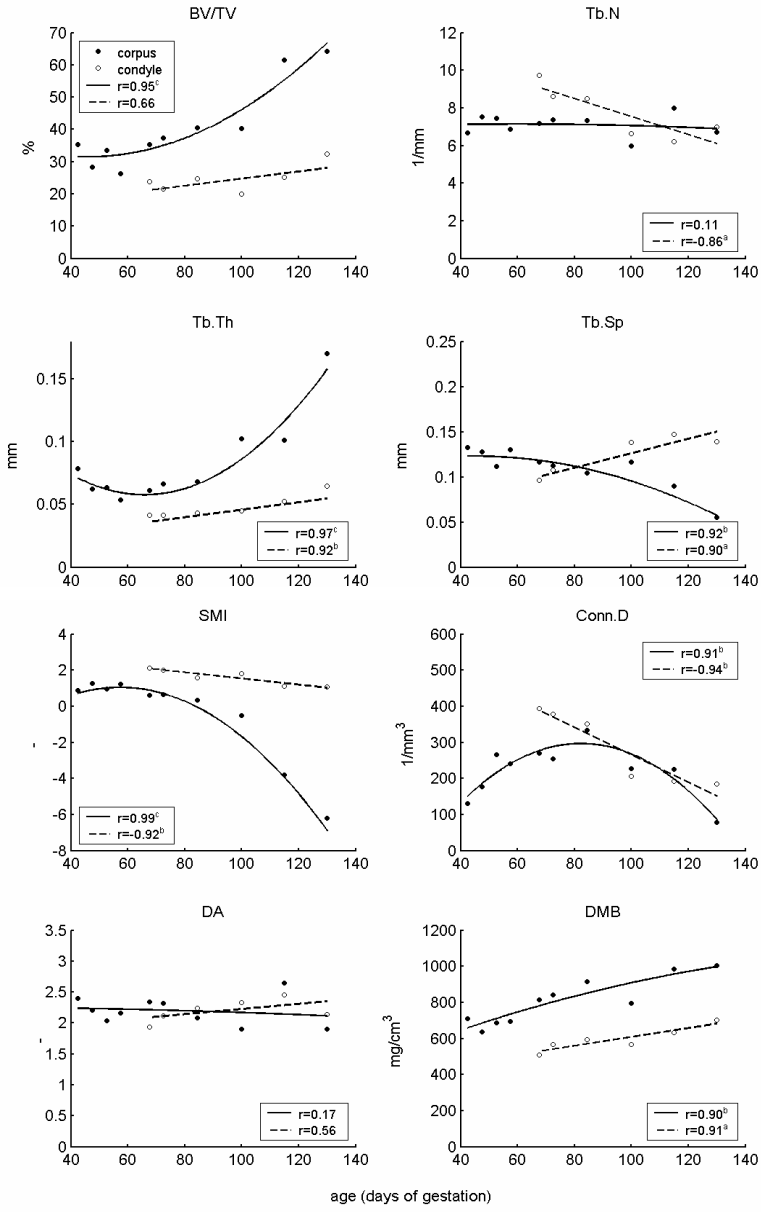

Figure 3. Results of all the investigated parameters in this study plotted against age. Closed circles: values for the corpus. Open circles: values for the condyle. BV/TV: bone volume fraction; Tb.N: trabecular number; Tb.Th: trabecular thickness; Tb.Sp: trabecular separation; SMI: structure model index; Conn.D: connectivity density; DA: degree of anisotropy; DMB: degree of mineralization of bone. Solid line: second-degree polynomial regression for corpus data points. Dashed line: linear regression for condyle data points. The significance of the r-values of the regression is indicated as follows: [a] $P < 0.05$; [b] $P < 0.01$; [c] $P < 0.001$. Values for the condyles of the youngest specimens are absent, due to absence of a mineralized trabecular structure in these specimens.

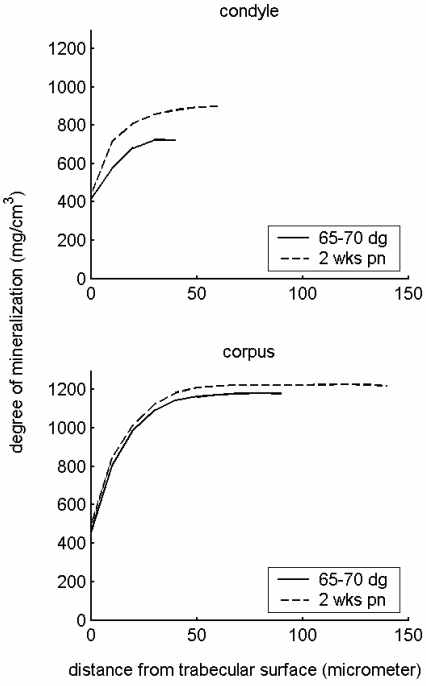

Figure 4. Distribution of the degree of mineralization within trabecular elements from a 65-70 days old specimen and from a two week old specimen as a function of the distance from the surface of the trabecular elements. With increasing developmental age a steeper gradient in the degree of mineralization from the surface to the center was observed in the condyle (top figure). Besides this, a relatively larger "constant" region of higher mineralized bone was present in the centers of the trabecular elements of the condyle of older specimens. These two phenomena cause the increase in the average degree of mineralization with developmental age. For the corpus, only the latter was present (bottom figure).

Discussion

Although both the presumptive cortical bone in the corpus and the presumptive trabecular bone in the condyle had initially a similar trabecular appearance during development, the current study shows that there is a considerable difference in development between the two. The bone volume fraction of the corpus increased significantly with age with values up to approximately 70%. In the condylar bone, where no significant increase with age was observed, the bone volume fraction was much less. It is known that the bone volume fraction

in adult compact bone can reach values as high as 95%; often referred to as a porosity of 5% (Wachter et al., 2001; Cooper et al., 2004).

Architecture

The increase in bone volume fraction in the corpus could be mainly attributed to an increasing trabecular thickness and to a decrease in trabecular separation, while there was no change in trabecular number (Fig. 3). Despite the increase in trabecular thickness with age in the condyle, no change in bone volume fraction was observed. This could be explained by the decrease in trabecular number and the increase in their separation, which counteracts the effect of the increasing trabecular thickness.

The presumptive trabecular bone in the mandibular condyle displayed an ongoing change from a rod-like structure towards a more plate-like one as was characterized by a significant decrease in the structure model index. The presumptive cortical bone in the corpus showed a more plate-like structure from the beginning and the structure model index values for this region decreased sharply towards values well below zero with age. The negative values of the structure model index indicate a very compact bone structure. Normally, the structure model index varies between the values 0 for perfect plates and 3 for perfect rods. However, values up to 4 are also possible, indicating spherically shaped structures. Negative values can come from isolated marrow spaces (Hildebrand and Rüegsegger, 1997). When bone is getting more compact, these spaces might increase in number.

The significant decrease in connectivity density of the presumptive trabecular bone in the condyle is most probably caused by the decreasing number of trabecular elements within the chosen volume of interest. During the earlier developmental stages in the corpus, an increase in the number of connections was established, while in the later stages, a decrease was observed. This decrease could be caused by the fusion of rod-like trabecular elements into more plate-like elements and filling up of perforations in plates. The degree of anisotropy in both investigated structures remained unchanged, but was relatively high (generally values above 2) as compared to values that were found in juvenile pigs (Teng and Herring, 1995). Both in the condyle and corpus the main orientation of the trabecular elements was anteroposteriorly. This is also the direction in which the condyle grows in fetal pigs (Wissmer, 1927). Also in the corpus, where ossification starts in a single ossification centre located near the future mental foramen, bone grows in an anterior, upward, and posterior direction (Radlanski et al., 2003). This preferred orientation is during later development and

adulthood still reflected in the orientation of the Haversian canal system in the mandibular corpus (van Eijden, 2000).

However, besides growth being responsible for the obtained results, it has also been demonstrated that mechanical loading of bone that occurs during development influences bone morphology and that the structure present is optimal to resist the loading on the bone structures, which also occurs *in utero* (Goret-Nicaise, 1981; Burger et al., 1991). It has furthermore been suggested that, during adulthood, mechanical loading is also responsible for observed bone morphology in the mandibular condyles of humans (Giesen and van Eijden, 2000; van Ruijven et al., 2002).

Onset of mechanical loading of the mandible might be reflected in the curves of the bone volume fraction, trabecular thickness, structure model index, connectivity density, and to a lesser extent the trabecular separation of the presumptive cortical bone in the mandibular corpus, as they show a clear curvilinear character during development. During the earlier ages little change was found in these parameters, while at ages around 70 days of gestation they exhibited sharp increases or decreases. This is also the age at which the presumptive trabecular bone in the mandibular condyle starts to develop. It has been shown that at a corresponding developmental age in the human fetus repetitive jaw movements as well as suckling and swallowing reflexes appear, suggesting functional loading of the mandible by developing muscles (de Vries et al., 1985).

Degree and distribution of mineralization

The degree of mineralization was quantified by comparing linear attenuation values found in bone specimens with that of homogeneous K_2HPO_4 solutions. K_2HPO_4 has exactly the same absorption properties as hydroxyapatite (Nuzzo et al., 2002), the main constituent of mineralized bone in adults, but also in fetal bone hydroxyapatite is already abundantly present (Nuzzo et al., 2003; Meneghini et al., 2003). Increasing average degrees of mineralization with developmental age, observed in both the presumptive trabecular bone of the condyle and the presumptive cortical bone of the corpus (Fig. 3), might be based on several phenomena. Firstly, in the condyle minerals in the trabecular centers apparently continue to mature showing an increasing degree of mineralization (Fig. 4 top panel). This more mineralized central region also gets larger with age as the average trabecular thickness increases (Fig. 3 and 4) thus contributing to a higher average value of the degree of mineralization of the structure. This latter phenomenon seems to be the dominant contributor to the observed increase in average degree of mineralization observed in the corpus, as no difference in degree

of mineralization was found between the centers of younger and older specimens (Fig. 4 bottom panel). Secondly, the bone surface to bone volume ratio decreases with developmental age in both the condyle and corpus (data not shown). Therefore, poorly mineralized tissue at the surface of bone elements contributes less to the overall degree of mineralization at later stages. Similarly, the higher degree of mineralization in the corpus compared to the condyle is most probably caused by the higher degrees of mineralization in the centers of the trabecular elements as well as by a markedly larger center region, and the lower bone surface to bone volume ratio in the corpus.

The values for the average degree of mineralization found in this study were low compared to values found in other studies that focused on healthy adult bone and adult bone suffering from disease like osteoporosis (Meunier and Boivin, 1997; Boivin and Meunier, 2002; Follet et al., 2004). In the papers mentioned, the average values for the degree of mineralization were generally higher than 1100 mg/cm^3, with maximum values going beyond 1600 mg/cm^3. This could indicate that the mineralized tissue in the developing skeletal structures in the fetus is fairly young mineral tissue that still has to undergo maturation. The lower degrees of mineralization could also suggest that the bone in these developing structures is subjected to extensive remodeling and that, therefore, the mineralized tissue is not long-lasting and constantly renewed and replaced by younger and less mineralized tissue.

In can be concluded from this study that marked changes in architectural as well as in mineralization properties of bone occur during its development in the mandible of pigs. Moreover, differences between different bone structures within the mandible were evident. Bone in the condyle develops into a spongy trabecular structure whereas the bone in the corpus starts out as a trabecular-like structure where gradually the trabecular elements coalesce to transform into compact bone. Considerable changes in architectural parameters of bone in the corpus at the age of approximately 70 days of gestation and the appearance of trabecular bone in the condyle at this age are assumed to relate to the onset of functional loading of the mandible by developing masticatory muscles. Considerable changes in the pace of mineralization at this age were not found. It seems reasonable to conclude that the increase in dimensions of the trabecular elements occurs via apposition of new bone material at their surfaces which is reflected in the differences in degree of mineralization observed between their surface and their centers.

CHAPTER 5

REGIONAL DIFFERENCES IN ARCHITECTURE AND MINERALIZATION OF DEVELOPING MANDIBULAR BONE

Abstract

The goal of this study was to investigate the mutual relationship between architecture and mineralization during early development of the pig mandible. These factors are considered to define the balance between the requirements for bone growth on the one hand and for load bearing on the other. Architecture and mineralization were examined using microCT, whereas the mineral composition was assessed spectrophotometrically in groups of fetal and newborn pigs. The development of the condyle coincided with a reorganization of bone elements without an increase in bone volume fraction, but with an increase in mineralization and a change in mineral composition. In the corpus the bone volume fraction and mineralization increased simultaneously with a restructuring of the bone elements and a change in mineral composition. The growth of the condyle was reflected by regional differences in architecture and mineralization. The anterior and inferior regions were characterized by a more dense bone structure and a higher mineralization as compared to posterior and superior regions, respectively. In the corpus growth was mainly indicated by differences between buccal and lingual plates as well as between anterior, middle, and posterior regions characterized by a more compact structure and higher mineralization in the lingual and middle regions. In conclusion, the architecture and mineralization in the condyle and corpus started to deviate early during development towards their destiny as trabecular and compact bone, respectively. These results were compatible with those obtained with mineral composition analysis. Regional differences within condyle and corpus reflected known developmental growth directions.

Introduction

The mineral component is a main constituent of bone tissue and is important in that it confers much of the hardness and rigidity of bone. Therefore, it is a major determinant of its mechanical properties. Studies have been performed using ashed bone samples to investigate the mineral composition of cortical (Biltz and Pellegrino, 1969; Pugliarello et al., 1973; Driessens et al., 1986; Aerssens et al., 1998) as well as trabecular bone (Gong et al., 1964; Dyson and Whitehouse, 1968; Wong et al., 1986; Aerssens et al., 1997; van der Harst et al., 2004) from a wide variety of species and anatomical locations. Generally, this concerned bone in a growing, adult or aging state. In a few studies changes of bone mineral composition during fetal development have been analyzed (Dickerson, 1962a,b; Birckbeck and Roberts, 1971; Bonar et al., 1983; Grynpas et al., 1984; Oyedepo and Henshaw, 1997; Roschger et al., 2001). Of these studies only Dickerson examined differences between presumptive cortical and trabecular bone using ashed samples (Dickerson, 1962a,b). However, the studies mentioned above were all limited to mineral composition determination alone and were not related to bone architecture or its degree of mineralization, which contribute considerably to the mechanical strength of bone tissue (Boskey, 2002).

Most long bones develop endochondrally, whereas many bones of the calvarium and face develop through intramembranous ossification. In the developing mandible, however, both processes can be found, i.e. endochondral ossification gives rise to the condyle, and intramembranous ossification is responsible for the development of the corpus. The mandible thus appears to be a suitable model by which the differences in bone structure, mineralization, and mineral composition between these two regions can be studied (Hall, 1982; Atchley and Hall, 1991). Besides, the mandible is among the first bones in the body to ossify during fetal development (Hodges, 1953), thus providing the opportunity to study the development of bone at early fetal stages.

Earlier studies have shown that the condyle grows mainly in a superoposterior direction and that the ossification of the corpus commences from the mandibular primary growth centre in an anterior, posterior, and lateral direction. Furthermore, an increase in width and a change in shape of the corpus have been put forward (Wissmer, 1927; Goret-Nicaise and Dhem, 1984; Lee et al., 2001; Radlanski et al., 2002; Radlanski, 2003). These studies, however, do not give information on how the growth is reflected in architecture and mineralization of the bone tissue in multiple regions within condyle and corpus. In previous

studies both the architecture and the degree of mineralization have been demonstrated to change in the developing mandibular condyle and corpus (Mulder et al., 2005; 2006b). Mineral composition analysis was, however, not included and detailed regional differences were not explored.

Therefore, in the present study multiple regions were examined in the condyle and corpus of the pig mandible, thus examining both the trabecular and cortical bone compartments. Architecture, degree of mineralization, and mineral composition measurements were performed in order to be able to better understand the developmental processes of the bone compartment of the mandible and the relationships between the parameters mentioned. Regional differences were expected as bone tissue in different regions of the developing condyle and corpus has a different developmental age and older bone has had more time to mature and mineralize. In the condyle, inferior and anterior regions are believed to contain the oldest bone tissue. In the corpus, the bone in the centre region is expected to be more mature than anterior and posterior ones. Multiple specimens were investigated per age group and architectural parameters and degree of mineralization were investigated using microCT. To assess the mineral composition, the specimens were ashed and examined for their calcium and phosphate content.

Material and methods

Samples

The mandibular condyle and corpus from four fetal and four newborn pigs (standard Dutch commercial hybrid race) were examined. The fetal specimens (estimated age: 75 days of gestation, mean weight: 375 g) were obtained from slaughtered sows in a commercial slaughterhouse and their age was estimated from the mean weight of the litter using growth curves (Evans and Sack, 1973). The newborn specimens (approximately 112-115 days post conception, mean weight: 1351 g) were acquired from the experimental farm of the Faculty of Veterinary Medicine in Utrecht, the Netherlands, and were euthanized by an intravenous overdose of ketamine (Narcetan) after premedication. These specimens were obtained from other experiments that had been approved by the Committee for Animal Experimentation of the Faculty of Veterinary Medicine, Utrecht, the Netherlands. The specimens were stored at -20°C prior to assessment.

The mandibles were dissected from the heads and cut in half at the symphyseal region. The right halves were prepared for analysis (Fig. 1). The condyle was separated with a frontal cut at the incisura mandibulae and with a horizontal cut at the ramus mandibulae. The corpus was isolated with a cut just behind the canine tooth and behind the last molar. Before further processing, teeth were removed by dissection and the samples were disposed of adhering soft tissue.

Architecture and degree of mineralization

Three-dimensional reconstructions of the bony structures of condyle and corpus were obtained by using a high-resolution microCT system (μCT 40; Scanco Medical AG., Bassersdorf, Switzerland). The specimens were mounted in cylindrical specimen holders (polyetherimide; outer diameter: 20 mm, wall thickness: 1.5 mm) and secured with synthetic foam. The scans yielded an isotropic spatial resolution of 10 μm. A 45 kV peak-voltage X-ray beam was used, which corresponds to an effective energy of approximately 24 keV. The microCT was equipped with an aluminum filter and a correction algorithm that reduced the beam hardening artifacts sufficiently to enable quantitative measurements of the degree and distribution of mineralization of developing bone (Mulder et al., 2004). The computed attenuation coefficient for each voxel was represented by a grey value in the reconstruction.

To determine the architecture and degree of mineralization, volumes of interest (approximately 1 mm^3), built up out of 10 x 10 x 10 μm^3 voxels, were defined in different regions. These volumes of interest were not necessarily cubical. In the condyle a total of six volumes were defined, i.e. inferiorly and superiorly, anteriorly and posteriorly, medially and laterally (Fig. 1). The corpus was virtually divided into three equal parts: anterior, middle, and posterior. In the middle of each of these parts, volumes of interest were selected in the areas where presumptive compact bone will form, i.e. lingually, buccally, and apically (Fig. 1). Hence, a total of nine volumes of interest were selected in the corpus. In data analyses, different volumes of interest were combined to gain a more complete representation of the region. The anterior region was characterized by combining the lingual, buccal, and apical volumes. The same holds true for the middle and posterior regions. The volumes selected on the lingual side in the anterior, middle, and posterior regions were combined to represent the lingual region of the mandible. Similar combinations were applied to the buccal and apical regions.

The reconstructions were segmented using an adaptive method, in which the 3D grey value reconstruction of a volume of interest was segmented at multiple levels. The threshold, where the bone volume fraction changed the least, was selected and visually checked (Ding et al., 1999). It was assured that the threshold corresponded to the minimum between the background and bone tissue peak in the grey value histogram. By repeating every scan projection four times and averaging these, the signal to noise ratio was improved substantially and the determination of the suitable threshold was facilitated. In a segmented image every voxel with a linear attenuation value below the threshold (assumingly representing soft tissue or background) was made transparent and voxels above this threshold (representing bone) were made opaque. From these segmented images, several bone architectural parameters (BV/TV: bone volume fraction, Tb.N: trabecular number, Tb.Th: trabecular thickness, Tb.Sp: trabecular separation, SMI: structure model index) were calculated (Software Revision 3.2, Scanco Medical AG). SMI was analyzed to quantify the structural appearance of trabecular bone. Normally, the SMI varies between the value 0, for perfect plates, and 3, for perfect rods. Negative values can come from isolated marrow spaces (Hildebrand and Rüegsegger, 1997). When the bone is getting more compact, these spaces might increase in number.

For determination of the degree of mineralization, voxels with a value above the threshold kept their original grey value that can be considered proportional to the local degree of mineralization (Nuzzo et al., 2003). The outermost voxel layer characterized as bone was disregarded as this layer is likely to be corrupted by partial volume effects. The degree of mineralization was quantified by comparing the average linear attenuation coefficient of the segmented volume of interest with reference measurements of a series of solutions with different concentrations of the mineral K_2HPO_4 (Mulder et al., 2004). The degree of mineralization is expressed as the mass of mineralized tissue (mg) relative to its volume (cm^3) in a volume of interest after thresholding has been performed.

Mineral composition

After microCT analysis, the specimens were defatted in a 1:1 mixture of acetone and alcohol for 24 hours and subsequently rinsed in demineralized water. After drying for an hour at approximately 105ºC in an oven, the dry weight of the specimens was determined. The fat-free, dry samples were placed in crucibles and ashed overnight at 620ºC in a muffle furnace, the ash was weighed, dissolved in 12M hydrochloric acid, and this was subsequently diluted. Calcium content was measured by flame atomic absorption spectrophotometry (Perkin Elmer, Wellesley, USA) and the phosphate content was analyzed using the method of Chen (Chen et

al., 1956). Both the calcium and phosphate content were expressed by their relative weight (%) with respect to that of the ash weight. Furthermore, ash fraction (ash weight divided by dry weight) and the Ca/P molar ratio were calculated.

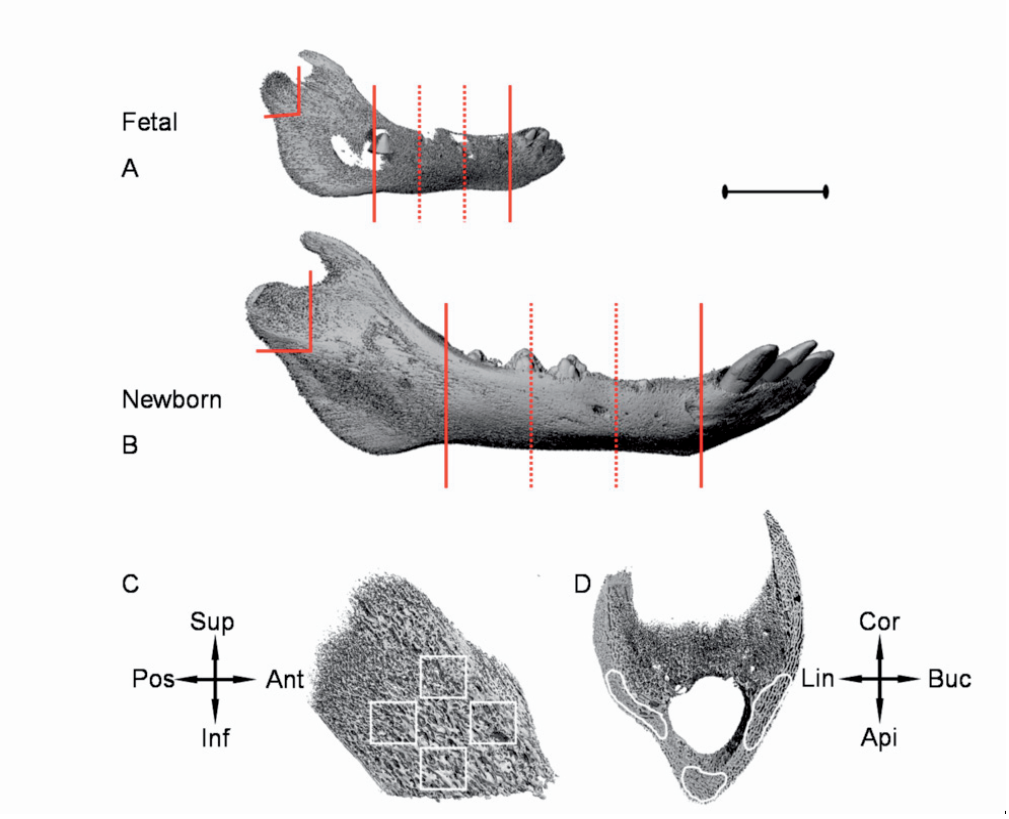

Figure 1. Regions defined in the developing mandible. A: 3D microCT reconstructions of a fetal mandible (70-75 days). B: Newborn mandible. Solid red lines: physical cuts to isolate the condyle and corpus from the specimens. Dotted red lines: separation between anterior, middle, and posterior regions in the corpus. Note that the teeth present in these reconstructions were removed before the analyzing scan was performed. Bar: 20 mm. C: Sagittal cross-section through the condyle. D: Frontal section of the corpus. White enclosures: volumes of interest (approximately 1 mm^3). Not shown are the medial and lateral regions that were selected in the condyle.

Statistics

All measured parameters were expressed as mean ± SD. Statistical analysis of the data was performed using the software package SPSS (11.5.1). Differences between parameters measured in fetal and newborn specimens were analyzed using independent-sample t tests. Comparison between different regions selected within the condyle and within the corpus and

also the differences between condyle and corpus of the same age group were tested with paired-sample t tests. A p-value of less than 0.05 was considered statistically significant.

Results

Whole condyle and corpus

The newborn condyle had increased in size and the superior and posterior orientation of the trabecular elements suggests that the expansion of the condyle had mainly occurred in these directions. Furthermore, an evident increase in degree of mineralization could be observed. No subchondral or cortical bone had formed in both the fetal and newborn condylar specimens (Fig. 2).

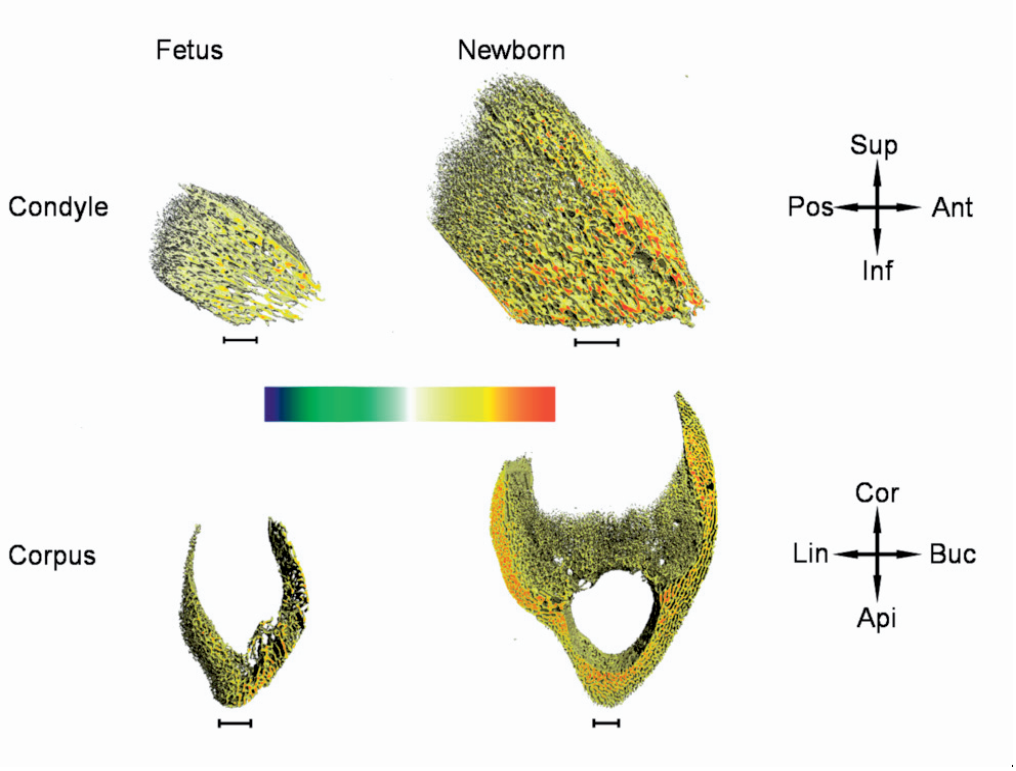

Figure 2. Mineralization in developing mandibular bone. 3D microCT reconstructions of fetal (top-left) and newborn condyles (top-right) and of fetal (bottom-left) and newborn corpus (bottom-right). Color bar: degree of mineralization, increasing from blue to red. Bar: 1.0 mm. Sup: superior, Inf: inferior, Ant: anterior, Pos: posterior, Lin: lingual, Buc: buccal, Api: apical, Cor: coronal.

Development coincided with a reorganization of bone elements of the presumptive trabecular structure without an increase of the bone volume fraction itself (Table 1). There was, however, an increase in trabecular thickness and separation with a concurring decrease in trabecular number.

Whereas in the fetal corpus no trace of alveolar bone was found, in the newborn specimens it had formed between the developing teeth. This also led to a clear confinement of the mandibular canal (Fig. 2). Furthermore, a distinction between the trabecular structure of the alveolar bone and the more compact presumptive cortical bone could be observed. In contrast to the condyle, in the corpus the bone volume fraction did increase together with restructuring of the bone elements towards a more compact structure. This was reflected by an increase in trabecular thickness and trabecular number with a concurrent decrease in trabecular separation and backed by a decrease in structure model index towards negative numbers (Table 1).

Table 1. Architecture and mineralization of the condyle and corpus[a].

		Condyle		Corpus	
		Fetal	Newborn	Fetal	Newborn
BV/TV	(%)	19.3$^{\#}$ (4.8)	16.7$^{\#\#}$ (2.4)	26.9* (6.3)	51.8 (12.4)
Tb.Th	(mm)	0.04*$^{\#}$ (0.01)	0.05$^{\#\#}$ (0.01)	0.05** (0.01)	0.09 (0.01)
Tb.N	(1/mm)	6.7** (0.3)	5.2$^{\#\#}$ (0.3)	7.0* (0.3)	8.1 (0.5)
Tb.Sp	(mm)	0.14** (0.01)	0.19$^{\#\#}$ (0.01)	0.13** (0.01)	0.09 (0.01)
SMI		1.9 (0.5)	1.9$^{\#\#}$ (0.2)	1.5** (0.4)	-1.5 (1.1)
DMB	(mg/cm^3)	665**$^{\#\#}$ (26)	783$^{\#\#}$ (13)	899** (20)	990 (22)
Ash fraction	(%)	39.3** (9.7)	61.7 (4.1)	42.0** (7.3)	60.2 (1.5)
Wt% Ca[b]	(%)	12.5**$^{\#\#}$ (4.1)	30.3$^{\#\#}$ (1.6)	30.9** (2.5)	37.2 (3.3)
Wt% P[b]	(%)	6.1**$^{\#\#}$ (2.0)	14.6$^{\#\#}$ (0.9)	15.5** (1.2)	18.3 (1.7)
Ca/P molar ratio		1.56* (0.02)	1.61 (0.01)	1.54* (0.04)	1.64 (0.03)

[a] Values for architecture and DMB in both condyle and corpus were obtained by averaging the data acquired from the regional volumes of interest. Mean values with standard deviation (in parenthesis).

[b] Weight percentages of calcium and phosphate were determined relative to ash weight.

* = Significant difference between fetal and newborn specimens of the same anatomical location (*$P < 0.05$; ** ($P < 0.01$). $^{\#}$ = Significant difference between condyle and corpus in the same age group ($^{\#}P < 0.05$; $^{\#\#}P < 0.01$). BV/TV: bone volume fraction, Tb.Th: trabecular thickness, Tb.N: trabecular number, Tb.Sp: trabecular separation, SMI: structure model index, DMB: degree of mineralization of bone.

Differences between the fetal condyle and corpus were scarce in terms of the architectural parameters used in this study. When comparing the newborn condyle with the newborn corpus, a divergence of architectural parameters between these two regions evidently took place. The bone volume fraction, trabecular thickness, and number were higher in the corpus than in the condyle. On the other hand, trabecular separation and structure model index were lower.

There was an increase in the degree of mineralization (DMB) with developmental age in both the condyle and corpus (Table 1). The DMB in the corpus in both the fetal and newborn group was higher than in the condyles of the same age.

The ash analysis provided information on ash fraction, the relative amounts of calcium and phosphate, and the molar ratio between these two elements (Table 1). A significant increase in ash fraction took place with developmental age in both the condyle and corpus. The calcium as well as the phosphate content increased significantly from the fetal stage to newborns. In both the fetal and newborn group the calcium and phosphate content was lower in the condyle than it was in the corpus. The Ca/P ratio increased in both the condyle and corpus with developmental age.

Heterogeneity within condyle and corpus

Dissimilarities in architecture were evident when comparing various regions in the condyle with each other (Table 2). In the fetal condyle a higher bone volume fraction and trabecular thickness and a lower structure model index were found anteriorly than posteriorly. These differences were maintained in the newborn condyle. Additionally in the newborn specimens the bone volume fraction and trabecular thickness were found to be higher inferiorly than superiorly and the structure model index was lower inferiorly. Hardly any differences were discerned between lateral and medial parts of the fetal and newborn condyle.

Anteriorly, the condyle was always more highly mineralized than posteriorly (Table 2). No differences in DMB were noted between inferior and superior regions in the fetal group. Though, in the newborn group the inferior regions were more highly mineralized than superiorly. No differences in DMB between the lateral and medial regions were observed irrespective of age.

The presence of plates at the buccal surface of the corpus and to a lesser degree at the inner side of the lingual part of the corpus (transited into the alveolar structure) was evident (Fig. 2). In the fetal corpus (Table 3) buccal regions differed from both the lingual and apical ones. These differences included a lower BV/TV and Tb.Th and a higher SMI on the buccal

side when compared to the lingual and apical regions. In the fetal group, the anterior region displayed a lower BV/TV, Tb.Th, and Tb.N and a higher Tb.Sp and SMI than the middle and posterior regions. When dealing with newborn specimens, nearly the same relationships occurred between buccal vs. lingual and apical. In the newborn group, however, the middle region of the corpus showed a higher BV/TV and Tb.Th and a lower Tb.Sp and SMI than both the anterior and posterior regions.

Table 2. Architecture and degree of mineralization (means and standard deviations) in the different regions of the developing condyle.

	Anterior		Posterior	
	Fetal	Newborn	Fetal	Newborn
BV/TV	22.7$^{\#\#}$ (4.5)	20.0$^{\#}$ (3.5)	12.9 (5.6)	10.8 (1.4)
Tb.Th	0.05*$^{\#\#}$ (0.01)	0.06$^{\#}$ (0.01)	0.03** (0.01)	0.05 (0.01)
Tb.N	6.4* (0.4)	5.1(1.0)	6.7** (0.5)	4.6 (0.4)
Tb.Sp	0.14* (0.01)	0.19 (0.04)	0.14** (0.01)	0.21 (0.02)
SMI	1.6$^{\#\#}$ (0.5)	1.6$^{\#\#}$ (0.2)	2.6 (0.6)	2.4 (0.2)
DMB	682**$^{\#\#}$ (27)	804$^{\#\#}$ (8)	610** (33)	766 (18)
	Inferior		**Superior**	
	Fetal	Newborn	Fetal	Newborn
BV/TV	18.7 (5.4)	23.3$^{\#\#}$ (2.8)	20.1** (5.6)	9.5 (1.2)
Tb.Th	0.04** (0.01)	0.06$^{\#\#}$ (0.01)	0.04 (0.01)	0.04 (0.01)
Tb.N	6.7** (0.3)	4.9 (0.7)	6.3* (0.5)	4.8 (0.6)
Tb.Sp	0.14* (0.01)	0.19 (0.03)	0.14** (0.02)	0.21 (0.03)
SMI	2.0 (0.7)	1.3$^{\#\#}$ (0.1)	1.8 (0.6)	2.4 (0.1)
DMB	664** (36)	808$^{\#\#}$ (19)	666** (26)	749 (9)
	Lateral		**Medial**	
	Fetal	Newborn	Fetal	Newborn
BV/TV	15.5 (6.9)	10.5 (4.3)	20.1 (4.1)	20.9 (1.2)
Tb.Th	0.04 (0.01)	0.04 (0.01)	0.04 (0.01)	0.06 (0.02)
Tb.N	6.7*$^{\#}$ (0.4)	5.8 (0.3)	7.4** (0.4)	5.9 (0.4)
Tb.Sp	0.14*$^{\#}$ (0.01)	0.17 (0.01)	0.12** (0.01)	0.16 (0.01)
SMI	2.3 (0.7)	2.7 (0.4)	1.9 (0.5)	1.7 (1.1)
DMB	654* (60)	754 (12)	669** (28)	804 (40)

* = Significant difference between fetal and newborn specimens while comparing the same anatomical location (*$P < 0.05$; **$P < 0.01$). $^{\#}$ = Significant difference between locations at the same age, i.e. anterior vs. posterior, inferior vs. superior, medial vs. lateral ($^{\#}P < 0.05$; $^{\#\#}P < 0.01$). Mean values with standard deviation (in parenthesis).

Between buccal, lingual, and apical regions in the fetal corpus no differences in DMB were distinguished but it was significantly lower in anterior regions when compared to middle and posterior regions (Table 3). In the newborn group though, the buccal region was significantly less mineralized than lingual and apical regions. The posterior region was significantly less mineralized than anterior and middle regions.

Table 3. Architecture and degree of mineralization (means and standard deviations) in the different regions of the developing corpus[a].

	Buccal		Lingual		Apical	
	Fetal	Newborn	Fetal	Newborn	Fetal	Newborn
BV/TV	19.8*$^{\#\dagger\dagger}$ (6.7)	39.6†† (13.4)	28.6* (3.1)	52.7 (18.2)	32.2** (9.3)	63.1 (8.6)
Tb.Th	0.05$^{\#\#\dagger}$ (0.01)	0.06$^{\#\#\dagger\dagger}$ (0.01)	0.06** (0.01)	0.10 (0.02)	0.06** (0.01)	0.10 (0.01)
Tb.N	6.9** (0.2)	8.8† (0.8)	6.5 (1.1)	7.5 (0.7)	7.5 (0.2)	7.9 (0.5)
Tb.Sp	0.13**†† (0.01)	0.09† (0.01)	0.14* (0.02)	0.09 (0.02)	0.11** (0.01)	0.08 (0.01)
SMI	2.1*$^{\#\dagger}$ (0.5)	0.1$^{\#\dagger\dagger}$ (1.1)	1.4** (0.1)	-2.1 (1.2)	1.2** (0.8)	-2.4 (1.7)
DMB	992 (24)	969$^{\#\dagger}$ (16)	1005 (17)	988 (22)	999 (25)	1014 (36)

	Anterior		Middle		Posterior	
	Fetal	Newborn	Fetal	Newborn	Fetal	Newborn
BV/TV	15.4**$^{\#\#\dagger}$ (3.7)	54.4 (16.9)	34.0* (7.7)	61.8‡ (16.9)	31.2 (8.5)	39.2 (4.8)
Tb.Th	0.04**$^{\#\dagger}$ (0.01)	0.09$^{\#\#\dagger}$ (0.02)	0.06** (0.01)	0.11‡‡ (0.01)	0.06 (0.01)	0.06 (0.01)
Tb.N	6.3**$^{\#\dagger}$ (0.4)	8.0 (0.6)	7.2* (0.3)	8.2 (0.7)	7.4 (0.5)	8.0 (0.7)
Tb.Sp	0.16**$^{\#\dagger}$ (0.02)	0.08† (0.02)	0.12** (0.01)	0.08‡ (0.02)	0.12 (0.01)	0.10 (0.01)
SMI	2.3**$^{\#\#\dagger}$ (0.2)	-1.7 (1.9)	1.1** (0.6)	-3.0‡‡ (1.2)	1.3* (0.6)	0.3 (0.5)
DMB	969*$^{\#\#\dagger\dagger}$ (21)	1005† (11)	1013 (17)	1014‡‡ (41)	1013* (26)	952 (22)

[a] A total of nine volumes of interest were selected in the corpus. Anteriorly, the lingual, buccal, and apical regions were averaged to obtain values for the anterior region and the same holds for the middle and posterior regions. The value for the lingual region was obtained by averaging lingual volumes of interest in the anterior, middle, and posterior regions. The same was done for the buccal and apical regions. Mean values with standard deviation (in parenthesis).

* = Significant difference between fetal and newborn specimens while comparing the same anatomical location (* $P < 0.05$; **$P < 0.01$). # = Significant difference between buccal and lingual location at the same age and between anterior and middle ($^{\#}P < 0.05$; $^{\#\#}P < 0.01$). † = Significant difference between buccal and apical location at the same age and between anterior and posterior. ($^{\dagger}P < 0.05$; $^{\dagger\dagger}P < 0.01$). ‡ = Significant difference between lingual and apical location at the same age and between middle and posterior ($^{\ddagger}P < 0.05$; $^{\ddagger\ddagger}P < 0.01$).

Discussion

To our knowledge, this is the first study in which architectural analysis, mineralization, and mineral composition were simultaneously investigated in developing bone. Additionally, a detailed regional analysis offered information on growth of trabecular and cortical bone elements in the mandible for the first time.

A clear orientation of the trabecular elements in the condyle was evident. In both the fetal and newborn group, this orientation was directed posteriorly and superiorly. This has also been found in earlier studies on the fetal mandibular condyle (Mulder et al., 2005) and on the condyle of juvenile pigs (Teng and Herring, 1995). This orientation of the trabecular elements is presumably a reflection of the growth course in the condyle. A remarkable finding was that, despite growth and changes in architecture, the relative amount of bone (BV/TV) remained constant in the condyle. In the corpus noticeable compaction of the bone structure occurred, which was also backed by changes in the structure model index values. Whereas in the fetal group an equal amount of rod-like and plate-like trabecular elements was present, in the newborn group the bone structure became more compact as characterized by negative values of the structure model index (Mulder et al., 2006b). The orientation of bony elements was mainly upwards and longitudinally, which presumably coincides with the governing growth directions.

A lower degree of mineralization of the condyle with respect to the corpus was found. It suggests that the condyle grows more rapidly and that the turnover of bone material is higher, giving rise to abundant younger bone tissue with a lower degree of mineralization (Dyson and Whitehouse, 1968; Bigi et al., 1997). Another explanation might be the fact that the corpus starts to ossify earlier during development than the condyle and thus contains more mature bone tissue (Mulder et al., 2006b).

The ash fraction in the condyle and corpus was similar in both age groups. In both structures it increased with age. In addition, the relative amount of both calcium and phosphate increased significantly with age. However, in the condyle they were lower than in the corpus. In both the condyle and corpus the increase in calcium was higher than the increase in phosphate as the ratio between them increased. In the condyle and corpus, the increase in degree of mineralization might have been caused by a change into more calcium and phosphate rich minerals, more resembling hydroxyapatite (Ca/P ratio of 1.67) and by a better organization and more dense stacking of the crystals (Grynpas and Holmyard, 1988).

During this process, calcium and phosphate ions might have replaced other extraneous ions like sodium, magnesium, and HPO_4^{2-} ions. Furthermore, an increase in crystal size and perfection may have influenced the degree of mineralization (Grynpas, 1993; Bigi et al., 1997; Fratzl et al., 2004).

The ash fraction value in the newborns closely matches the values found in postnatal and adult specimens of bone of different species (Biltz and Pellegrino, 1969; Wong et al., 1985; Aerssens et al., 1997; van der Harst et al., 2004) and developing cranial bones of humans (Kriewall et al., 1981). The calcium and phosphate content in the newborn corpus approaches the values normally obtained for stoichiometric hydroxyapatite (Dyson, 1968). A similar developmental change in composition has been found in studies concerning human bone development (Dickerson, 1962b; Birckbeck and Roberts, 1971; Oyedepo and Henshaw, 1997). In comparison to other anatomical sites, the mandibular corpus in the developing pig matched developing cortical bone of the humerus excellently with respect to bone mineral composition. The condyle on the other hand exhibited higher values in comparison with epiphyseal bone in both the pig femur and humerus (Dickerson, 1962a).

A significantly lower bone volume fraction and degree of mineralization were noted in the condylar growth regions (posterior and superior) as compared to opposite regions (anterior and inferior). The higher bone volume fractions in the latter two regions were most likely caused by a higher thickness of the trabecular elements, whereas no regional differences were perceived in number and separation. The regional differences also corroborated with changes in the shape of trabecular elements as expressed by the structure model index. In the anterior and inferior regions, the elements had a predominant plate-like form. In the growth regions rod-like trabeculae had the upper hand. Both the results of architecture and degree of mineralization pointed out that the condyle remained a trabecular structure and that it grows in superoposterior direction.

The architecture and degree of mineralization of the buccal region of the corpus differed clearly from both lingual and apical regions. Bone volume fraction in this region was significantly lower as reflected by thinner bony elements. The more compact lingual and apical structure was also reflected in the negative numbers of their structure model index. The structure at the buccal side of the corpus in the newborn group could indicate a rapid growth of the corpus in lateral direction by the accretion of plates of bone tissue on the preexisting bony surface (Stover et al., 1992) with the concurring presence of anastomosing trabeculae. This was also discerned on the inner surface of the lingual cortex, but to a lesser degree. This might imply a lateral growth and an increase in width of the corpus. The features just

mentioned are equivalent with those observed in earlier studies on human fetal specimens (Goret-Nicaise, 1981; Goret-Nicaise and Dhem, 1984).

Generally, the middle portion of the corpus had the highest bone volume fraction, degree of mineralization, and thickest bony elements in both fetal and newborn group. This might indicate that in this region the bone mineralization had been going on for a longer period than anteriorly and posteriorly. This seems in corroboration with previous findings that the mandibular corpus develops from the so-called mandibular primary growth centre that appears near the future mental foramen (Radlanski et al., 2002).

In conclusion, architectural and mineralization differences between condyle and corpus align with those obtained with mineral composition analysis. The known developmental growth of the condyle in posterosuperior direction and that of the corpus laterally and longitudinally and the increase in width are reflected by concomitant changes in architecture and mineralization.

CHAPTER 6

BIOMECHANICAL CONSEQUENCES OF DEVELOPMENTAL CHANGES IN TRABECULAR ARCHITECTURE AND MINERALIZATION OF THE PIG MANDIBULAR CONDYLE

Abstract

The purpose of the present study was to examine the changes in apparent mechanical properties of trabecular bone in the mandibular condyle during fetal development and to investigate the contributions of altering architecture, and degree and distribution of mineralization to this change. Three-dimensional micro-computed tomography (microCT) reconstructions were utilized to assess the altering architecture and mineralization during development. From the reconstructions, inhomogeneous finite element models were constructed, in which the tissue moduli were scaled to the local degree of mineralization of bone (DMB). In addition, homogeneous models were devised to study the separate influence of architectural and DMB changes on apparent mechanical properties. It was found that the bone structure became stiffer with age. Both the mechanical and structural anisotropies pointed to a rod-like structure that was predominantly oriented from anteroinferior to posterosuperior. Resistance against shear, also increasing with age, was highest in the sagittal plane. The reorganization of trabecular elements during development, which occurred without a change in bone volume fraction, contributed to the increase in apparent stiffness. The increase in DMB, however, contributed more dominantly. Incorporating the observed inhomogeneous distribution of mineralization decreased the apparent stiffness, but increased the mechanical anisotropy. This denotes that there might be a directional dependency of the DMB of trabecular elements, i.e. differently orientated trabecular elements might have different DMBs. In conclusion, changes in DMB and its distribution are important to consider when studying mechanical properties during development and should be considered in other situations where differences in DMB are expected.

Introduction

During fetal life bone develops into a load bearing structure. From early on in this phase, it has to withstand the gradually increasing loads from involuntary contractions of developing muscles causing fetal movement. How the increased loading during fetal development is reflected in mechanical stiffness and strength of the trabecular structure has not yet been established.

Numerous studies have investigated the stiffness and strength of trabecular bone using physical mechanical tests (Linde, 1994; Teng and Herring, 1996; McCalden et al., 1997; Giesen et al., 2001). However, these tests do not allow the distinction between, for instance, the influences of changes in architecture and mineralization on the apparent mechanical properties. Finite element (FE) models have been applied to simulate and replace physical mechanical tests, where these were unfeasible or even impossible to perform (van Ruijven et al., 2003; van Eijden et al., 2004). Furthermore, they provide an excellent means to isolate the biomechanical effects of the changing architecture, and the degree of mineralization of bone (DMB) and its distribution. Finally, they allow for fast and realistic simulations of multiple uniaxial testing procedures, yielding the relevant components of the apparent stiffness matrix (van Rietbergen et al., 1995).

Generally, the elements in FE models of trabecular bone have been assigned a tissue modulus that was assumed to be homogeneous, isotropic and linearly elastic (Kabel et al., 1999a; Ulrich et al., 1999). However, the plates and rods of adult trabecular bone are composed of packets of remodeled bone of different ages which have a different DMB (Ziv et al., 1996; Paschalis et al., 1997), indicating varying tissue mechanical properties. Such variations have indeed been confirmed by nanoindentation studies (Rho et al., 1997; Roy et al., 1999). The tissue modulus has been found to be proportional to the DMB (Choi et al., 1990; Currey, 1999).

Inhomogeneity in the way the DMB is distributed over the bony elements in the developing mandibular condyle has been shown in recent studies on fetal development of trabecular bone (Mulder et al., 2005; 2006b). In trabecular elements, a gradual increase in the DMB from the surface towards their centers has been observed. This is in agreement with the mechanism of apposition of new bone material with a relatively low DMB on the surface of trabeculae, which becomes more mineralized and rigid with tissue age (Ziv et al., 1996). As bone matures, the relative contribution of new bone tissue decreases and the average

trabecular DMB increases. Simultaneous with the increase in average DMB, a distinct condylar trabecular architecture develops from the presumptive trabecular structure. This development, however, proceeds without a change in bone volume fraction (Mulder et al., 2005). It is unknown what the biomechanical consequences of these changes are and how they contribute individually to changes in the apparent mechanical properties of the trabecular structure.

The goal of the present study was to investigate the changes in apparent mechanical properties of trabecular bone in the mandibular condyle during fetal development. This goal was pursued by applying FE models of early fetal and newborn pig mandibular condyles, in which the architecture, and the degree and distribution of mineralization, as quantified by microCT, were incorporated. A second goal was to investigate the relative contributions of the changing architecture, and the changing DMB and its distribution during development to the changes in apparent mechanical properties. For that purpose, separate simulations were performed in which the altering DMB or its distribution was disregarded.

Material and methods

Samples

The right mandibular condyle of four fetal and four newborn pigs from different litters (standard Dutch commercial hybrid race) were examined. The fetal specimens (estimated age: 75 days of gestation, mean weight: 375 g) were obtained from commercially slaughtered sows and their age was estimated from the mean weight of the litter using growth curves (Evans and Sack, 1973). The newborn specimens (approximately 112-115 days post conception, mean weight: 1351 g) were acquired from the experimental farm of the Faculty of Veterinary Medicine in Utrecht, the Netherlands, and were euthanized by an intravenous overdose of ketamine (Narcetan) after premedication. These specimens were obtained from other experiments that had been approved by the Committee for Animal Experimentation of the Faculty of Veterinary Medicine, Utrecht, the Netherlands. The specimens were stored at -20°C prior to assessment.

The mandibles were dissected from the heads and cut in half at the symphyseal region. The right halves were prepared for analysis. The condyle was separated with a frontal cut at

the mandibular notch and with a horizontal cut at the mandibular ramus parallel to the occlusal plane.

Architecture and DMB

Three-dimensional reconstructions of the bony condylar structures were obtained by using a high-resolution microCT system (μCT 40; Scanco Medical AG., Bassersdorf, Switzerland). The specimens were mounted in cylindrical specimen holders (polyetherimide; outer diameter: 20 mm, wall thickness: 1.5 mm) and secured with synthetic foam. The scans yielded an isotropic spatial resolution of 10 μm. A 45 kV peak-voltage X-ray beam was used, which corresponds to an effective energy of approximately 24 keV (Mulder et al., 2004). The microCT was equipped with an aluminum filter and a correction algorithm that sufficiently reduced the beam hardening artifacts to enable quantitative measurements of the degree and distribution of mineralization of immature bone (Mulder et al., 2004). The computed attenuation coefficient of the X-ray beam for each voxel was stored in an attenuation map and represented by a grey value in the reconstruction.

The architecture and DMB were determined in cubic volumes of interest defined in the condyles (fetal: approximately 1.5 mm^3, newborn: approximately 7.5 mm^3), which were built up out of 10 x 10 x 10 μm^3 voxels (Fig. 1). The top and bottom plane of the cubes were oriented parallel to the occlusal plane. To discriminate between bone and background, the reconstructions were segmented using an individually determined threshold using an adaptive threshold determination procedure, which was visually checked. In a segmented image every voxel with a linear attenuation value below the threshold (assumingly representing soft tissue or background) was made transparent and voxels above this threshold (representing bone) were made opaque. From these segmented images, relevant bone architectural parameters (BV/TV: bone volume fraction, Tb.N: trabecular number, Tb.Th: trabecular thickness, Tb.Sp: trabecular separation, Conn.D: connectivity density, SMI: structure model index) were calculated. To determine the direction and structural anisotropy of the trabecular structure, a mean intercept length (MIL) tensor was calculated (Harrigan and Mann, 1984). The eigenvectors of this tensor align with the principal directions of the trabecular structure. The eigenvalues (H_1, H_2, and H_3) express the prevalence of the bone material in the corresponding directions. They were sorted such that $H_1 > H_2 > H_3$. The degrees of structural anisotropy (DA_{MIL}) were defined by H_1/H_3, H_1/H_2, and H_2/H_3. To determine the direction of the trabecular structure relative to the mandibular condyle, the projections of the principal

directions on the sagittal and frontal planes were used (Software Revision 3.2, Scanco Medical AG).

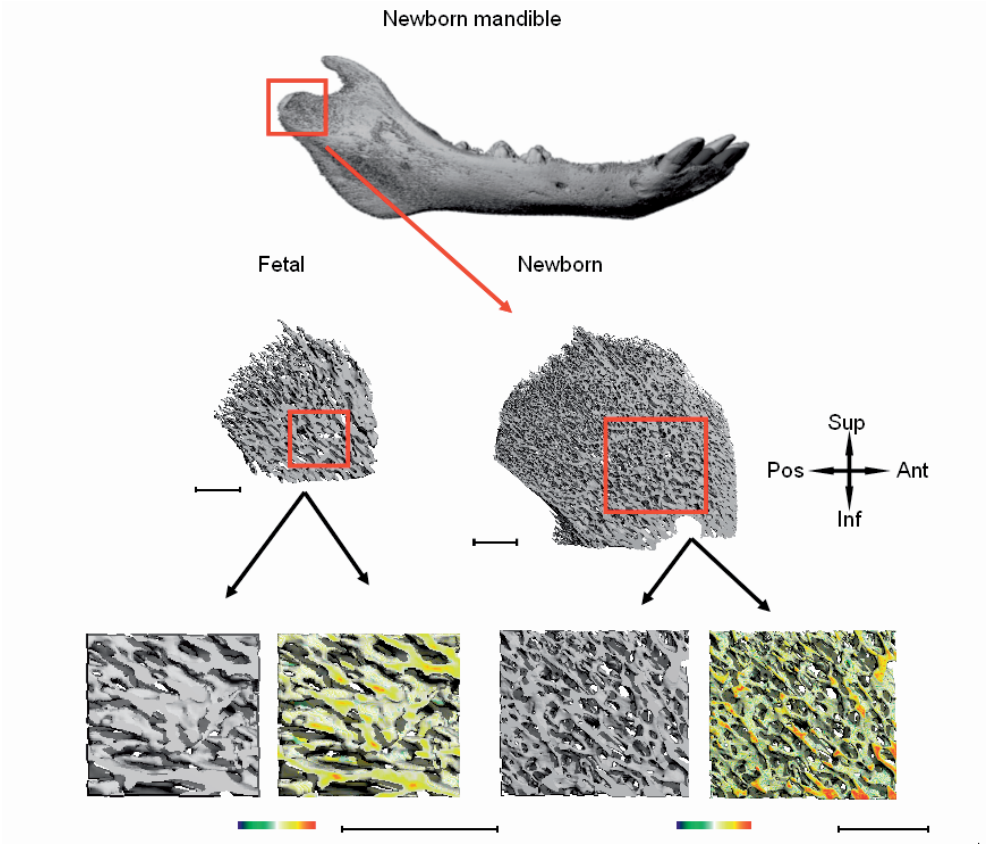

Figure 1. Selection of the volumes of interest. Top: 3D reconstruction of a newborn mandible. Middle: 3D reconstructions of sagittal cross-sections from a fetal and newborn pig mandibular condyle. The red squares represent the location of the cubic volumes of interest that were used to calculate architecture, degree and distribution of mineralization, and mechanical properties. Bottom: Top view of homogeneous and inhomogeneous reconstructions of the cubes. The colors represent the degree of mineralization, increasing from blue to red. Bars: 1.0 mm.

For determination of the DMB, voxels with a value above the threshold kept their original grey value, which can be considered proportional to the local DMB (Nuzzo et al., 2003). The bone voxels in the layer adjacent to the marrow space were disregarded as this layer is likely to be corrupted by partial volume effects. The DMB was quantified by comparing the attenuation coefficient with reference measurements of a phantom containing hydroxyapatite of 0, 200, 400, 600, and 800 mg/cm^3.

FE analyses

Using the reconstructions created with microCT, inhomogeneous FE models in which architecture, degree and distribution of mineralization are incorporated, were created. The voxels in the three-dimensional microCT reconstructions were directly converted into cubic eight-node brick elements. The tissue modulus (E_t) was calculated by scaling it to the DMB value of the corresponding microCT voxel according to $\log E_t = -8.58 + 4.05 * \log[Ca]$ (Currey, 1999). In this relationship the concentration of calcium [Ca] was recalculated to the concentration of hydroxyapatite [HA] or DMB by multiplying [Ca] by a factor 2.5 (approximately 40% of hydroxyapatite consists of calcium) and subsequently multiplying this by 1.4 g/cm^3, i.e. the specific density of trabecular bone tissue (Ouyang et al., 1997; Kabel et al., 1999b).

The apparent mechanical properties of the FE models were estimated using an element-by-element FE-solver (van Rietbergen et al., 1995). This program was modified to permit the assignment of a different tissue modulus to each individual element. Six uniaxial mechanical tests (three compression and three shear tests) were simulated by applying a uniform displacement at the surfaces of the specimen cubes. Each simulated test yielded a part of the apparent stiffness matrix of the specimen. Using an optimization procedure, the best orthotropic representation of the apparent stiffness matrix of the specimen was calculated by rotating the original condylar coordinate system until the principal mechanical directions were found for which the Young's moduli, and the directions for which the shear moduli were greatest. The Young's moduli (E_1, E_2, and E_3) and shear moduli (G_{12}, G_{23}, and G_{31}) were approximated relative to these directions. Together, these directions constitute an orthogonal coordinate system. They were sorted such that $E_1 > E_2 > E_3$. The degrees of mechanical anisotropy (DA_E) were defined by E_1/E_3, E_1/E_2, and E_2/E_3. To determine the orientation of the principal mechanical directions relative to the condyle, they were projected on the sagittal and frontal planes.

Another goal was to investigate separately the effects on apparent mechanical properties of a) developmental changes in architecture and b) the distribution of mineralization. To investigate the influence of architecture the results of the simulations described above were compared with those where a homogeneous tissue modulus was applied. Therefore, an isotropic tissue modulus of 4000 MPa, as calculated from the average DMB of the fetal specimens, was applied to all elements of both the fetal and newborn specimens. To investigate the influence of the distribution of mineralization with respect to developmental age, simulations were performed where each element in a specific specimen

model received the same average tissue modulus, approximated from the average DMB of that specimen.

Statistics

Components of the global stiffness matrix (E_1, E_2, E_3, G_{12}, G_{23}, and G_{13}) and mechanical anisotropies were averaged per age group and compared between age groups using independent-sample t-tests. The influences of architecture, and degree and distribution of mineralization on apparent mechanical properties were investigated by comparing the differences in mechanical variables between the various models using paired sample t-tests. Correlations between architectural and mechanical properties were explored by taking all specimens into account.

Results

Changes in architecture and DMB during development

Compared to the fetal one, the newborn condyle had increased in size and an anteroinferior towards posterosuperior orientation of the trabecular elements was clearly visible (Fig. 1). No discernable subchondral or cortical bone had been formed in either the fetal or newborn specimens. Development coincided with a reorganization of bone of the trabecular structure without a significant change in the bone volume fraction itself (Table 1). There was an increase in mean trabecular thickness (from 0.049 mm to 0.063 mm) and mean separation (from 0.122 mm to 0.228 mm) with a concurring decrease in mean trabecular number (from 6.99/mm to 3.95/mm) and connectivity (from 161.82/mm^3 to 76.96/mm^3). No differences in structural anisotropy were discerned between the fetal and newborn group.

Table 1. Morphometric and mineralization parameters of the trabecular bone in the condyle.

		Fetal mean (sd)	Newborn mean (sd)
BV/TV	(%)	24.14 (4.14)	19.65 (1.64)
Tb.Th	(mm)	0.049** (0.002)	0.063 (0.005)
Tb.N	(1/mm)	6.99** (0.47)	3.95 (0.22)
Tb.Sp	(mm)	0.122** (0.012)	0.228 (0.016)
SMI		1.62 (0.35)	1.53 (0.10)
Conn.D	($1/mm^3$)	161.82** (31.09)	76.96 (4.92)
DA_{MIL1}	H_1/H_3	2.50 (0.23)	2.27 (0.20)
DA_{MIL2}	H_1/H_2	2.40 (0.24)	2.11(0.22)
DA_{MIL3}	H_2/H_3	1.04 (0.02)	1.07 (0.03)
DMB	(mg/cm^3)	630** (31)	730 (13)
E_{tissue}[a]	(MPa)	4000** (770)	6664 (466)

[a] Tissue moduli were calculated according to the relationship contrived by Currey et al. (1999).

** Significant difference between fetal (n=4) and newborn (n=4) specimens ($P < 0.01$).

BV/TV: bone volume fraction; Tb.Th: trabecular thickness; Tb.N: trabecular number; Tb.Sp: trabecular separation; SMI: structure model index; Conn.D: connectivity density; DA_{MIL1-3}: degrees of structural anisotropy; DMB: degree of mineralization of bone; E_{tissue}: tissue modulus.

The DMB of the newborn specimens was larger than that of the fetal ones. It increased from 630 mg/cm^3 (fetal) to 730 mg/cm^3 (newborn), while the variation in mineralization, as characterized by the width of the frequency distributions (Fig. 2), displayed no change.

Changes in mechanical properties during development

The increase in average DMB during development led to an increase in average tissue modulus from 4000 MPa to 6664 MPa (Table 1) according to the applied relationship between the hydroxyapatite concentration and tissue modulus (Currey, 1999). Approximately a doubling of both apparent Young's and shear moduli during development was predicted (Table 2, column [a]). No differences in mechanical anisotropy were found between the fetal and newborn group.

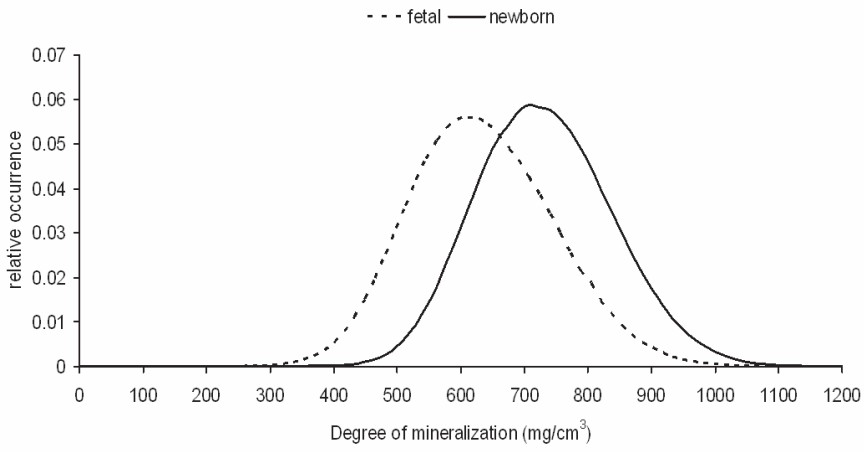

Figure 2. Frequency distributions of mineralization. Dashed line: Grouped distribution of the fetal specimens. Solid line: Grouped distribution of the newborn specimens. Note the increased average degree of mineralization of the newborn group and equal width of the curves.

In both age groups the principal mechanical directions coincided with the principal structural directions. In both age groups, the first and second principal directions were approximately in the sagittal plane (Fig. 3). The first principal direction corresponded to the trabecular alignment, i.e. from anteroinferior towards posterosuperior. The second principal direction was pointing from posteroinferior to anterosuperior and the third mediolaterally. Resistance against shear was large in the sagittal and frontal planes.

Changes in the magnitudes of the Young's and shear moduli were generally significantly related to changes in DMB (on average $R = 0.83$; $P = 0.015$; Fig. 4), trabecular thickness (on average $R = 0.87$; $P = 0.007$), trabecular number (on average $R = -0.78$; $P = 0.028$), and trabecular separation (on average $R = 0.80$; $P = 0.022$), while there were also significant mutual correlations between degree of mineralization and trabecular thickness, number, and separation. There was, however, no correlation of the Young's and shear moduli with bone volume fraction.

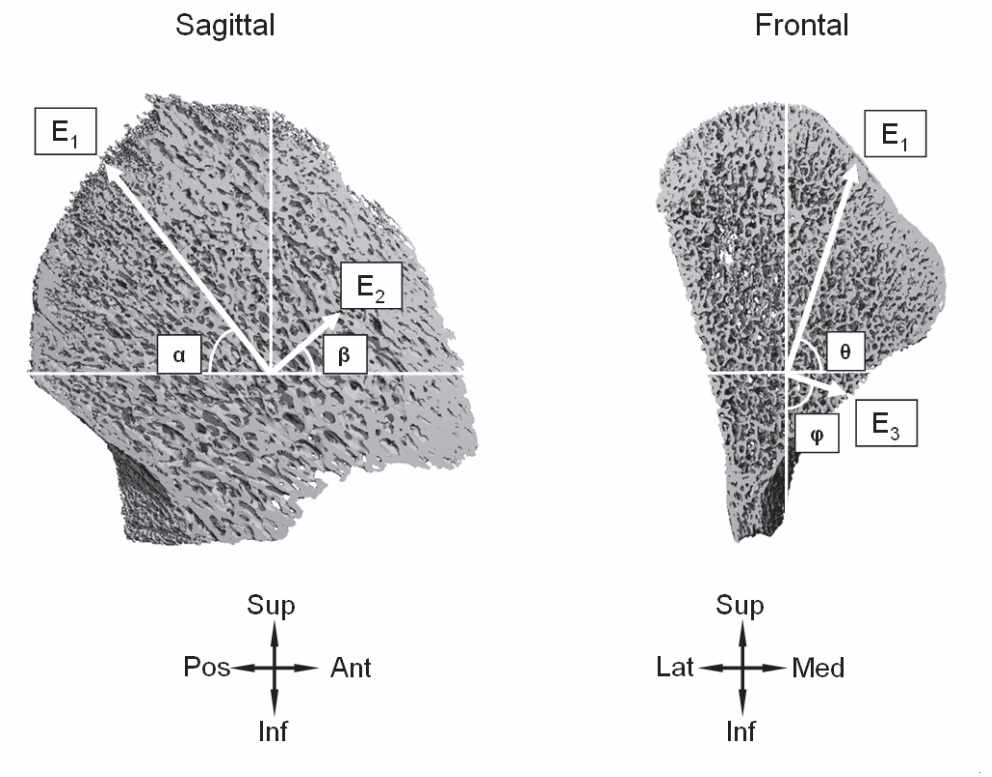

Figure 3. Size and orientation of the projections of principal stiffness components ($E_1 > E_2 > E_3$) from the original model on the sagittal and frontal planes. Left: Sagittal cross-section of a newborn mandibular condyle. α = 51.5°, β = 41.4°. Right: Frontal cross-section of a newborn condyle. θ = 73.4°, φ = 84.4°. For clarity: E_3 is not shown in the sagittal view; E_2 is not shown in the frontal view.

Influence of changing architecture and degree and distribution of mineralization on the mechanical properties

When the influence of the degree and distribution of mineralization on the tissue stiffness was disregarded completely, no differences in apparent Young's and shear moduli, and degrees of mechanical anisotropy between fetal and newborn specimens were observed (Table 2, column [b]), except for E_2, which increased from the fetal to newborn stage. This indicates a limited influence of the changes in architecture on the apparent mechanical properties.

When the distribution of mineralization was disregarded by implementing the tissue modulus according to the specimen-specific average DMB, significant increases in apparent Young's and shear moduli were observed during development (Table 2, column [c]). The values

for the Young's and shear moduli predicted with this model were, however, always higher than the ones found in the original model and degrees of mechanical anisotropy lower. Incorporating the distribution of mineralization thus lowers the values of Young's and shear moduli. The predicted principal mechanical directions of E_1 to E_3 were always the same as in the original model.

Table 2. Apparent mechanical parameters of the trabecular bone in the condyle.

Mechanical parameter		Original model [a]		Influence of changed architecture [b]		Influence of changed architecture and changed DMB [c]	
		Fetal Mean (sd)	Newborn Mean (sd)	Fetal Mean (sd)	Newborn Mean (sd)	Fetal Mean (sd)	Newborn Mean (sd)
$E_1^{‡‡}$	(MPa)	180.91* (104.63)	373.39 (92.68)	220.69 (110.51)	245.15 (44.83)	219.33* (111.08)	409.98 (91.94)
$E_2^{\#‡‡}$	(MPa)	41.28** (15.28)	118.63 (24.26)	55.76* (18.98)	87.46 (15.64)	55.50** (20.07)	147.01 (35.74)
$E_3^{‡‡}$	(MPa)	33.12 (23.50)	62.43 (34.69)	43.52 (25.01)	45.76 (17.94)	44.63 (29.74)	76.63 (33.19)
$G_{12}^{\#‡‡}$	(MPa)	40.53** (20.02)	89.19 (15.81)	49.10 (20.57)	62.17 (8.52)	49.27* (22.90)	104.13 (20.52)
$G_{23}^{\#‡‡}$	(MPa)	21.90* (13..27)	44.02 (9.14)	27.31 (14.04)	30.97 (3.63)	27.36* (15.97)	51.66 (7.85)
$G_{13}^{‡‡}$	(MPa)	36.69 (24.17)	81.18 (29.35)	44.22 (25.78)	53.33 (14.95)	44.36 (27.60)	89.76 (30.36)
$DA_{E1}^{††‡‡}$	E_1/E_3	6.44 (2.48)	6.73 (2.21)	5.51 (1.96)	5.71 (1.42)	5.51 (1.96)	5.71 (1.42)
DA_{E2}	E_1/E_2	3.58 (0.95)	3.21 (0.82)	3.43 (0.55)	2.85 (0.60)	3.43 (0.55)	2.85 (0.60)
DA_{E3}	E_2/E_3	1.97 (1.50)	2.28 (1.18)	1.62 (0.92)	2.10 (0.82)	1.62 (0.92)	2.10 (0.82)

[a] Isotropic, inhomogeneously distributed, specimen specific tissue modulus distribution.

[b] Isotropic, homogeneously distributed, constant tissue modulus (4000 MPa).

[c] Isotropic, homogeneously distributed, specimen specific, constant tissue modulus (fetal: 4000 MPa, newborn: 6664 MPa).

* Significant difference between fetal (n=4) and newborn (n=4) specimens ($P < 0.05$); ** ($P < 0.01$).

[#] Significant difference between [b] and [c] ($P < 0.05$), including the fetal and newborn specimens (n=8).

[††] Significant difference between [a] and [b] ($P < 0.01$).

[‡‡] Significant difference between [a] and [c] ($P < 0.01$).

$E_{1\text{-}3}$: apparent Young's moduli; $G_{12,23,13}$: apparent shear moduli; $DA_{E1\text{-}3}$: degrees of mechanical anisotropy.

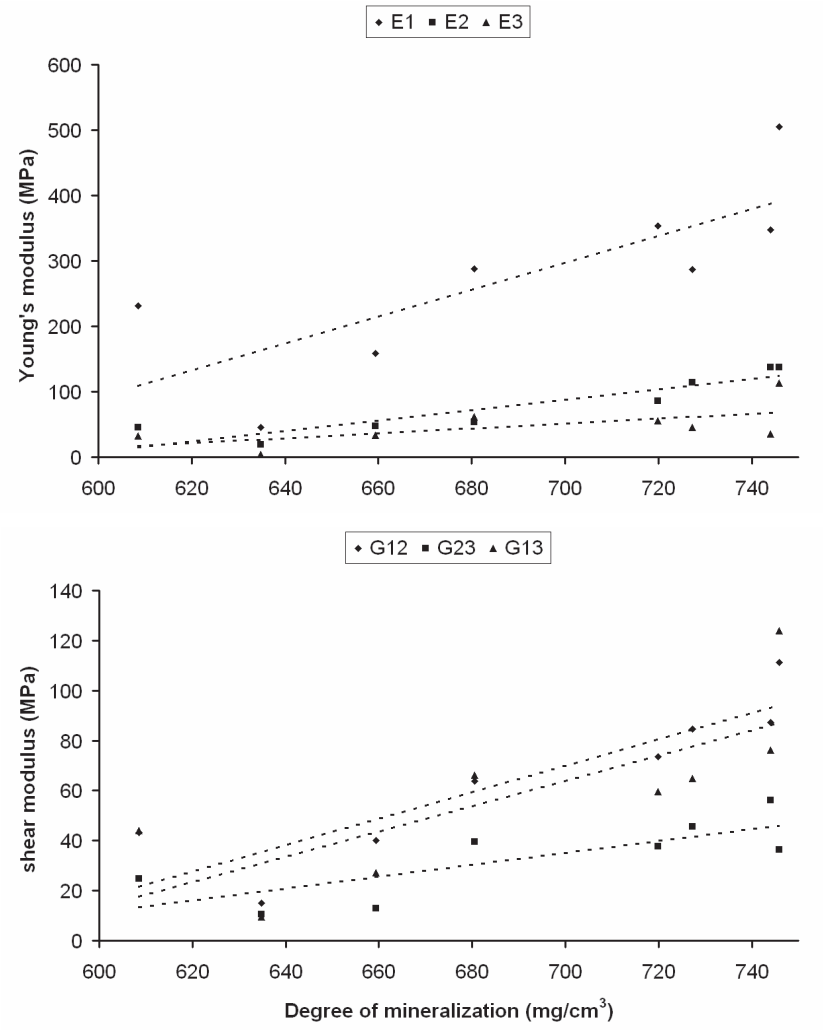

Figure 4. Relationship between the degree of mineralization (DMB) and apparent mechanical properties from the original model; each data point represents a specimen. Top: DMB versus apparent Young's moduli. E_1 vs. DMB: $R = 0.78$; $P = 0.022$; E_2 vs. DMB: $R = 0.92$; $P = 0.001$; E_3 vs. DMB: $R = 0.61$; $P = 0.106$. Bottom: DMB versus shear moduli. G_{12} vs. DMB: $R = 0.89$; $P = 0.003$; G_{23} vs. DMB: $R = 0.78$; $P = 0.021$; G_{13} vs. DMB: $R = 0.77$; $P = 0.026$.

Discussion

This study was concerned with the biomechanical properties of the developing trabecular bone in the pig mandibular condyle. Differences in architecture and DMB between the fetal

and newborn group were reflected by an increase of the Young's and shear moduli. By isolating the effects of changing architecture and DMB, we were able to study their separate influence on the increasing apparent mechanical properties during development. This was assessed by comparing the predictions of the original model with those obtained from simulations in which the tissue moduli were altered accordingly.

The effect of increasing DMB and its distribution was most substantial; in most cases, the Young's and shear moduli displayed a doubling in value. From the increase in average DMB (Table 1) an approximately 1.5 times increase in tissue moduli from fetal to newborn was expected. However, a doubling in Young's and shear moduli was observed, indicating an additional contribution of altered architecture. This suggests that especially the increase in DMB and its distribution are important to consider for mechanical properties during development. Using FE analyses, the change in apparent Young's moduli is generally attributed to changes in the bone volume fraction (van Rietbergen et al., 1998; Giesen et al., 2001; Ding et al., 2002). The absence of such a relationship in this study might be caused by the small bone volume fraction differences between our samples. The reorganization and adaptation of the trabecular elements in the condyle during development did not result in a change in the bone volume fraction. Therefore, the effects of changes in architecture could have been caused, for instance, by the increasing mean thickness of trabecular elements, although paralleled by a decrease in mean trabecular number and an increase in mean separation (Table 1). The correlation between DMB and trabecular thickness strengthens this notion. The thicker the trabeculae are, the larger in an absolute sense the region of highly mineralized and thus stiffer bone tissue, in their centers is (Mulder et al., 2005). The increased mechanical stiffness might indicate that the condyle is increasingly loaded during development. The loading might be from involuntary contractions by developing muscles and from yawn and swallowing reflexes of the fetus. The constant principal directions might indicate that the loading direction roughly remains the same during development.

The degrees of mechanical anisotropy were substantially larger than the structural ones, implying that, besides trabecular orientation, other parameters such as directionally dependent trabecular thickness and shape might also contribute to this property (van Ruijven et al., 2003). Furthermore, the dissimilarity between the stiffness in the different principal directions indicates that the structure in the mandibular condyle is not perfectly plate-like. Also the structure model index backs this notion; the values signify either an equal distribution of plate-like and rod-like trabecular elements or an intermediate trabecular shape. The fact that the degree of mechanical anisotropy was increased when the distribution of

mineralization was incorporated in the FE models denotes that there might be a directional dependency of the degree of mineralization of trabecular elements, i.e. differently orientated trabecular elements might have different degrees of mineralization.

Comparison of the present results with other FE studies that concerned trabecular bone is limited due to differences in the choices of tissue stiffness. In several studies postnatal development of architecture and mechanical properties were investigated using FE models (e.g. Tanck et al., 2001; Ding et al., 2002). However, the DMB was not incorporated in these studies although changes in DMB might be expected (Nafei et al., 2000a). A study in which the tissue moduli were arbitrarily scaled to mineralization distribution and incorporated in FE models found that the inhomogeneous models matched the mechanical properties, as measured by physical compression tests, closest (Bourne and van der Meulen, 2004). As was the case in the present study, other studies in which mineralization variation was incorporated in FE models found that this affected the trabecular bone mechanical properties appreciably (van der Linden et al., 2001; Jaasma et al., 2002). This implies that changes in DMB and its distribution are of great importance when studying mechanical properties and should be considered in situations where differences in DMB are expected, e.g. development, growth, and changes in functional loading. The stiffness of trabecular bone in the adult pig condyle is substantially higher than the ones found here (Teng and Herring 1995; 1996). However, in the adult condyle the amount of bone is considerably larger and also a higher DMB may be expected.

A few remarks have to be made about the methods used. First, the removal of the surface layer of voxels characterized as bone would unavoidably cause the omission of voxels with some bone in them. Including them causes a sharp falling off in DMB towards the periphery. The exclusion of these voxels could imply that the mechanical effect of changes in DMB is actually smaller than one might genuinely expect. Second, the volumes of interest, selected in the mandibular condyles, were relatively small. However, despite this small size the continuum assumption for trabecular bone was fulfilled, i.e. the sides of the cubes were larger than three to five trabecular thicknesses (Harrigan et al., 1988). Third, it must be mentioned that only four fetal and four newborn specimens were used. However, the strong correlations found in this study justify this choice and rules out any coincidence based on interindividual variation. Forth, the applied material model for bone tissue was linear elastic and isotropic. At the structural and tissue level, however, bone exhibits non-linear, visco-elastic behavior. Consequently, extrapolating the present results to dynamical and/or large deformation situations has to be performed with care. Fifth, from nanoindentation studies it

has been inferred that the stiffness of bone material displays anisotropy (Rho et al., 1997; Roy et al., 1999). This is probably not the case for woven bone (Su et al., 2003). Finally, the exponential relationship, contrived by Currey (1999), used in this study to scale the tissue moduli from the degree of mineralization included multiple species, but not the domestic pig and also no fetal specimens were taken into account. It is unknown if and how the fetal pig specimens fit into this relationship.

In conclusion, it was found that the apparent mechanical stiffness of trabecular bone in the pig mandibular condyle increased during development. This increase was mainly instigated by an increase in the degree of mineralization, but also architectural changes of the trabecular structure, without altering the bone volume fraction, contributed. Disregarding the distribution of mineralization appeared to lead to a considerable overestimation of the apparent Young's and shear moduli.

CHAPTER 7

THE INFLUENCE OF MINERALIZATION ON INTRATRABECULAR STRESS AND STRAIN DISTRIBUTION IN DEVELOPING TRABECULAR BONE

Abstract

Trabecular bone is assumed to distribute mechanical loads from the subchondral bone of the epiphysis to the cortical shell of the diaphysis. The load-transfer pathway is largely determined by its architecture. However, the influence of variations in mineralization is not known. The goal of this study was to examine the influence of inhomogeneously distributed degrees of mineralization (DMB) on intratrabecular stresses and strains and how they might change during development. Cubic mandibular condylar bone specimens from fetal and newborn pigs were used. Three-dimensional high-resolution microCT reconstructions were utilized to construct finite element models, in which the element tissue moduli were scaled to the local DMB. Disregarding the observed distribution of mineralization was associated with an overestimation of average equivalent strain and underestimation of von Mises equivalent stress. From the surface of trabecular elements towards their core the equivalent strain decreased irrespective of tissue stiffness distribution. This indicates that the trabecular elements were bended during the compression experiment. Inhomogeneously distributed tissue stiffness resulted in a low equivalent stress at the trabecular surface that increased towards the core. In contrast, disregarding this tissue stiffness distribution resulted in a high stress at the surface which decreased towards the core. The average equivalent strain did not change from fetal to newborn stages, whereas the von Mises equivalent stress increased. Intratrabecular distribution profiles of both strain and stress showed similar trends in both the fetal and newborn specimens. It was concluded that the increased DMB, together with concurring alterations in architecture, during development leads to a structure which is able to resist increasing loads without an increase in average deformation, which may lead to damage. Furthermore, incorporating inhomogeneously distributed tissue stiffness in finite element models, scaled to the local degree of mineralization, has substantial influence on intratrabecular stress and strain distribution.

Introduction

The trabecular bone of the mandibular condyle is considered to transfer a multitude of mechanical loads, applied to the relatively thin subchondral bone, to the cortical shell of the mandibular ramus. The load-transfer pathway is largely determined by the architecture and local stiffness of the trabecular bone. During early development, the condyle is increasingly loaded due to involuntary contraction of developing muscles (de Vries et al., 1985). Owing to this loading, the trabecular elements are subjected to deformations (i.e. strains) leading to stresses in the bone tissue. These stresses and strains are considered to modulate the growth of the bone (Burger et al., 1991). Due to this mechanism, bone is able to adapt to a changing mechanical environment during development. Most likely this will result, at the stage of birth, in a structure that is able to adequately withstand the forces that go along with early feeding behavior.

Over the past couple of years finite element (FE) analysis based on micro-computed tomography (microCT) reconstructions has become a powerful tool to determine the apparent mechanical properties of selected trabecular bone volumes (van Ruijven et al., 2003; van Eijden et al., 2004) or even complete bone parts (van Rietbergen et al., 1995; Pistoia et al., 2002; Homminga et al., 2004; Verhulp et al., 2005). In many cases these analyses have replaced physical mechanical tests where these were unfeasible or even impossible to perform. They can be used to predict the apparent mechanical properties of some volume of interest composed of irregularly shaped trabeculae. In addition to apparent mechanical properties, local strains and stresses within the trabeculae can be approximated.

The results of FE studies are heavily dependent on the implemented mechanical properties of the applied materials. Regarding bone tissue, these properties depend on the degree and distribution of mineralization. It has been shown that mineralization is not homogeneously distributed over the trabecular bone tissue of, for example, developing bone (pig mandible: Mulder et al., 2005; 2006b) and mature bone (rabbit femur: Bourne and van der Meulen, 2004; human mandibular condyle: van Ruijven et al., 2006). The degree of mineralization appears to increase systematically from the surface of the trabeculae towards their centers. In recent studies, differences in degree of mineralization at the trabecular level have been demonstrated to be related with concomitant differences in mechanical properties (Rho et al., 1997; Roy et al., 1999). The resulting inhomogeneity of tissue stiffness can affect the apparent mechanical properties of the complete trabecular structure (Bourne and van der

Meulen, 2004; Jaasma et al., 2005; van Ruijven et al., 2006). Thus far, the effect of the degree and distribution of mineralization has insufficiently been taken into account as determinant of bone quality. It is unknown what the biomechanical consequences of these variations in mineralization are for the apparent biomechanical behavior of trabecular bone and for intratrabecular distributions of stresses and strains, and herewith how they change during development. In the previous chapter (Mulder et al., 2006d), the effect on the apparent mechanical properties is described. In the present chapter, the influence on intratrabecular distribution of stress and strain is investigated.

Quantitative knowledge about the three-dimensional intratrabecular tissue stress and strain distributions provides information on the nature of trabecular deformation during loading. It could, furthermore, be a key factor to quantify bone integrity according to Wolff's trajectorial hypothesis, which suggests that, normally, stresses and strains should be distributed rather evenly over the trabecular structure. It may additionally give insights into micro-crack initiation and propagation behavior, which is influenced considerably by heterogeneity in bone mineralization (Ciarelli et al., 2003). It may, furthermore, provide information about stimuli that are the bases for modeling and remodeling of bone tissue. Finally, knowledge regarding the mechanical properties during development will augment the understanding of normal trabecular bone development.

The goal of this study is, therefore, two-fold. First, to investigate how variations in distribution of mineralization in the mandibular condyle affect intratrabecular distribution of stresses and strains. Second, to investigate how these are altered during development (Mulder et al., 2005; 2006b).

To pursue these goals, finite element models of specimens from the mandibular condyle of developing pigs were analyzed. Their geometry was modeled according to high resolution microCT reconstructions. The tissue stiffness was approximated from the local degree of mineralization, as measured also by microCT. The influence of the inhomogeneity of mineral distribution was analyzed by comparing the results with those of simulations where this inhomogeneity was neglected. The distribution of stresses and strains was assessed in a simulated compression test, applied along the vertical condylar axis.

Material and methods

Samples

The mandibular condyles of four fetal and four newborn pigs from different litters (standard Dutch commercial hybrid race) were examined. The fetal specimens (estimated age: 75 days of gestation, mean weight: 375 g) were obtained from commercially slaughtered sows and their age was estimated from the mean weight of the litter using growth curves (Evans and Sack, 1973). The newborn specimens (approximately 112-115 days post conception, mean weight: 1351 g) were acquired from the experimental farm of the Faculty of Veterinary Medicine in Utrecht, the Netherlands, and were euthanized by an intravenous overdose of ketamine (Narcetan) after premedication. These specimens were obtained from other experiments that had been approved by the Committee for Animal Experimentation of the Faculty of Veterinary Medicine, Utrecht, the Netherlands. The specimens were stored at -20°C prior to assessment.

The mandibles were dissected from the heads and cut in half at the symphyseal region. The right halves were prepared for analysis. The condyle was separated with a frontal cut at the mandibular notch and with a horizontal cut at the mandibular ramus parallel to the occlusal plane.

MicroCT

Three-dimensional reconstructions of the bony condylar structures were obtained by using a high-resolution microCT system (µCT 40; Scanco Medical AG., Bassersdorf, Switzerland). The specimens were mounted in cylindrical specimen holders (polyetherimide; outer diameter: 20 mm, wall thickness: 1.5 mm) and secured with synthetic foam. The scans yielded an isotropic spatial resolution of 10 µm. A 45 kV peak-voltage X-ray beam was used, which corresponds to an effective energy of approximately 24 keV (Mulder et al., 2004). An integration time of 1200 ms was applied to reduce noise substantially and to facilitate the discrimination between bone and background. The microCT was equipped with an aluminum filter and a correction algorithm that sufficiently reduced the beam hardening artifacts to enable quantitative measurements of the degree and distribution of mineralization (Mulder et al., 2004). The computed attenuation coefficient of the X-ray beam for each voxel was stored in an attenuation map and represented by a grey value in the reconstruction.

Cubic volumes of interest were defined in the condyles (fetal: approximately 1.5 mm^3, newborn: approximately 7.5 mm^3), and were built up out of 10 x 10 x 10 μm^3 voxels from which degree of mineralization and architecture were determined. The top and bottom plane of the cubes were oriented parallel to the occlusal plane. To discriminate between bone and background, the reconstructions were segmented using an adaptive threshold determination procedure, which was visually checked. In a segmented image every voxel with a linear attenuation value below the threshold (assumingly representing soft tissue or background) was made transparent and voxels above this threshold (representing bone) kept their original grey value. The latter can be considered proportional to the local degree of mineralization (DMB) (Nuzzo et al., 2003).

The DMB was quantified by comparing the attenuation coefficient with reference measurements of a phantom containing hydroxyapatite of 0, 200, 400, 600, and 800 mg/cm^3. To investigate the radial distribution of the degree of mineralization in the trabeculae a so-called peeling algorithm was used (Mulder et al., 2005). Consecutive layers of bone-containing voxels (7-8 μm thick) were peeled from the trabeculae, going from their surface inwards, towards the core. After a layer had been peeled off, its average degree and variation (SD) of mineralization were calculated. In this procedure, the bone voxels in the layer adjacent to the marrow space were disregarded as this layer is likely to be corrupted by partial volume effects. The trabecular architecture was quantified by a number of architectural parameters (BV/TV: bone volume fraction, Tb.N: trabecular number, Tb.Th: trabecular thickness, Tb.Sp: trabecular separation, Conn.D: connectivity density, SMI: structure model index, DA: degree of anisotropy) (Software Revision 3.2, Scanco Medical AG).

FE analyses

Using the three-dimensional reconstructions created with microCT, an FE model was created for every specimen. The voxels in the three-dimensional microCT reconstructions were directly converted into cubic eight-node brick elements. The tissue modulus (E_t) was approximated from the DMB value of the corresponding microCT voxel according to $\log E_t = -8.58 + 4.05*\log[Ca]$ (Currey, 1999). The concentration of calcium [Ca], expressed as mg/g by Currey (1999) was recalculated to the concentration of hydroxyapatite [HA] or DMB by multiplying [Ca] by a factor 2.5 (approximately 40% of hydroxyapatite consists of calcium) and subsequently multiplying this by 1.4 g/cm^3, i.e. the specific density of trabecular bone tissue (Ouyang et al., 1997; Kabel et al., 1999a). When the inhomogeneous distribution of

DMB was disregarded, all elements were equipped with the same tissue modulus, corresponding to the average DMB of that specimen.

The FE problems were solved using an element-by-element FE-solver (van Rietbergen et al., 1995). This program was modified to permit the assignment of a different tissue modulus to each individual element. A uniaxial compression test, corresponding to the superoinferior direction, was simulated by applying a uniform displacement (strain: 1%) on the superior surface of the specimen cubes. The vertical direction was assumed to correspond most closely to the average joint loading direction.

From the resulting components of the strain and stress tensor, the average equivalent strain and von Mises equivalent stress were calculated, respectively. Frequency distributions of the parameters mentioned and of the component of principal strain with the largest magnitude were constructed. The radial distribution of the equivalent strain and von Mises equivalent stress in the trabecular elements was studied by applying a similar peeling algorithm as applied for the DMB.

Statistics

To analyze the results from the peeling-algorithm, a general linear model (repeated measures) was applied. To study the difference between models per layer a general linear model (multivariate) was used. From the frequency distributions of the equivalent strain and von Mises equivalent stress, the mean and standard deviation of these parameters were determined. Differences between fetal and newborn specimens were statistically assessed using independent-sample t-tests. A p-value of less than 0.05 was considered statistically significant.

Results

Values for and differences in architectural parameters between fetal and newborn stages are given in Table 1. Architectural development coincided with a reorganization of bone of the trabecular structure without a significant change in the bone volume fraction itself. There was an increase in trabecular thickness (from 0.049 mm to 0.063 mm) and separation (from 0.122 mm to 0.228 mm) with a concurring decrease in trabecular number (from 6.99/mm to

3.95/mm) and connectivity (from 161.82/mm^3 to 76.96/mm^3). No differences in structural anisotropy were discerned between the fetal and newborn group.

Table 1. Architectural parameters of the trabecular bone in the condyle.

		Fetal mean (sd)	Newborn mean (sd)
BV/TV	(%)	24.14 (4.14)	19.65 (1.64)
Tb.Th	(mm)	0.049 (0.002)[a]	0.063 (0.005)
Tb.N	(1/mm)	6.99 (0.47)[a]	3.95 (0.22)
Tb.Sp	(mm)	0.122 (0.012)[a]	0.228 (0.016)
SMI		1.62 (0.35)	1.53 (0.10)
Conn.D	(1/mm^3)	161.82 (31.09)[a]	76.96 (4.92)
DA		2.50 (0.23)	2.27 (0.20)

[a] Significant difference between fetal and newborn specimens ($P < 0.01$).

BV/TV: bone volume fraction; Tb.Th: trabecular thickness; Tb.N: trabecular number; Tb.Sp: trabecular separation; SMI: structure model index; Conn.D: connectivity density; DA: degree of anisotropy.

The degree of mineralization significantly increased ($P < 0.05$) during development from fetal to newborn age. Whereas in fetal specimens the average DMB was approximately 630 mg/cm^3, in the newborn specimens it was approximately 730 mg/cm^3 (Fig. 1A). The variation in mineralization as characterized by the width of the frequency distribution remained constant. The increase in DMB led to an increase in average tissue stiffness from fetal (approximately 4.0 GPa) to newborn (approximately 6.7 GPa) specimens. Using the peeling-algorithm, it was demonstrated that the mineralization was distributed inhomogeneously in a systematic pattern over the trabecular elements (Fig. 1B). From the surface of trabeculae towards their core, the degree of mineralization increased significantly in both the fetal and newborn specimens. For the fetal ones, the second and third layers were statistically different from each other and successive layers ($P < 0.05$). The increase in DMB reached a plateau after the third layer as there was no difference between the more central layers. In the newborn ones, layers two through five were different from each other and successive layers ($P < 0.05$), whereas layers six through nine were not significantly different and thus also reaching a plateau.

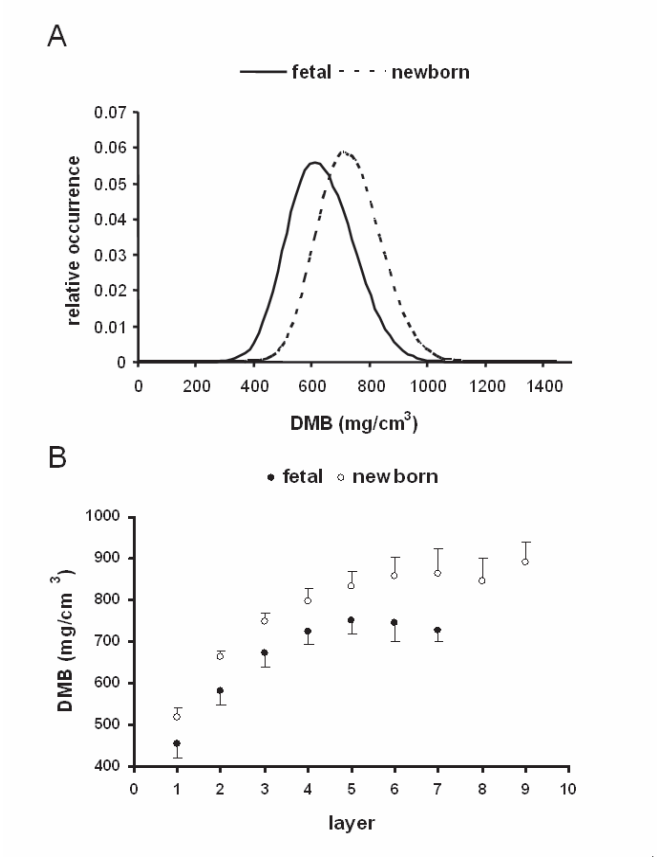

Figure 1. Distribution of degree of mineralization (DMB) in fetal (n=4) and newborn (n=4) trabecular bone specimens. A: Frequency distributions. Note the increase in average DMB from fetal to newborn B: Distribution from the surface of trabecular elements (layer 1) to their cores (fetal: layer 7; newborn: layer 9). Layer 1 was omitted in calculations of average values and histograms.

The average equivalent strain did not change significantly from fetal to newborn stages (Table 2). However, when the influence of mineralization on the tissue elasticity was disregarded, the average equivalent strain was overestimated ($P < 0.01$). This was also noticeable from the frequency distributions (Fig. 2A) and detectable in the profile through trabecular elements as obtained by the peeling procedure. In both fetal and newborn specimens, the strain was largest in the superficial layers of the trabecular elements, and was significantly reduced when getting closer to the cores (Fig. 2B, C, D), eventually leveling off towards the center of the trabecular elements. When the distribution of mineralization was disregarded, the equivalent strain was overestimated starting from layer three (fetal) and four (newborn).

Table 2. Equivalent strain and stress**.**

	Fetal mean (sd)	Newborn mean (sd)
Equivalent microstrain, inhomogeneous model	440 (130)	510 (70)
Equivalent microstrain, homogeneous model	530 (140)[c]	620 (150)[b]
Equivalent stress, inhomogeneous model (MPa)	1.29 (0.38)[a]	2.53 (0.94)
Equivalent stress, homogeneous model (MPa)	1.08 (0.30)[ab]	2.16 (0.74)[b]

[a] Significant differences between fetal and newborn specimens, $P < 0.05$.

[b] Significant differences between the homogeneous and inhomogeneous model per parameter, $P < 0.05$; [c] $P < 0.01$.

The average values of the von Mises equivalent stress increased from fetal to newborn stages (Table 2). Also, the frequency distribution changed during development (Fig. 3A). In the newborn specimens the stresses with the most frequent occurrence were larger than in the fetal specimens. These stresses were reduced in value when the influence of mineral distribution was disregarded (Table 2; Fig 3A). This influence was also evident in the radial distribution of equivalent stress over the trabecular elements. It was shown that the highest stress occurred near their center (Fig. 3B). The profiles from both fetal (Fig. 3C) and newborn specimens (Fig. 3D) showed similar trends as examined by the peeling procedure. The surface of trabecular elements contained the lowest stress, which significantly increased to its maximum about halfway between the surface and the cores and subsequently decreased again near the cores, but not reaching the values present at the surface. Disregarding the inhomogeneous distribution of mineralization resulted in a different profile; the highest stresses were then observed at the surface, which decreased towards the cores. It, thus, caused an overestimation of the equivalent stress at the surface of trabecular elements and an underestimation at their cores.

The distribution of the component of the principal strain with the largest magnitude (Fig. 4) was equally wide for the fetal and newborn specimens. However, distributions obtained while disregarding mineral distribution clearly overestimated the larger strains in compression. In both age groups the larger part of the component of the principal strain with the largest magnitude was compressive. The balance seemed to shift even more to compression in newborn specimens.

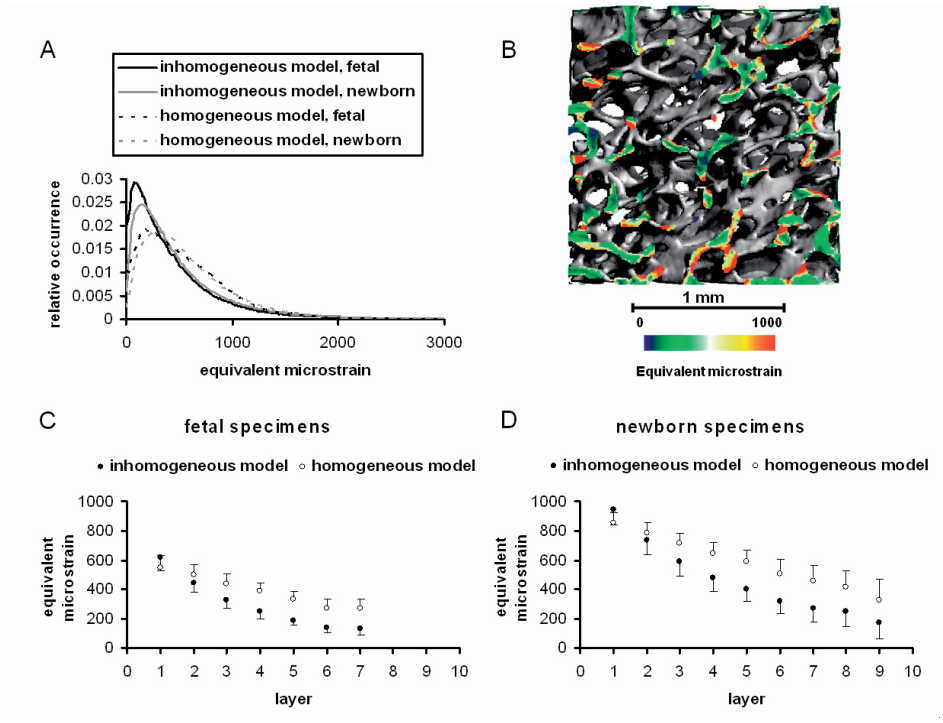

Figure 2. Distribution of equivalent strain in fetal (n=4) and newborn (n=4) specimens. The histograms do not contain surface voxels. A: Frequency distributions. Note the similarity between fetal and newborn specimens and the difference between the models. B: Frontal cross-section of the cubic volume of interest of a newborn specimen. Note the decreasing trend of the equivalent strain from the trabecular surfaces to the cores. C: Three-dimensional distribution from the surface of fetal trabecular elements (layer 1) to their core (layer 7). D: Three-dimensional distribution from the surface of newborn trabecular elements (layer 1) to their core (layer 9).

Discussion

To our knowledge this is the first study in which the influence of mineral distribution, related to tissue stiffness, on the local distribution of tissue stress and strain over the trabecular bone was investigated. We found that the cores of the trabeculae have higher mineralization than superficial regions. This indicates that modeling and remodeling occurs predominantly at the surface. Consequently, the youngest bone is present at the surface and the oldest bone at the core of the trabeculae. From a mechanical point of view, it should be noted that the bone mineral provides rigidity to the bone (Currey, 1988). Bone tissue with a high DMB can be expected to be relatively stiff and brittle, which is likely to have reduced fracture toughness.

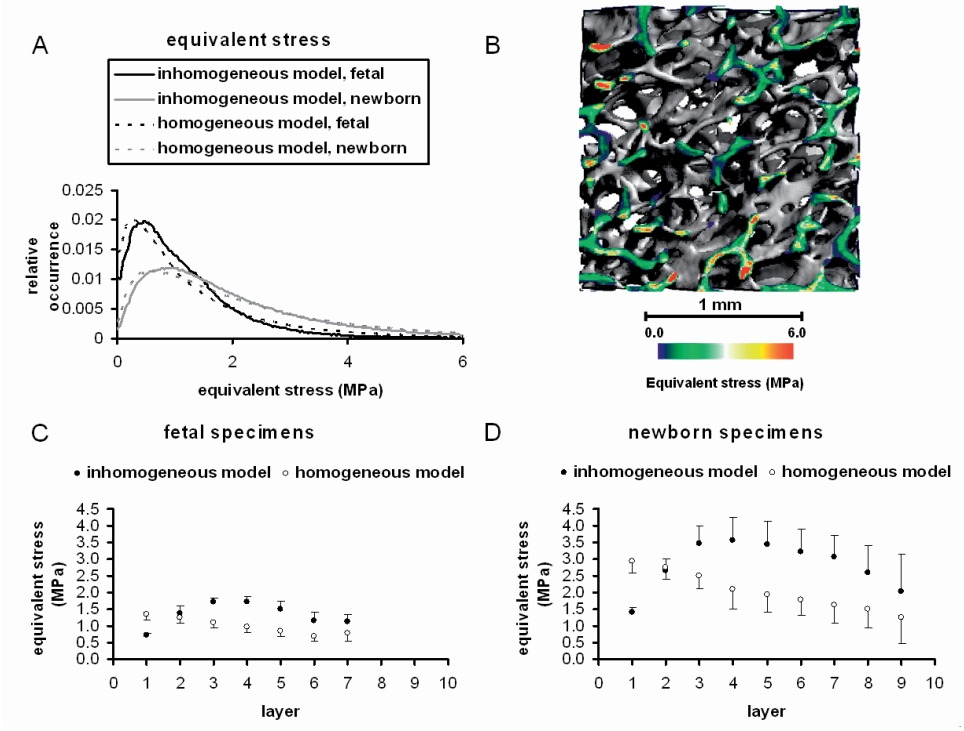

Figure 3. Distribution of equivalent stress in fetal (n=4) and newborn (n=4) specimens. A: Frequency distributions. Note the difference between fetal and newborn specimens and between the models. B: Frontal cross-section of the cubic volume of interest of a newborn specimen. Note the increasing trend of the equivalent stress from the trabecular surfaces to the cores. C: Three-dimensional distribution from the surface of fetal trabecular elements (layer 1) to their core (layer 7). D: Three-dimensional distribution from the surface of newborn trabecular elements (layer 1) to their core (layer 9).

From that perspective, heterogeneity in bone mineralization may have a considerable influence on crack initiation and propagation behavior and is therefore essential for the bone toughness (Ciarelli et al., 2003). The observed heterogeneity makes the trabeculae relatively compliant to bending and rigid to compression along their main axis. A less mineralized surface presumably demonstrates a greater ability to withstand the strains without breaking, as present when trabeculae are loaded in bending, and hence the trabeculae are less prone to fracture. Moreover, due to the relatively low degree of mineralization, the accompanying stresses remain relatively low. In the cores of trabecular elements, the high degree of mineralization retains the material from excessive deformation, thus resulting in low strains, but higher stresses. This composition can be considered preferable to prevent crack propagation. The highly mineralized cores provide high compression stiffness, but with a

relatively low failure energy (Currey, 1984). Cracks initiated in this tissue might be prevented from continuing through the surface layers, which have lower mineral content and are more compliant (Zioupos and Currey, 1994). This prevents complete fracture of the trabecular elements and enables repair of the damage. This is confirmed by observation of damaged trabecular elements, where the highly mineralized core contains microcracks, while the mechanical integrity of the trabecular elements is maintained by the undisturbed, less mineralized surface (Fyhrie and Schaffler, 1994; Mori et al., 1997).

We found that incorporating inhomogeneously distributed tissue stiffness, according to the local degree of mineralization, had a profound effect on frequency distributions and three-dimensional profiles of stress and strain through trabecular elements. Disregarding this inhomogeneously distributed tissue stiffness was demonstrated to lead to an overestimation in average equivalent strain, with vertical compression. The von Mises equivalent stress on the other hand was underestimated in that case. The three-dimensional stress and strain profile through the trabecular elements indicates that the deformation scheme of trabecular elements during loading is affected by the distribution of mineralization. Higher strains at the surface of trabecular elements than in the cores point to bending deformation. However, in pure bending the amount of compressed and stretched tissue should be equal, which is not the case for the presently applied deformation which was mainly compressive (see Fig. 4).

The present study does not confirm the paradigm that, normally, strains should be distributed rather evenly over the trabecular architecture. In contrast, it is in agreement with previous studies where frequency distributions in human and canine femurs were of similar shape (van Rietbergen et al., 1999; 2003). The fact that no uniform distributions of stress and strain were found is probably due to the fact that both the bone architecture and mineralization are adapted to multiple loading directions. Moreover, an optimal trabecular structure may appear differently under multi-directional loads than the 'trajectorial' organization proposed by Wolff (Pidaparti and Turner, 1997). Obviously, a perfectly even distribution cannot be expected for one single load case because the condyle is subjected to varying loading magnitudes and directions during normal use. Not only joint forces but also muscle forces are applied on it. A trabecular structure created through load adaptive remodeling should reflect all these different loading configurations in a weighted manner (van Rietbergen et al., 2003).

With the development from fetal to newborn, the distribution of the equivalent strain as a result of the applied compression did not change. Between the stages a similar frequency distribution and profile through trabecular elements was observed. However, an increased

amount of stress, probably due to the increase in DMB was found, indicating a larger load bearing capacity. This increase was not accompanied by a change in the profiles through trabecular elements. Between these stages, changes in trabecular architecture, without altering the bone volume fraction have occurred (Mulder et al., 2005; 2006b). These changes included an increase in thickness of the trabecular elements, a reduction in their number, and a doubling of the intertrabecular spacing (Table 1). Furthermore, the average DMB had increased. These phenomena together show us that the increased DMB leads to a structure which is able to resist larger amounts of load without an increase in average deformation. Furthermore, the largest strains occur in the surface regions of the trabecular elements where the bone is able to adapt its structure best.

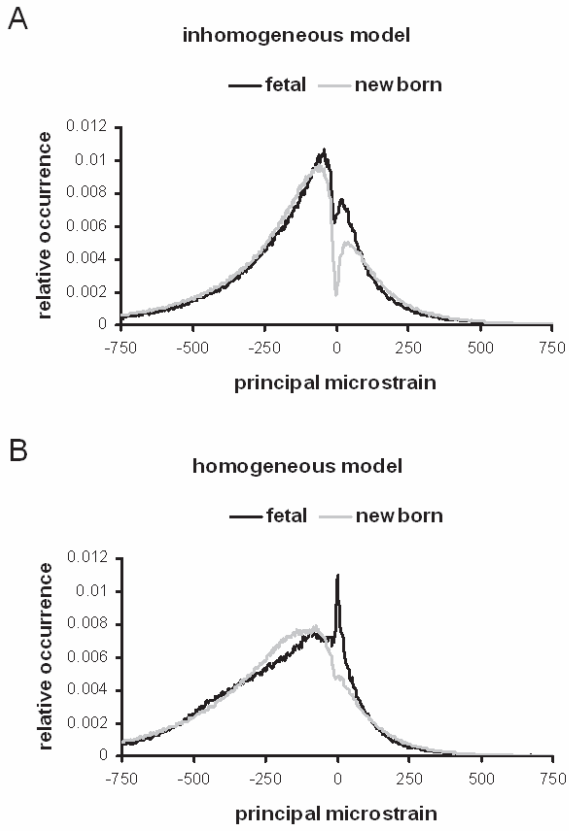

Figure 4. Frequency distributions of the principal strain with the largest magnitude for fetal (n=4) and newborn (n=4) specimens. A: Inhomogeneous models. B: Homogeneous models.

In the present analysis, a number of simplifications have been applied. First, in the calculation of the average values for DMB and equivalent stress and strain the superficial

bone layer was disregarded. This was done because the superficial voxels are likely to be corrupted by partial volume effects. Their inclusion would have led to an underestimation of mean DMB as they will have a DMB less than this average. Second, the material property of the bone tissue in our model was assumed to be isotropic and linearly elastic. The latter is applicable for trabecular bone for small deformations (Keaveny et al., 1994). Third, trabecular bone tissue has a preferred orientation which affects isotropy (Roy et al., 1999). This means that bone tissue properties may vary when different loading directions are applied. As trabeculae are likely to be loaded primarily along their long axis, the effects of anisotropy can be assumed to be primarily qualitative. Forth, the exponential relation used to scale tissue stiffness from local degree of mineralization was derived from experiments using cortical bone samples from several species (Currey, 1999). Although it is very likely that a similar relation will be valid in pig trabecular bone tissue, it is unknown if and how these fit into this relationship. A possible aberration from this relationship, however, does presumably not affect the findings in a qualitative sense as it is not likely that the proportional character of the relationship will be affected. Finally, the trabecular bone has been modeled morphologically by cubic elements. This approach produces 'jagged' surfaces. It has been shown that this can lead to local computational oscillations and errors in the stress-strain calculations, near these surfaces (Camacho et al., 1997; Guldberg et al., 1998). Because the surface layer was omitted in the determination of the histograms, the effect on the histograms and the calculated average and standard deviation will be small (van Rietbergen et al., 1999). Furthermore, due to averaging the results over neighboring elements, possible instabilities were reduced (Guldberg et al., 1998).

It can be concluded that the inhomogeneous distribution of mineralization has a decreasing effect on the average equivalent strain, while it tends to raise the von Mises equivalent stress in the trabecular bone. The equivalent strain was largest at the surface of trabecular elements and decreased towards their core. The equivalent stress was found to have its maximum about halfway between the surface and the core. This indicates that the trabecular elements are bended during compression. No changes in equivalent strain were observed during development from fetal to newborn specimens, but equivalent stress increased. The profiles from surface to core were similar between fetal and newborn specimens. Incorporating inhomogeneously distributed tissue stiffness, scaled to the local degree of mineralization, in FE models is essential for a better understanding of bone mechanical behavior.

CHAPTER 8

RELATIONSHIP BETWEEN TISSUE STIFFNESS AND DEGREE OF MINERALIZATION OF DEVELOPING TRABECULAR BONE

Abstract

It is unknown how the degree of mineralization of bone in individual trabecular elements is related to the corresponding mechanical properties at the bone tissue level. Understanding this relationship is important for the comprehension of the mechanical behavior of bone at both the apparent and tissue level. The purpose of the present study was, therefore, to determine the tissue stiffness and degree of mineralization of the trabecular bone tissue and to establish a relationship between these two variables. A second goal was to assess the change in this relation during development. Mandibular condylar specimens of four fetal and four newborn pigs were used. The tissue stiffness was measured using nanoindentation. A pair of indents was made in the cores of 15 trabecular elements per specimen. Subsequently, the degree of mineralization of these locations was determined with microCT. The mean tissue stiffness was 11.2 GPa (± 0.5 GPa) in the fetal group and 12.0 GPa (± 0.8 GPa) in the newborn group, which was not significantly different. The degree of mineralization of the fetal trabecular cores was 744 mg/cm^3 (± 28 mg/cm^3). The one in the newborn bone measured 719 mg/cm^3 (± 34 mg/cm^3). Again, no significant difference between them was found. A significant relationship between tissue stiffness and degree of mineralization was obtained for fetal (R = 0.40; $P < 0.001$) and newborn (R = 0.72; $P < 0.001$) groups. The slopes of the regression lines were significantly different. It was concluded that bone tissue in fetal and newborn trabecular cores is already highly mature and resembles adult trabecular bone tissue properties and is strongly correlated with degree of mineralization.

Introduction

Adult bone material contains predominantly lamellar bone. The fetal skeleton, however, is formed by woven bone which has a rapid rate of deposition. Woven and lamellar bone differ with regard to their formation, composition, organization, and mechanical properties (Buckwalter et al., 1995). The irregular collagen-fibril orientation and irregular pattern of mineralization of woven bone make it more flexible and more easily deformable than, but mechanically inferior to lamellar bone, despite a higher degree of mineralization (Currey, 1998).

It has been previously shown that, besides changes in architecture, the average degree of mineralization of presumptive trabecular bone of the pig mandibular condyle increases during development (Mulder et al., 2005). The relationship between the degree of mineralization in individual trabecular elements and the mechanical properties at the tissue level has not been established unambiguously yet. Understanding this relationship is important for the comprehension of the mechanical behavior of bone at both the tissue and apparent level (Turner et al., 1990; van der Linden et al., 2001; Bourne and van der Meulen, 2004; Follet et al., 2004; Mulder et al., 2006d). Furthermore, quantification of bone tissue properties is a prerequisite for the characterization of the mechanical environment in which bone cells reside (Jee, 2001).

One way of measuring the tissue mechanical properties is nanoindentation (Malzbender et al., 2002). Over the past 10 years, nanoindentation has been used frequently to assess the intrinsic mechanical properties of bone tissue. These mechanical properties were found to vary greatly between different species (Currey, 2003), individuals (Zysset et al., 1998), anatomical locations (Rho et al., 2001; Hengsberger et al., 2005), bone structural units (Rho et al., 1997; Rho et al., 1999; Roy et al., 1999; Zysset et al., 1999; Xu et al., 2003), and direction of testing (longitudinal vs. transverse) (Rho et al., 1997; Rho et al., 1999; Roy et al., 1999; Swadener et al., 2001; Fan et al., 2002). In mature humans, the mechanical properties of bone tissue appeared not to change with age (Zysset et al., 1998; Rho et al., 2002). However, it was found that newly formed bony lamellae in human fetal femurs, deposited during early development on the periosteal surface, have a lower tissue stiffness than bone lamellae already present (Su et al., 1997). Furthermore, it was established that tissue stiffness increases with fetal age. However, such measurements were not performed on trabecular elements. Neither were they related to other properties like degree of mineralization on a

trabecular level. It is known that the mechanical properties of bone tissue are strongly dependent on the amount of mineral present. As more and more mineral displaces water, the bone becomes stiffer (Currey, 1998). The general approach to 'explaining' the mechanical properties of bone is to relate statistically the mechanical behavior to other features of the bone, such as its mineral content. With this phenomenological approach, one can explain mechanical properties in terms of other variables and use such relationships for prediction (Currey, 1999).

The goal of this study was to determine the tissue stiffness and degree of mineralization of the trabecular bone tissue and to establish a relationship between these two variables. A second goal was to assess the change in this relation during development. To pursue these goals, mandibular condyles of pigs of two different developmental ages were investigated. The tissue stiffness was assessed using nanoindentation, whereas the degree of mineralization of the corresponding location was determined using micro-computed tomography (microCT).

Material and methods

Samples

The trabecular bone in the left mandibular condyle of eight pigs (standard Dutch commercial hybrid race) was examined. The pigs were divided into two groups; there were four fetal ones (estimated age: 70 days of gestation, mean weight: 375 g) and four newborns (approximately 112-115 days post conception, mean weight: 1351 g). The fetuses were obtained from slaughtered sows in a commercial slaughterhouse and their age was estimated from the mean weight of the litter using growth curves (Evans and Sack, 1973). The newborn specimens were acquired from the experimental farm of the Faculty of Veterinary Medicine in Utrecht, the Netherlands, and were euthanised by an intravenous overdose of ketamine (Narcetan) after premedication. The specimens were obtained from other experiments that were approved by the Committee for Animal Experimentation of the Faculty of Veterinary Medicine, Utrecht, the Netherlands. They were stored at -20°C prior to assessment.

The mandibles were prepared by dissection from the heads and cut in half at the symphyseal region. In the fetal group, the ramus along with the coronoid and condylar process was isolated from the rest of the left hemi-mandible. In the newborn group only the top part of the ramus including coronoid and condylar process was isolated.

All specimens were dehydrated in graded ethanol solutions (70-100%) and embedded in polymethylmethacrylate (PMMA) (Merck, Darmstadt, Germany) with the lateral side facing down. The embedded bones were sectioned using a microtome (Leica, Nussloch, Germany) in the sagittal plane approximately halfway between the medial and lateral condylar pole, exposing the trabecular microstructure at the surface. The exposed surface was ground with successively finer grades of abrasive paper (grit size: 400, 600, 1200) under deionized water and polished on microcloth with aluminum polishing solution (0.05 μm particle size) (Buehler, Lake Bluff, IL, USA).

A coordinate system was created on the polished surface in order to be able to retrace the locations of individual indents in microCT scans, as the indentations themselves were too small to be detected in microCT reconstructions (see below). Crosshairs (approximate width 10 μm) were etched on the polished surface of the specimens (Fig. 1B). Near the end of the lines, just within the confines of the sample as well as on the crossing, small holes (diameter approximately 20 μm) were drilled that were filled with an aluminumoxide powder and sealed with wax. The crosshairs and filled holes were detectable under the nanoindentation optical microscope, whereas in microCT reconstructions only the latter were perceptible clearly. Coordinates were attributed to the approximate center of the holes under the optical microscope. The coordinates of all indents were established relative to the same coordinate system and, therefore, the position of an indent relative to the holes could be determined. This enabled to determine the exact positions of the indents in trabecular tissue as reconstructed with microCT.

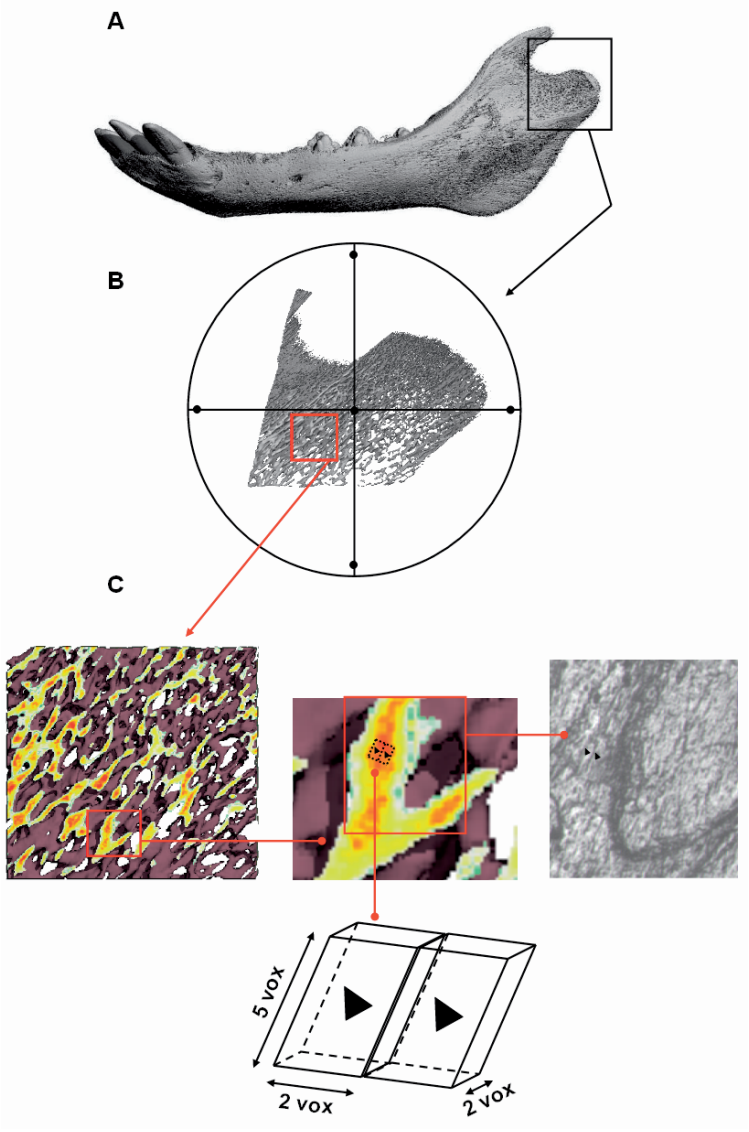

Figure 1. Sample preparation. A: Three-dimensional reconstruction of a newborn pig mandible. B: Graphical representation of an embedded newborn specimen, which was cut sagittally through the condyle, revealing the trabecular structure envisioned here with a microCT reconstruction. Note the vertical and horizontal crosshairs and the holes (dots), which acted as a coordinate system. C: Left: Magnified portion of B, visualizing the trabecular structure and the distribution of mineralization in the cutting plane in the front. Middle: Magnified portion from the left image. Degree and distribution of mineralization depicted with color scale (increasing degree of mineralization from blue to red). Dashed rectangles: regions, containing location of indents, in which mean degree of mineralization was determined (see also magnification below that). Right: Optical microscope image of the same trabecular element as in middle image. The locations of indentation (triangles) are depicted.

Nanoindentation

Load-control nanoindentation tests (Nano Indenter XP, MTS Systems Co., Oak Ridge, TN, USA) were performed on the embedded specimens using a Berkovich diamond indenter. The tests were performed in a vibration isolation cabinet at room temperature and stable humidity to ensure that the influence from thermal drift was minimal. Based on optical microscope observations, trabecular elements were identified in the anterior part of the mandibular condyle as this region contains abundant trabeculae of considerable thickness (Mulder et al., 2005). Trabecular elements with the same width were selected (110 µm). Subsequently, two indents were performed halfway the width of each of the selected trabeculae and the coordinates of the indents were registered (Fig. 1). The distance between the two consecutive indents was 15 micrometer. In total, 15 trabecular elements were tested per condylar specimen leading to a total of 240 indents (8 specimens x 15 trabecular elements per specimen x 2 indents per trabecular element).

The load protocol (similar to Mittra et al., 2006) comprised two conditioning steps before maximal load was applied (Fig. 2A). In the first conditioning step a 2 mN load was realized in 100 s and was followed by a 50 s holding period. Thereafter, unloading to 10% of the load was realized in 100 s followed by a second conditioning step to a load of 4 mN. In the following the peak load of 8 mN (load rate: 80 µN/s) was achieved. A 50 s holding period was inserted prior to final unloading (unloading rate: 80 µN/s) to reduce viscoelastic deformation to a negligible rate (Rho et al., 1997; Mittra et al., 2006). A holding step at 10% of peak load for 100 s was used to establish the rate of thermal expansion of the indenter apparatus with which the displacement data was corrected afterwards. The indentation depths at maximum load were approximately one micrometer, which has been shown to be sufficient in relation to the surface roughness of the bone samples using similar polishing techniques (Hoc et al., 2006). From this protocol a typical load-displacement curve was obtained (Fig. 2B) and the Oliver and Pharr method was applied to determine the elastic modulus (Oliver and Pharr, 1992). Using the contact area A_c, and the contact stiffness S, which is the slope of the initial portion of the final unloading curve, assumingly representing a purely elastic effect, the reduced modulus (E_r) of the specimen-indenter combination was determined according to:

$$E_r = \frac{\sqrt{\pi}}{2}\frac{S}{\sqrt{A_c}}. \quad (1)$$

The contact area A_c was determined from the load-displacement curve according to the method described by Oliver and Pharr (1992). For this method, the tip shape of the indenter

needs to be known, and this was determined using calibration measurements on fused silica. The specimen (bone) tissue modulus (E_t) follows from

$$E_t = \frac{1-\nu_s^2}{\frac{1}{E_r} - \frac{1-\nu_i^2}{E_i}}, \tag{2}$$

where ν is the Poisson's ratio and the subscripts s and i refer to the bone specimen and the indenter, respectively, and E_i is the indenter's Young's modulus. The elastic properties of the Berkovich diamond indenter were: $\nu_i = 0.07$ and $E_i = 1140$ GPa. The Poisson's ratio of bone was assumed to be 0.3.

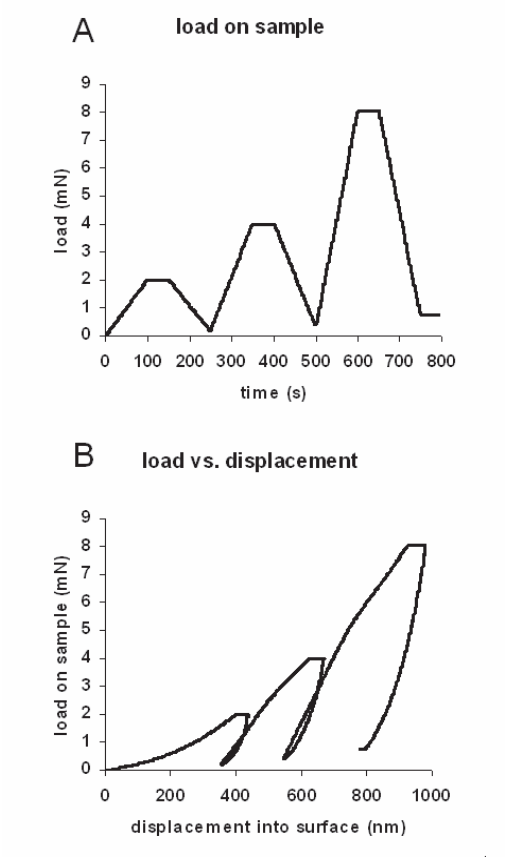

Figure 2. A: Nanoindentation protocol. The protocol comprised a loading step in 100 s to 2 mN followed by a 50 s holding period. After the holding period, unloading to 10% of the load was realized in 100 s followed by a similar procedure to a load of 4 mN and finally to the peak load of 8 mN (load rate: 80 μN/s). B: Typical load-displacement curve. The tissue stiffness was determined from the slope at the beginning of the final unloading step at maximum depth. Note that during the holding periods substantial time-dependent response is present, which points to the viscoelastic nature of the bone tissue.

MicroCT

Three-dimensional reconstructions of the trabecular bone in the mandibular condyle were obtained by using a high-resolution microCT system (μCT 40; Scanco Medical AG., Bassersdorf, Switzerland). The embedded specimens were ground to smaller dimensions in order to be able to analyze the specimens at a high resolution, which is limited to the diameter of the specimen holders. The coordinate system, however, was kept intact. The specimens were mounted in cylindrical specimen holders (polyetherimide; 20 mm outer diameter; wall thickness, 1.5 mm) and secured with synthetic foam. The specimens were completely submerged in deionized water. The scans yielded an isotropic spatial resolution of 10 μm. A 45 kV peak-voltage X-ray beam was used, which corresponds to an effective energy of approximately 24 keV (Mulder et al., 2004). The microCT was equipped with an aluminum filter and a correction algorithm that reduced the beam hardening artifacts sufficiently to enable quantitative measurements of the degree and distribution of mineralization of developing bone (Mulder et al., 2004). The computed linear attenuation coefficient in each voxel was stored in an attenuation map and represented by a grey value in the reconstruction. This attenuation coefficient can be considered proportional to the local degree of mineralization (Nuzzo et al., 2003).

Using the coordinate system mentioned, individual indent locations were identified in the microCT reconstructions. In this way, the local stiffness of the bone tissue obtained by nanoindentation was compared with the local degree of mineralization. To investigate the degree of mineralization of the indented locations, the area in which an indent had been performed was defined by a three-dimensional rectangular region of approximately two by five by two voxels (20 x 50 x 20 μm). The voxel layer defining the polished surface was omitted, because the absorption values assigned to them are biased due to partial volume effects, i.e. they contain both bone and background (embedding) tissue and the absorption values are thus severely underestimated. The defined region contained the location of an indent (Fig. 1).

The volumes of interest were segmented using an adaptive threshold which was equal for every specimen. The segmentation was visually checked. In a segmented image, every voxel with a linear attenuation value below this threshold (assumingly representing soft tissue or background) was made transparent and voxels above this threshold (representing bone) kept their original gray value. The outermost voxel layer characterized as bone, defining the cutting surface was removed as this is likely to be corrupted by partial volume effects. The degree of mineralization was quantified by comparing the attenuation coefficient with

reference measurements of a phantom containing hydroxyapatite of 0, 200, 400, 600, and 800 mg/cm^3.

Statistics

The relationship between degree of mineralization and tissue elastic modulus was assessed using linear regression in which the individual trabecular elements were treated as independent. The two values per trabecular element were averaged to obtain a mean value per trabecular element. Differences between fetal and newborn specimens with regard to tissue stiffness and degree of mineralization were statistically assessed using independent-sample t-tests. A p-value of 0.05 was considered statistically significant.

Results

The mean tissue stiffness of developing trabecular bone of the mandibular condyle of the fetal group (n=4), expressed as the elastic modulus, was measured to be 11.2 GPa (± 0.5 GPa), whereas in the newborn group (n=4) this was found to be 12.0 GPa (± 0.8 GPa). No significant difference was found between the two groups. The degree of mineralization of the fetal trabecular cores was 744 mg/cm^3 (± 28 mg/cm^3). The one in the newborn bone measured 719 mg/cm^3 (± 34 mg/cm^3). Again, no significant difference between them was found.

The relationship between the tissue stiffness and the degree of mineralization was analyzed for the fetal and newborn specimens separately (Fig. 3). In the fetal group (Fig. 3A), there was a significant correlation between them ($R = 0.40$; $P < 0.001$, n = 60). The regression equation was: E_t (GPa) = 0.013*DMB (mg/cm^3) + 1.81. In the newborn group (Fig. 3B), the relation between tissue stiffness was also found to correlate significantly ($R = 0.72$; $P < 0.001$, n = 60). The relationship was according to: E_t (GPa) = 0.024*DMB (mg/cm^3) - 5.17. Both slope and intercept of the regression line were significantly different between fetal and newborn ($P < 0.05$).

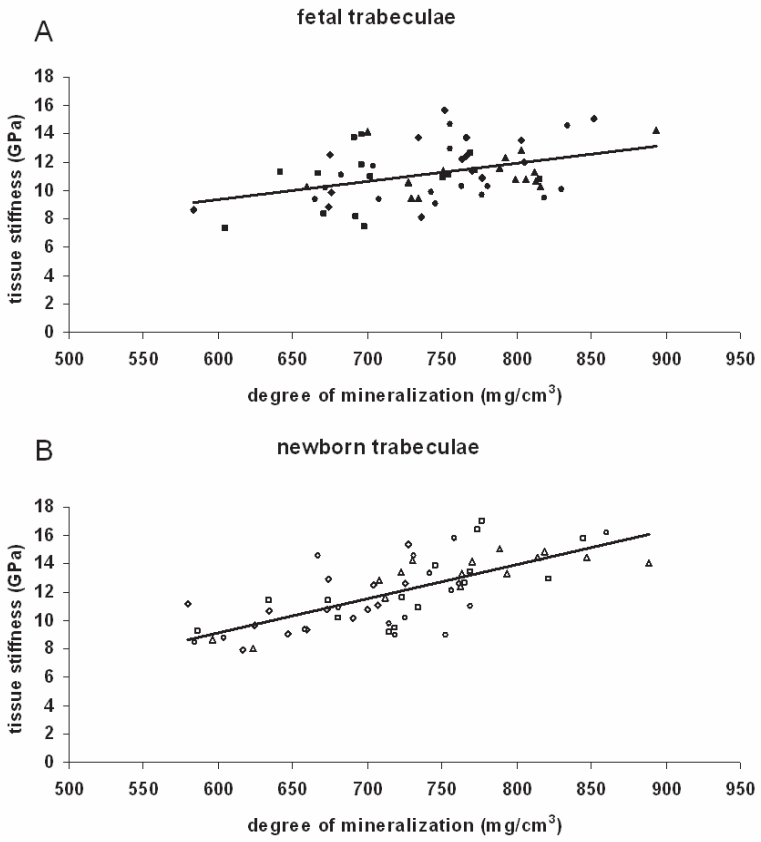

Figure 3. The relationship between tissue stiffness and degree of mineralization. A: Fetal trabeculae. B: Newborn trabeculae. Note that the four fetal and four newborn samples were individually represented using differently shaped cursors. Fetal: range over all indents: 7.4 - 15.6 GPa, Newborn: range over all indents: 8.0 - 17.0 GPa.

Discussion

In this study the relationship between mechanical properties as measured with nanoindentation and the degree of mineralization of trabecular bone was investigated for the first time. Understanding this relationship is important for the comprehension of the mechanical behavior of bone at both the tissue and apparent level. This may, for instance, add to the development of more accurate finite element models when tissue moduli need to be incorporated.

The values for tissue stiffness found in the present study (11.2 and 12.0 GPa) are low in comparison to adult bone tissue as characterized by nanoindentation. Generally the mean values are around 20 GPa for both trabecular and cortical bone tissue (e.g. Hengsberger et al., 2002; Rho et al., 2002). Comparison with the literature is, however, difficult due to the large variation in indentation load rates applied. Because of the viscoelastic nature of the bone tissue, the measured tissue modulus will be higher when higher load rates are applied (Fan and Rho, 2003). The rate applied in the present study (80 µN/s) is about a tenth of the load rate as applied in several other studies (Rho et al., 1999; Roy et al., 1999; Rho et al., 2002). The present results are in accordance with values found for adult trabecular bone tissue of the human femur characterized using nanoindentation in which similar load rates were applied (Zysset et al., 1998; 1999). Furthermore, the present results are in accordance with ones found in human fetal femurs (Su et al., 1997). Taking the differences in load rate into account, they also comply with those of adult trabecular bone of human vertebra (Rho et al., 1999; Roy et al., 1999; Rho et al., 2002), despite a difference in tissue type (woven vs. lamellar) (Currey, 1998). It seems therefore, that the elasticity of bone tissue in the cores of trabecular elements of fetal and newborn specimens is quite similar to that of adult trabecular bone in terms of tissue stiffness.

The finding that the degree of mineralization in the anterior regions of the mandibular condyle did not differ between fetal and newborn condylar specimens is in contrast to previous findings (Mulder et al., 2005; 2006b). This difference might be caused by the fact that in the present study for both age groups, trabecular elements of equal thickness (approximately 110 µm) were analyzed. The previous data related to all trabecular elements in a certain volume of interest, irrespective of their thickness. Thicker elements are presumably more highly mineralized than thinner ones as the bone tissue in their cores has had more time to mature (Paschalis et al., 1997; Mulder et al., 2005). Thus, the trabeculae of both groups might be made up out of bone tissue of similar age. The same explanation holds true for the similar values for tissue stiffness of the both age groups.

The observed relationship between degree of mineralization and tissue stiffness is in accordance with the relationship, which was constructed using a variety of species, according to $\log E_t = -8.58 + 4.05*\log[Ca]$ (Currey, 1999). Envelopes representing the variation in the determined variables show considerable overlap (Fig. 4). It thus seems that fetal and newborn trabecular bone tissue of the pig complies with bone material of other species in terms of mineralization and tissue stiffness. However, the relationship found in the present study

contrasts strongly with another relationship found using human femoral bone from two donors (Hengsberger et al., 2002).

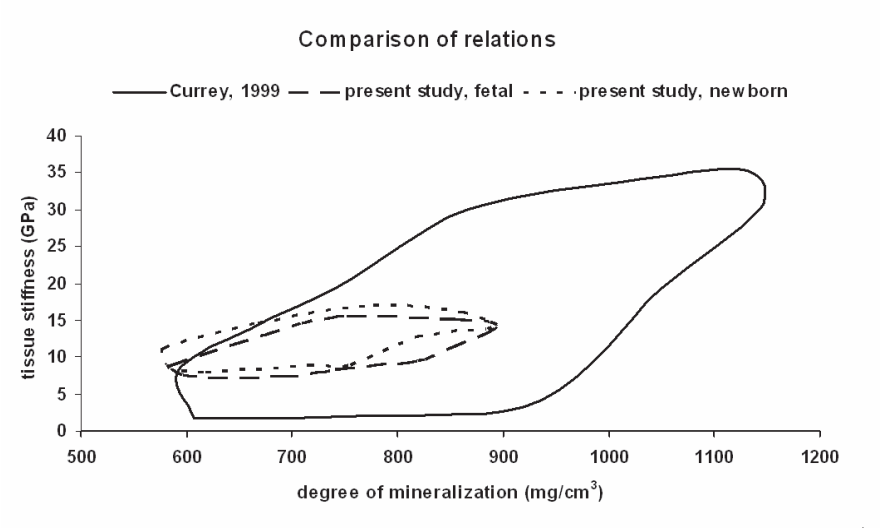

Figure 4. Comparison of the relationship between degree of mineralization and tissue stiffness found in the present study with a previously established relationship by Currey, 1999. Envelopes represent the variation in data points.

Despite the general agreement, the relationship differed between fetal and newborn groups. This might be caused by systematic differences in mineral composition. It has, for example, been shown that from the fetal to newborn stage, there is an increase in ash fraction, weight percentages of calcium and phosphate, and Ca/P ratio (Mulder et al., 2006c). This might in turn be related to differences in organization and stacking of minerals and differences in crystal size and perfection. Also, changes in overall tissue anisotropy could have influenced the tissue stiffness in the sagittal plane (Rho et al., 1997; Rho et al., 1999; Roy et al., 1999; Swadener et al., 2001; Fan et al., 2002). This means that for a similar regional difference in degree of mineralization between fetal and newborn specimens, the difference in tissue stiffness between the two age groups will be proportionally higher.

The results for nanoindentation in bone specimens are known to be dependent on the loading direction. Adult trabecular bone that has been subject to secondary remodeling consists mainly of lamellar bone tissue which displays a strong mechanical anisotropy (Rho et al., 1997; Swadener et al., 2001; Fan et al., 2002). This is reflected by the fact that indentation

testing on different planes in single bone specimens revealed that the bone tissue with the highest tissue stiffness corresponded with the long bone axis. As in the present study the specimens were tested in a mediolateral direction, this dependency was disregarded. The fetal and newborn specimens investigated here supposedly consist mostly of woven bone, which has almost no directional differences in mechanical properties (Currey, 1998). The almost random alignment of the collagen fibrils makes the mechanical properties of woven bone nearly isotropic under loading (Buckwalter et al., 1995). The collagen in woven bone is fine-fibred, 0.1 μm in diameter and oriented almost randomly, so it is difficult to make out any preferred direction over distances greater than about 50 μm (Currey, 1998). If anisotropy were present then our measurements would represent a weighted average of anisotropic moduli.

A few remarks have to be made about the methods used. First, the elastic modulus of the specimen (E_t) was derived from the stiffness using equations (1) and (2). Equation (1) was derived making the assumption that the tested material is elastically homogeneous and isotropic. When used to measure the tissue stiffness of an anisotropic material (such as adult and perhaps fetal bone), the modulus derived from this equation would be a weighted average of the anisotropic elastic constants (Rho et al., 1997). Second, a Poisson's ratio of 0.3 was assumed while determining the tissue stiffness. Although this is generally accepted as reasonable it is not unambiguously established (Guo and Goldstein, 2000). Third, the effects of the dehydration steps and embedding procedure on the mechanical properties have to be taken into consideration. While it is possible that PMMA embedding alters bone matrix properties either because of infiltration or high-temperature curing, it has been shown that this does not affect nanoindentation results (Silva et al., 2004). In contrast, the dehydration process has been demonstrated to be able to increase tissue stiffness by as much as 22.6% (Guo and Goldstein, 2000). It is unknown if the dehydration has a comparable effect on fetal bone. If this should be similar, it would imply that the tissue stiffness of the analyzed samples could be closer to 9-10 GPa. Such would augment the fit of the present results with the relationship between mineralization and tissue stiffness presented by Currey (1999). Finally, it is known that boundaries in microCT reconstructions are prone to so-called partial volume effects. Mineralization values of voxels at such boundaries will be underestimated as they only partially represent bone. Similarly, indentations performed close to the bone-embedding medium boundary can be unreliable as the embedding medium can be involved. In the present study, indentations near the trabecular edges were avoided as both the degree of mineralization and the nanoindentation results were acquired in the core of trabecular elements. It is, however, difficult to say if the indentations were truly performed in the cores

of trabecular elements as only the two-dimensional surface is exposed and the three-dimensional shape would only be determined from part of the trabecular element. This would give rise to a spread in degree of mineralization and tissue stiffness values as trabecular elements have an increasing degree of mineralization from the surface to their core (Mulder et al., 2005). It remains to be investigated how the tissue stiffness is distributed intratrabecularly.

In conclusion, both the bone tissue stiffness and the degree of mineralization in the cores of relatively thick trabecular elements were quantified and were found to be independent of fetal development. This suggests that bone tissue in these regions is already highly mature and resembles adult trabecular bone tissue properties. A strong relationship was found between the tissue stiffness and the degree of mineralization in both the fetal and newborn specimens.

CHAPTER 9

INTRATRABECULAR DISTRIBUTION OF TISSUE STIFFNESS IN DEVELOPING TRABECULAR BONE

Abstract

It is unknown how bone tissue stiffness is distributed within trabeculae and if it corroborates with intratrabecular variation in degree of mineralization. Understanding these variations is important for the comprehension of bone mechanical behavior at the tissue and apparent level and may provide insight into cell-mediated adaptation processes as modeling and remodeling activities and into deformation mechanisms of the bone microstructure. The purpose of the present study was, therefore, to investigate the tissue stiffness and the location corresponding degree of mineralization and second, to examine possible changes during prenatal development. Mandibular condylar specimens from four fetal and four newborn pigs were used. Tissue stiffness was measured using nanoindentation, whereas the degree of mineralization was assessed using three-dimensional microCT reconstructions. An array of eight indents was made over the trabecular width of 15 trabeculae in each of the eight specimens, leading to a total of 960 indents. Subsequently, the degree of mineralization of these locations was determined. The distribution of tissue stiffness and degree of mineralization showed similar and characteristic parabolic patterns, with the lowest values at the trabecular surface and highest values in their cores. Thereby, a significant relationship between tissue stiffness and degree of mineralization was found. From the fetal to the newborn stage, an increase in average tissue stiffness was observed, which was attributed to higher tissue stiffness at the trabecular surface of the newborns. It was concluded that bone tissue in fetal and newborn trabecular cores is already highly mature and resembles adult trabecular bone tissue properties. The similar distribution of tissue stiffness and degree of mineralization conforms and adds to previously reported relationships between mineralization and tissue stiffness. For the first time, it was shown that the intratrabecular tissue stiffness develops along the same path as the degree of mineralization and causality is suspected.

Introduction

Adult bone material is heterogeneous and at any moment comprises a collection of elements of older or younger 'tissue' (Parfitt et al., 1983; Rho et al., 2002). It has also been shown that tissue mineralization varies spatially within trabeculae of fetal bone (Meneghini et al., 2003; Mulder, 2005), similar to adult bone (Paschalis et al., 1997), due to continuous modeling and remodeling processes. The fetal skeleton is formed by woven bone which has a rapid rate of deposition, whereas adult bone is composed of lamellar bone. Little is known about the mechanical properties of woven bone. Its irregular collagen-fibril orientation and irregular pattern of mineralization make it more flexible and more easily deformable than lamellar bone. Despite a higher final degree of mineralization it remains mechanically inferior (Currey, 1998).

It has been previously shown that besides changes in micro-architecture, the average degree of mineralization of presumptive trabecular bone of the pig mandibular condyle increases during development (Mulder et al., 2005). Furthermore, it has been shown that the degree of mineralization increases gradually in a distinct pattern from the surface of trabecular elements towards their core. These intratrabecular variations are in agreement with the process of bone formation on the surface of trabeculae, after which it becomes more mineralized and rigid with age (Ziv et al., 1996). It is known that bone tissue stiffness depends heavily on its degree of mineralization (Currey, 1999; Mulder et al., 2006a). It is, however, still unknown how the degree of mineralization in individual trabecular elements is related to the mechanical properties at the tissue level, thus whether the stiffness and degree of mineralization display similar intratrabecular variation.

Understanding this tissue stiffness and degree of mineralization variation and their relationship is important for the comprehension of the mechanical behavior of bone at both the tissue and apparent level (Turner et al., 1990; van der Linden et al, 2001; Bourne and van der Meulen, 2004; Follet et al., 2004; Mulder et al., 2006e). Accurate finite element modeling of bones is limited by the accuracy of the parameters used as input. The use of inaccurate input values could lead to a misinterpretation of the structural functions of the bone as a whole as well as for the intratrabecular distribution of stress and strain related parameters (Mulder et al., 2006e). The latter may provide insight into cell-mediated adaptation processes as modeling and remodeling activities and into deformation mechanisms of the bone microstructure.

The local degree of mineralization of trabecular bone can be assessed by microCT (Mulder et al., 2004). The tissue stiffness can be measured using nanoindentation (Malzbender et al., 2002). Over the past 10 years, this technique has been used frequently to assess the intrinsic mechanical properties of bone tissue. These mechanical properties were found to vary greatly between different species (Currey 2003), individuals (Zysset et al., 1998), anatomical locations (Rho et al., 2001; Hengsberger et al., 2005), bone structural units (Rho et al., 1997; Rho et al., 1999; Roy et al., 1999; Zysset et al., 1999; Xu et al., 2003), and direction of testing (longitudinal vs. transverse) (Rho et al., 1997; Rho et al., 1999; Roy et al., 1999; Swadener et al., 2001; Fan et al., 2002). In mature humans, the bone tissue mechanical properties appeared not to change with age (Zysset et al., 1998; Rho et al., 2002). Using nanoindentation, it was found that newly formed bony lamellae in human fetal femurs, deposited during early development on the periosteal surface, have a lower tissue stiffness than bone lamellae already present (Su et al., 1997). Furthermore, it was established that on average bone tissue stiffness increases with fetal age. However, such measurements were not performed on trabecular elements. Neither was tissue stiffness related to other properties like the local degree of mineralization on trabecular level and its intratrabecular distribution has not been investigated.

The goal of this study was, to determine the intratrabecular variation in tissue mechanical properties of the trabecular bone tissue in the mandibular condyle, to relate it to the distribution of the degree of mineralization and to establish how both these variables change during development. To pursue these goals mandibular condyles of fetal and newborn pigs were investigated. The tissue stiffness was determined using nanoindentation and the degree of mineralization was assessed with micro-computed tomography (microCT).

Material and methods

The trabecular bone in the left mandibular condyle from eight pigs (standard Dutch commercial hybrid race) was examined. Four fetal specimens (estimated age: 70 days of gestation, mean weight: 375 g) and four newborn specimens (approximately 112-115 days post conception, mean weight: 1351 g) were used. The fetuses were obtained from slaughtered sows in a commercial slaughterhouse and their age was estimated from the mean weight of the litter using growth curves (Evans and Sack, 1973). The newborn specimens

were acquired from the experimental farm of the Faculty of Veterinary Medicine in Utrecht, The Netherlands, and were euthanised by an intravenous overdose of ketamine (Narcetan) after premedication. The specimens were obtained from other experiments that were approved by the Committee for Animal Experimentation of the Faculty of Veterinary Medicine, Utrecht, the Netherlands. They were stored at -20°C prior to assessment.

The mandibles were prepared by dissection from the heads and cut in half at the symphyseal region. In the fetal group, the ramus along with the coronoid and condylar process was isolated from the rest of the left hemi-mandible. In the newborn group only the top part of the ramus with attaching coronoid and condylar process was isolated.

All specimens were dehydrated in graded ethanol solutions (70-100%) and embedded in polymethylmethacrylate (PMMA) (Merck, Darmstadt, Germany) with the lateral side facing down. The embedded bones were sectioned using a microtome (Leica, Nussloch, Germany) in the sagittal plane approximately halfway between the medial and lateral condylar pole, exposing the trabecular microstructure at the surface. The exposed surface was ground with successively finer grades of abrasive paper (grit size: 400, 600, 1200) under deionized water and polished on microcloth with an aluminum polishing solution (0.05 μm particle size) (Buehler, Lake Bluff, IL).

A coordinate system was created on the polished surface in order to be able to retrace the locations of individual indents in microCT scans, as the indentations themselves were too small to be detected in microCT reconstructions (see below). Crosshairs (approximate width 10 μm) were etched on the polished surface of the specimens (Fig. 1). Near the end of the lines, just within the confines of the sample as well as on the crossing, small holes (diameter approximately 20 μm) were drilled that were filled with an aluminumoxide powder and sealed with wax. The crosshairs and filled holes were detectable under the nanoindentation optical microscope, whereas in microCT reconstructions only the latter were perceptible clearly. Coordinates were attributed to the approximate center of the holes under the optical microscope. The coordinates of all indents were established relative to the same coordinate system and, therefore, the position of an indent relative to the holes could be determined. This enabled to determine the exact positions of the indents in trabecular tissue as reconstructed with microCT.

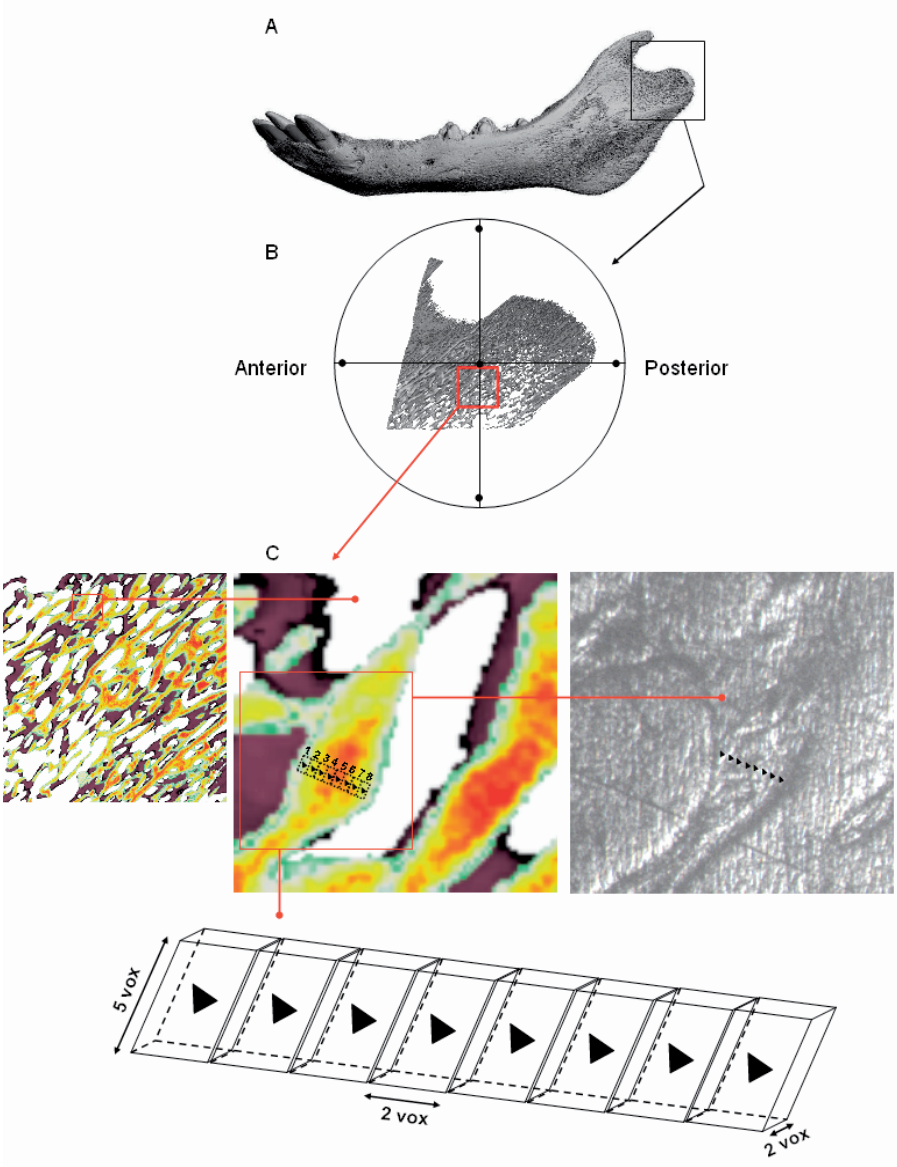

Figure 1. Sample preparation. A: Three-dimensional reconstruction of a newborn pig mandible. B: Graphical representation of an embedded newborn specimen, which was cut sagittally through the condyle, revealing the trabecular structure envisioned here with a microCT reconstruction. Note the vertical and horizontal crosshairs, which acted as a coordinate system. C: Magnified portion of B, visualizing the trabecular structure. Degree of mineralization depicted with color scale (increasing degree of mineralization from blue to red). Dashed rectangles: regions, containing location of indents, in which mean degree of mineralization was determined (see also magnification below that). Right: Optical microscope image of the same trabecular element as in middle image. The locations of indentation (triangles) are depicted.

Nanoindentation

Load-control nanoindentation tests (Nano Indenter XP, MTS Systems Co., Oak Ridge, TN) were performed on the embedded specimens using a Berkovich diamond indenter. The tests were performed in a vibration isolation cabinet at room temperature and stable humidity to ensure that the influence of thermal drift was minimal. Based on optical microscope observations, trabecular elements were selected in the anterior part of the mandibular condyle as this region contains abundant trabeculae of considerable thickness (Mulder et al., 2005). It was ensured that trabecular elements with approximately the same width were selected (approximately 110 µm). Subsequently, an array of eight indents was performed spanning the width of each of the selected trabeculae and the coordinates of the indents were registered (Fig. 1). The trabeculae that were assessed were oriented in an oblique superoinferior way. The array of indents ran from the anterior side to the posterior one. The distance between two consecutive indents was 15 micrometer. In total, 15 trabecular elements were tested per condylar specimen accumulating to a total of 960 indents in this study (8 specimens x 15 trabecular elements per specimen x 8 indents per trabecular element).

The load protocol (similar to Mittra et al., 2006) comprised two conditioning steps before maximal load was applied (Fig. 2A). In the first conditioning step a 2 mN load was realized in 100 s followed by a 50 s holding period. Thereafter, unloading to 10% of the load was realized in 100 s followed by a second conditioning step to a load of 4 mN. Finally, a load step with a peak load of 8 mN (load rate: 80 µN/s) was applied. A 50 s holding period was inserted prior to final unloading (unloading rate: 80 µN/s) to reduce viscoelastic deformation to a negligible rate (Rho et al., 1997; Mittra et al., 2006). A holding step at 10% of peak load for 100 s was used to establish the rate of thermal expansion of the indenter apparatus with which the displacement data was corrected afterwards.

The indentation depths at maximum load were approximately one micrometer, which has been shown to be sufficient in relation to the surface roughness of the bone samples polished using similar methods (Hoc et al., 2006).

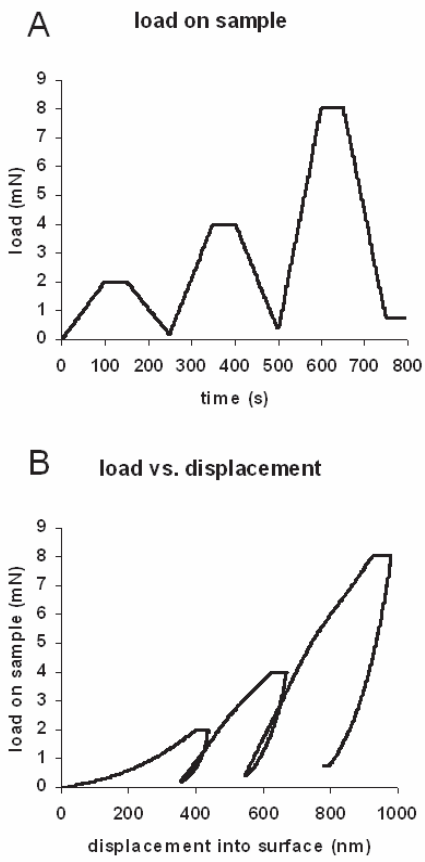

Figure 2. A: Nanoindentation protocol. The protocol comprised a loading step in 100 s to 2 mN followed by a 50 s holding period. After the holding period, unloading to 10% of the load was realized in 100 s followed by a similar procedure to a load of 4 mN and finally to the peak load of 8 mN (load rate: 80 µN/s). B: Typical load-displacement curve. The tissue stiffness was determined from the slope at the beginning of the final unloading step at maximum depth. Note that during holding periods substantial time-dependent response is present, which points to the viscoelastic nature of the bone tissue.

From this protocol a typical load-displacement curve was obtained (Fig. 2B) and the Oliver and Pharr method was applied to determine the elastic modulus (Oliver and Pharr, 1992). Using the contact area A_c, and the contact stiffness S, which is the slope of the initial portion of the final unloading curve, assumingly representing a purely elastic effect, the reduced modulus (E_r) of the specimen-indenter combination was determined according to:

$$E_r = \frac{\sqrt{\pi}}{2}\frac{S}{\sqrt{A_c}}. \quad (1)$$

The contact area A_c was determined from the load-displacement curve according to the method described by Oliver and Pharr (1992). For this method, the tip shape of the indenter needs to be known, and this was determined using calibration measurements on fused silica. The specimen (bone) tissue modulus (E_t) follows from

$$E_t = \frac{1-\nu_s^2}{\frac{1}{E_r} - \frac{1-\nu_i^2}{E_i}}, \quad (2)$$

where ν is the Poisson's ratio and the subscripts s and i refer to the bone specimen and the indenter respectively and E_i is the indenter's Young's modulus. The elastic properties of the Berkovich diamond indenter were: $\nu_i = 0.07$ and $E_i = 1140$ GPa. The Poisson's ratio of bone was assumed to be 0.3.

Successive unloading-loading trajectories exhibit hysteresis, as shown in Fig. 2B. This effect, together with the substantial displacement during the holding periods, suggests that the material responds viscoelastically, rather than purely elastically. For the present comparative study, however, an elastic analysis of the results suffices.

MicroCT

Three-dimensional reconstructions of the trabecular bone in the mandibular condyles were obtained by using a high-resolution microCT system (μCT 40; Scanco Medical AG., Bassersdorf, Switzerland). The embedded specimens were ground to smaller dimensions in order to be able to analyze the specimens at a high resolution, which is limited to the diameter of the specimen holders. The coordinate system, however, was kept intact. The specimens were mounted in cylindrical specimen holders (polyetherimide; 20 mm outer diameter; wall thickness, 1.5 mm) and secured with synthetic foam. The specimens were completely submerged in deionized water. The scans yielded an isotropic spatial resolution of 10 μm. A 45 kV peak-voltage X-ray beam was used, which corresponds to an effective energy of approximately 24 keV (Mulder et al., 2004). The microCT was equipped with an aluminum filter and a correction algorithm that reduced the beam hardening artifacts sufficiently to enable quantitative measurements of the degree and distribution of mineralization of developing bone (Mulder et al., 2004). The computed linear attenuation coefficient in each voxel was stored in an attenuation map and represented by a grey value in the reconstruction.

This attenuation coefficient can be considered proportional to the local degree of mineralization (Nuzzo et al, 2003).

Using the coordinate system, individual trabecular elements that had been indented could be retraced in the microCT reconstructions. This enabled to relate the local stiffness of the bone tissue obtained by nanoindentation with the local degree of mineralization determined by microCT. The local degree of mineralization of the indented locations was quantified in rectangular regions (approximately two by five by two voxels (20 x 50 x 20 µm) each containing the location of an indent (Fig. 1). The voxel layer defining the polished surface was omitted, because the absorption values assigned to them are biased due to partial volume effects, i.e. they contain both bone and background (embedding) tissue and the absorption values are thus underestimated.

To determine the average degree of mineralization in such a volume of interest it was segmented using an adaptive threshold which was equal for every specimen. The segmentation was visually checked. In a segmented image, every voxel with a linear attenuation value below this threshold (assumingly representing soft tissue or background) was made transparent and voxels above this threshold (representing bone) kept their original grey value. The outermost voxel layer characterized as bone, defining both the cutting surface as well as the bone-PMMA boundary, were removed as these are likely to be corrupted by partial volume effects. The degree of mineralization was quantified by comparing the attenuation coefficient with reference measurements of a phantom containing hydroxyapatite of 0, 200, 400, 600, and 800 mg/cm^3.

Statistics

Regression analysis was applied to study the relationship between degree of mineralization and tissue stiffness. To quantify the dependency of the tissue stiffness and the degree of mineralization on the distance to the trabecular core, the results of the indents and the location corresponding degree of mineralization were averaged over the specimen. Differences between fetal and newborn specimens with regard to mean tissue stiffness and mean degree of mineralization were statistically assessed using independent-sample t-tests. To analyze the difference between successive intratrabecular regions, a general linear model (repeated measures) was applied. A p-value of 0.05 was considered statistically significant.

Results

For both the fetal and newborn specimens, a clear relationship between tissue stiffness, expressed as elastic modulus, and degree of mineralization was established (Fig. 3). Each data point in this figure represents the average over 15 trabeculae at a specific indentation location (1-8) for each individual specimen. In the fetal group (Fig. 3A), the regression equations was: E_t (GPa) = 0.020*DMB (mg/cm^3) - 4.35 (R = 0.97; P < 0.001), with E_t being the tissue stiffness and DMB the degree of mineralization. In the newborn group (Fig. 3B), the equation was: E_t (GPa) = 0.025*DMB (mg/cm^3) - 5.83 (R = 0.98; P < 0.001).

The intratrabecular variation in tissue stiffness and degree of mineralization showed a regular and similar pattern (Fig. 4). Both the tissue stiffness and degree of mineralization of the trabeculae in both fetal and newborn specimen groups displayed an increase from the anterior surface towards the trabecular core and subsequently decreased again towards the posterior surface in a parabolic manner. Generally, the two anteriormost locations were significantly different from locations in the core, which were in turn significantly different from the three posteriormost locations (P < 0.05). When comparing corresponding indent locations between fetal and newborn specimens, it was observed that the values for tissue stiffness at both the anterior and posterior trabecular surface were always higher (P < 0.05) in the newborn ones. The same is true for the anterior surface regarding the degree of mineralization (P < 0.05).

The mean tissue stiffness of trabecular bone of the mandibular condyle of the fetal group (n=4) measured 7.9 GPa (± 0.6 GPa), whereas in the newborn group (n=4) this was 9.4 GPa (± 0.3 GPa). This was found to be a significant difference (P < 0.01). The average degree of mineralization of the fetal trabeculae was 602 mg/cm^3 (± 17 mg/cm^3). The one in the newborn bone measured 619 mg/cm^3 (± 21 mg/cm^3). No significant difference between them was found.

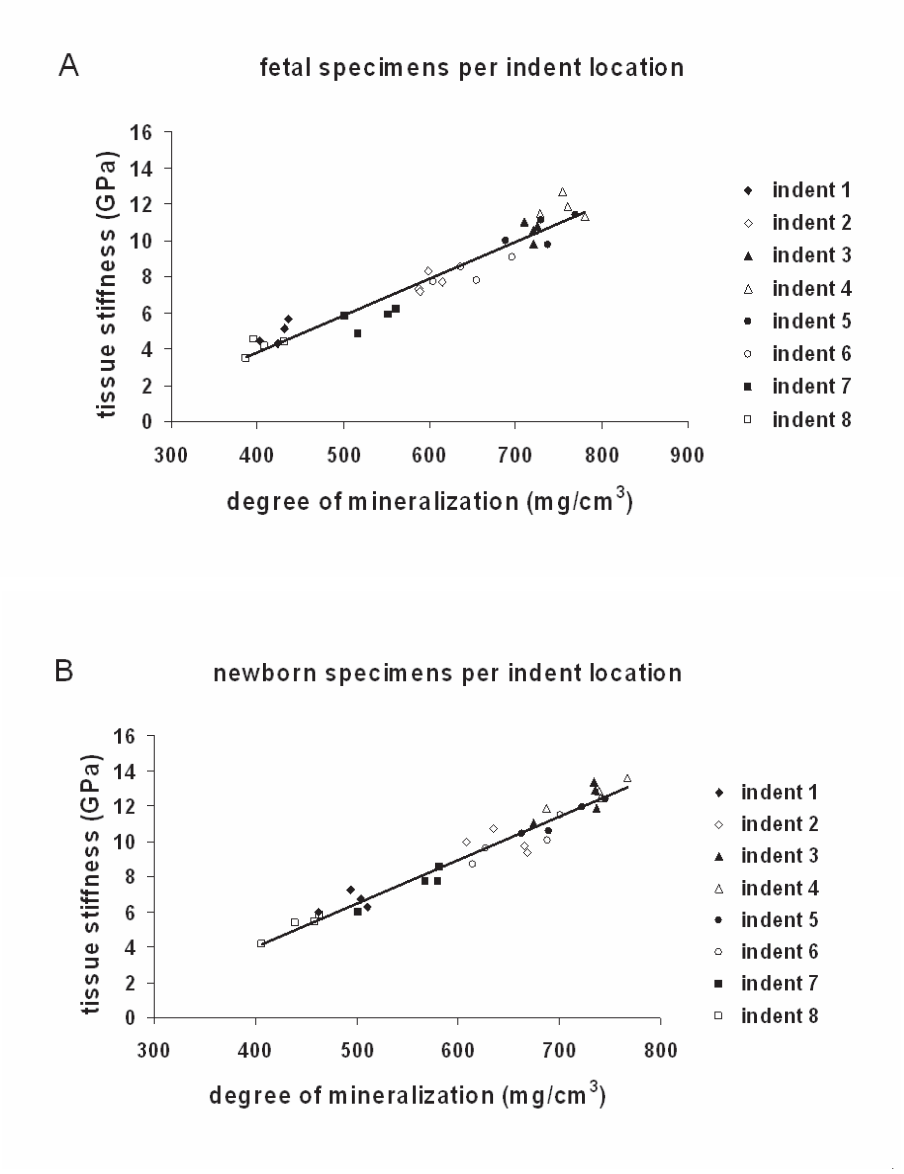

Figure 3. Relationship between tissue stiffness and degree of mineralization. Each data point represents the average over 15 trabeculae at a specific indentation location (1-8; 1 is the anteriormost indent and 8 is the posteriormost indent) for each individual specimen (n=4). A: Fetal specimens. B: Newborn specimens.

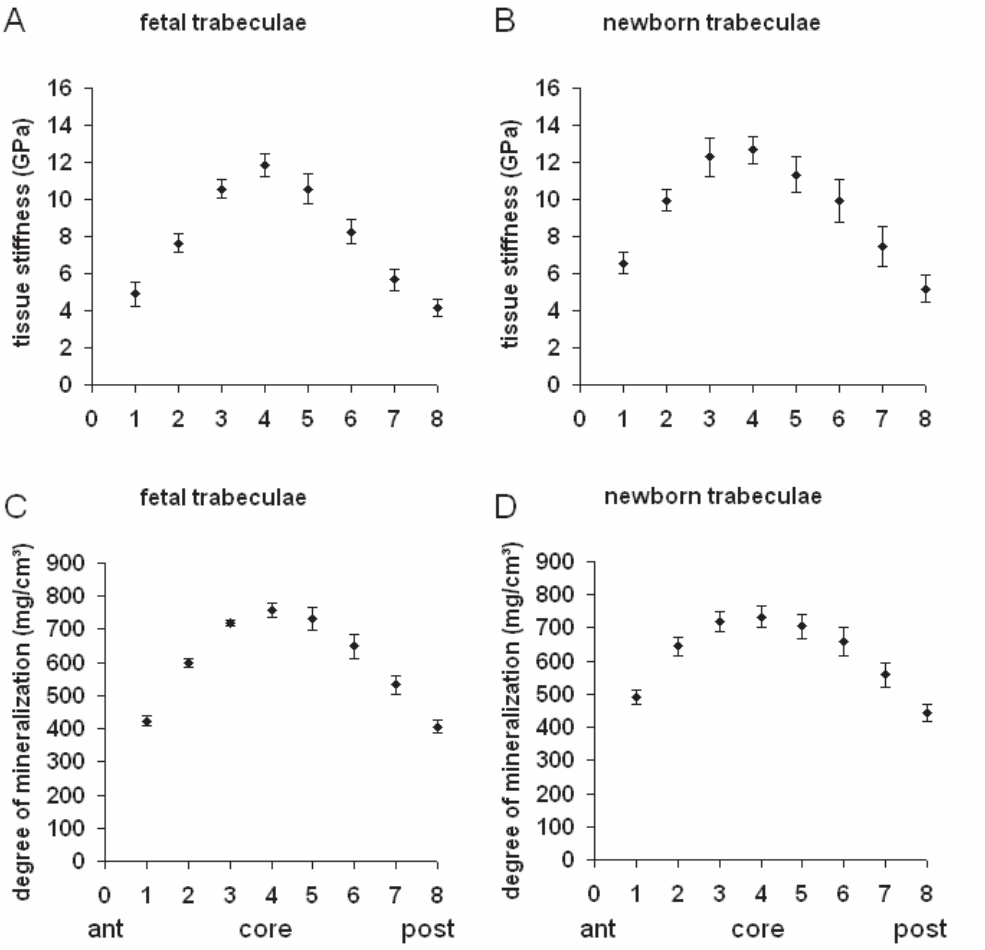

Figure 4. The intratrabecular distribution of tissue stiffness and degree of mineralization (DMB). A: Tissue stiffness distribution in fetal trabeculae. B: Newborn trabeculae. C: Distribution of mineralization in fetal trabeculae. D: Newborn trabeculae.

Discussion

In this study the intratrabecular distribution of bone tissue stiffness was investigated in combination with the degree of mineralization for the first time. These distributions showed a similar trend. A lower degree of mineralization and tissue stiffness were observed near the surface of trabeculae in comparison with their core. This implies a relationship between the degree of mineralization and tissue stiffness which was also established earlier (Mulder et al.,

2006a; Currey, 1999). The lower values at the trabecular surface might indicate modeling and/or remodeling activity and appear to be consistent with the preexisting notions that formation of trabecular bone takes place on the surface of trabeculae, and that newly formed collagenous tissue becomes more mineralized and rigid with age (Paschalis et al., 1997; Meneghini et al., 2003).

The observed intratrabecular heterogeneity of tissue stiffness makes the trabeculae relatively compliant to bending and rigid to compression along their main axis. A less stiff surface presumably results in a greater ability to endure high strains without breaking, as present when trabeculae are loaded in bending, and hence the trabeculae are less prone to fracture. Moreover, due to the relatively low stiffness, the accompanying stresses will remain relatively low. In the cores of the trabecular elements, the high stiffness shields the material from excessive deformation, thus resulting in low strains, but higher stresses. This composition can be considered preferable to prevent crack propagation. Cracks initiated in this tissue might be prevented from continuing through the surface layers, which have lower stiffness and are thus more compliant. This avoids complete fracture of the trabecular elements and enables repair of the damage. This has been confirmed by observation of damaged trabecular elements, where the highly mineralized core contains microcracks, while the mechanical integrity of the elements is maintained by the undisturbed, less mineralized surface (Fyhrie and Schaffler, 1994; Mori et al., 1997).

Many trabeculae displayed the highest values of tissue stiffness and degree of mineralization on the anterior side of the core (data not shown). This suggests a more modeling or remodeling activity on the posterior side of trabecular elements and might be responsible for an increase in thickness or even migration of the element in posterior direction, which has been shown to be the main growth direction of bone structure of the mandibular condyle (Teng and Herring, 1995; Mulder et al., 2005; 2006b).

The values for tissue stiffness found in the present study (4.1 to 12.7 GPa) are low in comparison to adult bone tissue characterized by nanoindentation. Generally the mean values are around 20 GPa for both trabecular and cortical bone tissue (e.g. Hengsberger et al., 2002; Rho et al., 2002). Comparison with the literature is, however, difficult due to the large variation in indentation load rates applied. Because of the viscoelastic nature of the bone tissue, the measured tissue modulus will be higher when higher load rates are applied (Fan and Rho, 2003). The rate applied in the present study (80 μN/s) is about a tenth of the load rate as applied in several other studies (Rho et al., 1999; Roy et al., 1999; Rho et al., 2002). Furthermore, in contrast to these studies, indentation locations relatively close to the boundary

between bone and embedding medium were not disregarded. The present indentation results in the cores of trabeculae are in accordance with values found for adult trabecular bone tissue of the human femur characterized using nanoindentation in which similar load rates were applied (Zysset et al., 1998; 1999), despite a difference in tissue type (woven vs. lamellar) (Currey, 1998). Furthermore, the present indentation results in the cores of trabeculae are in accordance with ones found in human fetal femurs (Su et al., 1997). It, therefore, seems that the elasticity of bone tissue in the cores of trabecular elements of fetal and newborn specimens is similar to that of adult trabecular bone.

In the present study, no significant difference was observed between fetal and newborn stadiums regarding degree of mineralization, whereas previously a significant increase in degree of mineralization was observed in anterior regions of the condyle with advancing development (Mulder et al., 2005; 2006b). This might be caused by the fact that trabecular elements with approximately equal width were selected in both age groups. Thus, the trabeculae of both groups might be made up out of bone tissue of similar age. However, in newborn specimens, higher values were found at the anterior trabecular surface, indicating a decreased modeling or remodeling activity in this region. A significant increase in average tissue stiffness from fetal to newborn stadiums was observed. As there was no increase in tissue stiffness in the cores of trabeculae (Mulder et al., 2006a), the increase in average trabecular tissue stiffness was instigated by an increase in tissue stiffness near the surface of the trabeculae. The increase in average tissue stiffness without an increase in average degree of mineralization might originate from systematic changes in mineral composition. It has been shown, for example, that from the fetal to newborn stage, there is an increase in ash fraction, weight percentages of calcium and phosphate, and Ca/P ratio. This might in turn be related to differences in organization and stacking of minerals and differences in crystal size and perfection (Mulder et al., 2006c).

A few remarks have to be made about the methods used. First, it is known that the estimation of mineralization from microCT reconstructions is prone to the so-called partial volume effect. Similarly, indentations close to the bone-embedding medium boundary may cause an unknown effect of the embedding medium on the measured tissue stiffness. Second, the elastic modulus of the specimen (E_t) is derived from the stiffness using equations (1) and (2). Equation (1) is derived with the assumption that the tested material is elastically homogeneous and isotropic. Third, the effects of the dehydration steps and embedding procedure on mechanical properties have to be taken into consideration. Finally, the results for nanoindentation in bone specimens are known to be dependent on the loading direction.

For a more extensive discussion regarding these points and the consequences that they might have on the results, we refer to chapter 8 (Mulder et al., 2006a).

In conclusion, both the distribution of tissue stiffness and degree of mineralization across trabecular elements were quantified. A characteristic distribution of both the tissue stiffness and the degree of mineralization in the fetal and newborn specimens was observed with lower values near the surface and higher ones in the core. The properties of the bone tissue in the investigated regions appeared to resemble adult trabecular bone tissue. This distribution of mineralization and tissue stiffness conforms and adds to previously reported relationships between mineralization and tissue stiffness. An increase in tissue stiffness with developmental age was observed, while the degree of mineralization remained unchanged. For the first time, it was shown that the tissue stiffness develops along the same path as degree of mineralization and causality is likely.

CHAPTER 10

SUMMARY AND CONCLUSIONS

Bones have a compact shell, which surrounds a core of trabecular bone. The bone is optimally adjusted to withstand forces and is responsible for the absorption, transfer, and distribution of loads that are exerted during daily function, such as mastication. These loads induce deformations (strains) and tensions (stresses) within the bone tissue. These instigate bone modeling and remodeling processes, during which the architecture of the bone structure and its degree and distribution of mineralization are adjusted to maintain the optimal load-resisting situation. Changes in architecture and mineralization of trabecular and compact bone are pronounced especially during prenatal development. Knowledge regarding architecture and mineralization of developing bone will augment the understanding of normal bone development and provides valuable information on bone formation and regeneration during, for example, fracture healing. Until now, precise information on changes in architecture and mineralization of developing bone is lacking.

Architecture and mineralization are dominant determinants of strength and deformability of bone and changes in them have consequences for the bone's mechanical properties on the apparent and tissue level. Apparent mechanical properties (e.g. apparent stiffness) are important characteristics of bones as they are, for example, a measure of their capability to resist deformation and thus of fracture risk. Tissue level mechanical properties (e.g. the tissue stiffness) are important, as they have an effect on, for example, intratrabecular distributions of stress and strain. Quantitative knowledge about the three-dimensional intratrabecular tissue stress and strain distributions provides information on the nature of bone deformation during loading. It may, additionally, give insight into micro-crack initiation and propagation behavior, which is considered to be influenced considerably by heterogeneity in bone mineralization. Thus far, it is unknown what the specific influence is of developmental changes in architecture and mineralization on the apparent and tissue level mechanical properties and what the relationship is between mineralization and tissue stiffness.

Therefore, the aim of the present study was to examine the changes in architecture and mineralization in developing bone and how this influences the bone's biomechanical properties on the apparent and tissue level. The jaw bone can be considered a suitable model for bone development, maturation and adaptation. In the present study, the jaw bone of developing pigs, from fetal to newborn stages, was investigated. The architectural and mineralization properties were assessed using micro-computed tomography (microCT). The separate influence of changes in these properties on the mechanical properties of the trabecular bone structure was explored by applying finite element models. They were applied to assess both the bone's apparent mechanical properties and the intratrabecular distribution of strains and stresses. The relationship between the degree of mineralization of bone and the tissue stiffness was examined by relating estimations obtained with microCT to measurements performed with nanoindentation.

Quantification of bone mineralization with microCT

Quantification of the degree of mineralization is not straightforward as commercial microCT systems are equipped with polychromatic X-ray sources, which may lead to beam hardening artifacts. The impact of this artifact is proportional to the bone mineral content. As developing bone is assumingly less mineralized than mature bone, the artifact is likely to be less pronounced. The accuracy was tested with reference salt solutions of known mineral concentrations (chapter 2). Up to the highest concentration (800 mg/cm^3) tested in this study, the relationship between attenuation and solution concentration appeared linear. The estimated uncertainty was proportional to the mineral concentration, the size of the sample, and the energy of the X-ray beam. In general, it was 10% or less. It was concluded that the accuracy of microCT can be considered adequate for the determination of the degree of mineralization of developing bone. It provides a means to simultaneously investigate the three-dimensional bone architecture and degree of mineralization during development in a non-destructive manner and with high resolution.

Architecture and mineralization of the developing jaw bone

Up till now, very limited quantitative information was available on the three-dimensional architecture and the degree of mineralization of the developing jaw bone. Developmental changes were closely monitored using microCT. The research was focused on the mandibular condyle (chapter 3), on the differences between compact and trabecular bone during

development (chapter 4), and on regional differences within and between the mandibular condyle and corpus (chapter 5).

It was found that the front side of the condyle displays a more advanced state of structural bone remodeling than the rear, where more active growth takes place (chapter 3). Furthermore, the intratrabecular distribution of mineralization indicated that apposition of new bone material takes place on the surface of trabeculae, where mineralized tissue with a low degree of mineralization was observed. In their cores, bone tissue with a higher degree of mineralization was detected that matures and becomes more highly mineralized during development, leading to an increase in average degree of mineralization of the condyle during development. Both the trabecular and compact bone of the mandible were found to develop from a trabecular-like structure (chapter 4). In presumptive compact bone the trabecular elements coalesce to transform into compact bone. Considerable changes in bone architecture in the corpus at the age of approximately 70 days of gestation and the appearance of trabecular bone in the condyle at this age are assumingly related to the onset of functional loading of the mandible by developing masticatory muscles. Considerable changes in the pace of mineralization at this age were not found. The growth of the condyle and corpus was reflected by regional differences. The anterior and inferior regions of the condyle were characterized by a more dense bone structure and a higher mineralization as compared to posterior and superior regions, respectively. In the corpus growth was mainly indicated by differences between buccal and lingual plates as well as between anterior, middle, and posterior regions, characterized by a more compact structure and higher mineralization in the lingual and middle regions. In conclusion, the architecture and mineralization of the bone in the condyle and corpus start to deviate early during fetal development towards their destiny as trabecular or compact bone. They reflect known developmental growth directions.

Biomechanical consequences of changes in architecture and mineralization

In order to analyze the biomechanical consequences of the observed changes in architecture and mineralization, finite element models were created from the microCT reconstructions of condylar trabecular bone of two groups of pigs with different developmental age. Models with and without the incorporation of the distribution of mineralization, expressed as tissue stiffness distribution, were developed to separately examine the influence that the developmental changes in architecture and the degree and distribution of mineralization had on the apparent mechanical properties (chapter 6) and on the intratrabecular distributions of tissue stress and strain (chapter 7).

It was found that changes in architecture from fetal to newborn stages had very little effect on the apparent mechanical properties, whereas the increase in the average degree of mineralization was the dominant factor leading to an increase in the apparent stiffness of the trabecular structure in both compression and shear (chapter 6). The distribution of mineralization appeared to cause a marginal decrease in average apparent stiffness. The effect on the directional dependency of the stiffness was stronger. The mechanical anisotropy increased significantly, when the distribution was taken into account. This denotes that differently oriented trabecular elements might have a different degree of mineralization. It was concluded that disregarding the distribution of mineralization is associated with an overestimation of apparent stiffness.

From the surface of trabecular elements towards their core the amount of strain decreased irrespective of the distribution of mineralization (chapter 7). This indicates that the trabecular elements are bended during compression of the whole bone. Stress appeared to increase from the trabecular surface towards the core. However, disregarding the distribution of mineralization resulted in a high stress at the surface which decreased towards the core. It was concluded that the observed heterogeneity in mineralization makes the trabeculae relatively compliant to bending and rigid to compression along their main axis. A less mineralized surface presumably demonstrates a greater ability to withstand the strains without breaking, as present when trabeculae are loaded in bending, and hence the trabeculae are less prone to fracture.

Relationship between tissue stiffness and degree of mineralization

As the relationship between the degree of mineralization in individual trabecular elements and the tissue stiffness had not been established unambiguously before, this was assessed by comparing results from nanoindentation with those obtained with microCT (chapter 8). In this analysis, the intratrabecular distribution of the degree of mineralization was taken into account (chapter 9). Nanoindentation was applied to measure the tissue stiffness and microCT for the estimation of the local degree of mineralization in two groups of pigs (fetal and newborn). An array of indents was performed spanning the width of each of the selected trabeculae.

A significant relationship existed between tissue stiffness and degree of mineralization for both fetal and newborn stages. Between these two groups, the relationship differed. The distribution of tissue stiffness and degree of mineralization showed similar characteristic parabolic patterns across trabecular elements, with the lowest values at the trabecular surface

and the highest values in their cores. From the fetal to the newborn stage, an increase in average tissue stiffness was observed, which was attributed to a higher tissue stiffness at the trabecular surface of the newborns. For the first time, it was shown that intratrabecular tissue stiffness is directly related to the degree of mineralization.

SAMENVATTING EN CONCLUSIES

Botten bestaan uit een kern van trabeculair bot die omgeven wordt door een omhulsel van compact bot. Het bot is optimaal aangepast om krachten op te vangen die er op worden uitgeoefend tijdens normale, dagelijkse functies, zoals het kauwen van voedsel. Daarbij treden vervormingen en spanningen in het botweefsel op. Deze spelen een rol bij de botvorming en botadaptatie. Hierdoor worden de vorm en de structuur van het bot steeds aangepast, waardoor een optimale situatie ten opzichte van het optredende krachtenpatroon gehandhaafd blijft. Tijdens de vorming van nieuw botweefsel worden daar mineralen in afgezet. De mineralisatiegraad neemt toe naarmate het botweefsel ouder wordt. Vooral gedurende de prenatale ontwikkeling treden er grote veranderingen op in de architectuur en mineralisatie van zowel compact als trabeculair bot. Het analyseren van deze veranderingen is belangrijk om de normale botontwikkeling beter te leren begrijpen. Bovendien levert het informatie op over de vorming en regeneratie van botweefsel tijdens bijvoorbeeld de genezing van botbreuken of als gevolg van therapie van botaandoeningen. De prenatale botontwikkeling vertoont daar vaak veel overeenkomsten mee. Tot nu toe is er over de prenatale veranderingen in architectuur en mineralisatie van bot nog weinig informatie beschikbaar.

Botarchitectuur en mineralisatiegraad hebben grote invloed op de mechanische eigenschappen (b.v. stijfheid, sterkte) van zowel de gehele botstructuur als het botweefsel. Op structuurniveau is bijvoorbeeld de structuurstijfheid (Engels: apparent stiffness) een maat voor de vervormbaarheid (elasticiteit) van de botstructuur. Op weefselniveau is bijvoorbeeld de weefselstijfheid (Engels: tissue stiffness) van invloed op de verdeling van spanningen en vervormingen in de botbalkjes (trabekels) ten gevolge van uitwendige belasting. Kwantitatieve kennis omtrent de driedimensionale verdeling van deze spanningen en vervormingen vertelt iets over het vervormingsgedrag van trabeculair bot tijdens botbelasting. Dit is onder andere van belang om inzicht te krijgen in het ontstaan en de verspreiding van scheurtjes in het botweefsel. Tot nu toe is het echter onbekend wat de exacte invloed is van veranderingen in architectuur en mineralisatie van bot tijdens de ontwikkeling op zijn

mechanische eigenschappen. Het is ook niet bekend wat de relatie is tussen mineralisatie en weefselstijfheid.

In dit proefschrift worden de veranderingen in architectuur en mineralisatie van het compacte en trabeculaire bot in de ontwikkelende onderkaak beschreven en worden de mechanische consequenties van deze veranderingen geanalyseerd. Het kaakbot is in deze een geschikt model omdat het relatief vroeg tijdens de prenatale ontwikkeling verbeent waardoor het hele scala van aanleg en adaptatie vanaf vroege prenatale stadia onderzocht kan worden. Daarbij komt dat de ontwikkeling en belasting in het kaakbot lokaal zeer verschillend zijn. In het huidige onderzoek is gebruik gemaakt van onderkaken van varkens in verschillende stadia van prenatale ontwikkeling. Daarvan werden de driedimensionale architectuur en mineralisatie onderzocht met behulp van microCT. De afzonderlijke invloed van architectuur- en mineralisatieveranderingen op de mechanische eigenschappen werd in kaart gebracht door het toepassen van eindige elementen modellen. Deze modellen kunnen gebruikt worden om de mechanische eigenschappen van het bot op zowel structuurniveau als op weefselniveau (de verdelingen van spanningen en vervormingen binnen de trabekels) te analyseren. De relatie tussen mineralisatiegraad en weefselstijfheid werd bepaald door de mineralisatiegraad gemeten met microCT te vergelijken met directe metingen van de weefselstijfheid met behulp van nanoindentatie.

Kwantitatieve bepaling van mineralisatie met behulp van microCT

Het bepalen van de mineralisatiegraad met microCT is niet vanzelfsprekend. Dit komt doordat microCT-apparatuur uitgerust is met polychromatische (meerdere energieën bevattende) röntgenbronnen. Dit leidt tot absorptieartefacten (Engels: beam hardening). Hierdoor is de röntgenabsorptie niet altijd evenredig met de mineralisatiegraad van het te onderzoeken object. De afwijkingen nemen toe met de mineralisatiegraad en de grootte van het object. Omdat nog niet volledig ontwikkeld bot minder sterk gemineraliseerd is, zullen de afwijkingen daar waarschijnlijk binnen acceptabele grenzen blijven. De nauwkeurigheid van het bepalen van de mineralisatiegraad met microCT werd bepaald met behulp van verschillende concentraties zoutoplossingen. De met microCT verkregen waarden werden vergeleken met theoretische waarden (hoofdstuk 2). Tot en met de hoogste concentratie (800 mg/cm^3) bleek de relatie tussen de gemeten absorptie en de zoutconcentratie een rechtlijnig verband te hebben. De afwijkingen tussen de gemeten en theoretische waarden bleken over het algemeen onder de 10% te liggen. We concludeerden daarom dat de nauwkeurigheid van microCT toereikend is voor bepaling van de mineralisatiegraad in zich ontwikkelend bot. Dit

geeft de mogelijkheid om op een niet-destructieve manier en met een hoge resolutie gelijktijdig zowel de driedimensionale botarchitectuur als de mineralisatiegraad te onderzoeken.

Architectuur en mineralisatie van het zich ontwikkelende kaakbot

Tot voor kort was er weinig kwantitatieve informatie beschikbaar over de ontwikkeling van de driedimensionale architectuur van het onderkaakbot. Bovendien was er nooit eerder gekeken naar de mineralisatiegraad van compact en trabeculair bot tijdens de ontwikkeling. Met behulp van microCT werden de architectuur en mineralisatie van het varkenskaakbot tijdens de prenatale ontwikkeling bestudeerd. Kaakbotmonsters van varkens van verschillende prenatale stadia werden geanalyseerd. Het onderzoek richtte zich op de ontwikkeling van de condylus (het kaakkopje) (hoofdstuk 3), op verschillen in ontwikkeling tussen compact en trabeculair bot (hoofdstuk 4) en op regionale verschillen binnen condylus en corpus (hoofdstuk 5).

De voorkant van de condylus bleek qua botarchitectuur en mineralisatiegraad verder in ontwikkeling te zijn dan de achterkant. Aan de achterkant vindt de meest actieve groei plaats (hoofdstuk 3). Verschillen in de mineralisatiegraad binnen de trabekels gaven aan dat ze in omvang groeien door de appositie van nieuw en daardoor weinig gemineraliseerd botweefsel aan hun oppervlak. In de kernen van de trabekels kan het botweefsel langer rijpen, waardoor de mineralisatiegraad daar hoger is. Tijdens de prenatale ontwikkeling neemt de gemiddelde mineralisatiegraad van de condylus toe. Zowel het toekomstige trabeculaire bot in de condylus als het toekomstige compacte bot in het corpus ontwikkelen zich vanuit een aanvankelijk trabeculair-achtige structuur (hoofdstuk 4). Compact bot ontstaat doordat de trabekels in omvang toenemen en met elkaar fuseren. Vanaf het moment dat het kaakbot voor het eerst serieus belast lijkt te worden door contraherende kauwspieren treedt er een versnelling op in de architectuurveranderingen van condylus en corpus. Zo'n snelle verandering in de mineralisatiegraad werd echter niet gevonden. De groei van de condylus en het corpus wordt verder gekarakteriseerd door regionale verschillen in architectuur en mineralisatie (hoofdstuk 5). Aan de voor- en onderkant van de condylus heeft het trabeculaire bot een dichtere structuur en een hogere mineralisatiegraad dan aan de achter- en bovenkant. In het corpus heeft het bot aan de linguale zijde een meer compacte structuur en hogere mineralisatiegraad dan aan de buccale zijde. Uit de waargenomen lokale verschillen in architectuur en mineralisatie kon de dynamiek van de botgroei tijdens de ontwikkeling worden afgeleid.

Biomechanische consequenties van veranderingen in architectuur en mineralisatie

Om de invloed van de gevonden veranderende architectuur en mineralisatie op de biomechanische eigenschappen te onderzoeken werden eindige elementen modellen gebruikt. Deze werden vervaardigd met behulp van de eerder gemaakte driedimensionale microCT reconstructies van het trabeculaire bot van de condylus van varkens in verschillende ontwikkelingsstadia. Er werd gekeken naar de afzonderlijke invloed van veranderingen in architectuur en mineralisatiegraad op de mechanische eigenschappen van het bot, op zowel structuurniveau (structuurstijfheid, hoofdstuk 6) als weefselniveau (intratrabeculaire verdeling van spanning en vervorming, hoofdstuk 7).

De prenatale veranderingen in architectuur bleken een geringe invloed te hebben op de structuurstijfheid. Deze bleek daarentegen in belangrijke mate afhankelijk van de gemiddelde mineralisatiegraad (hoofdstuk 6). Bij een gesimuleerde heterogene mineralisatieverdeling (de werkelijke situatie) bleek de structuurstijfheid lager te zijn dan bij een gesimuleerde homogene verdeling. De mechanische anisotropie, wat betekent dat de stijfheid van de botstructuur afhankelijk is van de richting van de belasting, nam toe bij een heterogene verdeling. Dit zou kunnen betekenen dat trabekels met verschillende oriëntatie een verschillende mineralisatiegraad hebben. We concludeerden dat eindige elementen modellen die geen rekening houden met verschillen in mineralisatiegraad en met een heterogene verdeling daarvan onnauwkeurige voorspellingen doen over de structuurstijfheid.

Als trabeculair bot belast wordt is in de trabekels de vervorming het grootst aan hun oppervlak en het kleinst in hun kern (hoofdstuk 7). Dit suggereert dat de trabekels tijdens belasting vooral worden gebogen. De spanningen in de trabekels zijn daarentegen het laagst aan het oppervlak en worden geleidelijk hoger in de richting van de trabekelkern. Bij een gesimuleerde homogene mineralisatieverdeling werden de spanningen in het oppervlak van de trabekels overschat en in hun kern juist onderschat. Door de heterogene mineralisatieverdeling zoals die in werkelijkheid voorkomt, zijn de trabekels relatief meegevend voor buiging en star voor compressie in hun lengterichting. Een lager gemineraliseerd trabekeloppervlak is waarschijnlijk beter in staat om grote vervormingen aan het oppervlak, zoals die voorkomen tijdens buiging, op te vangen zonder dat er schade optreedt. Dit zorgt ervoor dat de trabekels minder kans hebben om te breken.

De relatie tussen weefselstijfheid en mineralisatiegraad

Door het vergelijken van resultaten verkregen met behulp van nanoindentatie en microCT kon voor het eerst de relatie tussen weefselstijfheid en mineralisatiegraad op trabekelniveau

bestudeerd worden (hoofdstuk 8). Ook de intratrabeculaire verdeling van deze twee grootheden werd bestudeerd (hoofdstuk 9). Trabeculair bot van de condylus van twee groepen varkens in een verschillend ontwikkelingsstadium werd daarvoor gebruikt. Er werd een serie indentaties uitgevoerd over de gehele breedte van de trabekels.

Er werd een significante relatie tussen de weefselstijfheid en de mineralisatiegraad gevonden. Deze relatie verschilde tussen de twee ontwikkelingsstadia. De verdelingen van weefselstijfheid en mineralisatiegraad over de breedte van de trabekels vertoonden een identiek parabolisch patroon. Beide parameters waren het laagst aan het oppervlak van de trabekels en het hoogst in de kern. De gemiddelde weefselstijfheid neemt toe tijdens de ontwikkeling. Deze toename kan worden toegeschreven aan een stijging van de mineralisatiegraad aan het oppervlak van de trabekels.

REFERENCES

Aerssens J, Boonen S, Joly J, Dequeker J (1997). Variations in trabecular bone composition with anatomical site and age: potential implications for bone quality assessment. J Endocrinol 155: 411-421.

Aerssens J, Boonen S, Lowet G, Dequeker J (1998). Interspecies differences in bone composition, density, and quality: potential implications for in vivo bone research. Endocrinology 139: 663-670.

Atchley WR, Hall BK (1991). A model for development and evolution of complex morphological structures. Biol Rev Camb Philos Soc 66: 101-157.

Azeredo RA, Watanabe I, Liberti EA, Semprini M (1996). The arrangement of the trabecular bone in the vestibular surface of the human fetus mandible. I. A scanning electron microscopy study. Bull Assoc Anat 80: 7-12.

Barbier A, Martel C, de Vernejoul MC, Tirode F, Nys M, Mocaer G, Morieux C, Murakami H, Lacheretz F (1999). The visualization and evaluation of bone architecture in the rat using three-dimensional X-ray microcomputed tomography. J Bone Miner Metab 17: 37-44.

Baume LJ (1962). Ontogenesis of the human temporomandibular joint. I. Development of the condyles. J Dent Res 41: 1327-1339.

Ben-Ami Y, Lewinson D, Silbermann M (1992). Structural characterization of the mandibular condyle in human fetuses: Light and electron microscopy studies. Acta Anat 145: 79-87.

Berraquero R, Palacios J, Gamallo C, de la Rosa P, Rodriguez JI (1995). Prenatal growth of the human mandibular condylar cartilage. Am J Orthod Dentofacial Orthop 108: 194-200.

Bigi A, Cojazzi G, Panzavolta S, Ripamonti A, Roveri N, Romanello M, Noris Suarez K, Moro L (1997). Chemical and structural characterization of the mineral phase from cortical and trabecular bone. J Inorg Biochem 68: 45-51.

Biltz RM, Pellegrino ED (1969). The chemical anatomy of bone. I. A comparative study of bone composition in sixteen vertebrates. J Bone Joint Surg Am 51: 456-466.

Birkbeck JA, Roberts JA (1971). Skeletal composition in the early human fetus. Biol Neonate 19: 465-471.

Boivin G, Meunier PJ (2002). Changes in bone remodeling rate influence the degree of mineralization of bone. Connect Tissue Res 43: 535-537.

Bonar LC, Roufosse AH, Sabine WK, Grynpas MD, Glimcher MJ (1983). X-ray diffraction studies of the crystallinity of bone mineral in newly synthesized and density fractionated bone. Calcif Tissue Int 35: 202-209.

Borah B, Dufresne TE, Cockman MD, Gross GJ, Sod EW, Myers WR, Combs KS, Higgins RE, Pierce SA, Stevens ML (2000). Evaluation of changes in trabecular bone architecture and mechanical properties of minipig vertebrae by three-dimensional magnetic resonance microimaging and finite element modeling. J Bone Miner Res 15: 1786-1797.

Boskey AL (1992). Mineral-matrix interactions in bone and cartilage. Clin Orthop 281: 244-271.

Boskey AL (1996). Matrix proteins and mineralization: An overview. Connect Tissue Res 35: 357-363.

Boskey AL (2002). Variations in bone mineral properties with age and disease. J Musculoskel Neuron Interact 2: 532-534.

Bourne BC, van der Meulen MCH (2004). Finite element models predict cancellous apparent modulus when tissue modulus is scaled from specimen CT-attenuation. J Biomech 37: 613-621.

Braillon PM, Lapillonne A, Ho PS, Bouvier R, Bochu M, Salle BL (1996). Assessment of the bone mineral density in the lumbar vertebrae of newborns by quantitative computed tomography. Skeletal Radiol 25: 711-715.

Braillon PM, Salle BL, Brunet J, Glorieux FH, Delmas PD, Meunier PJ (1992). Dual energy X-ray absorptiometry measurement of bone mineral content in newborns: validation of the technique. Pediatr Res 32: 77-80.

Brooks RA, di Chiro G (1975). Theory of image reconstruction in computed tomography. Radiology 117: 561-572.

Brooks RA, di Chiro G (1976). Beam hardening in X-ray reconstructive tomography. Phys Med Biol 21: 390-398.

Buckwalter JA, Glimcher MJ, Cooper RR, Recker R (1996). Bone Biology. Part I: Structure, blood supply, cells, matrix, and mineralization. Instr Course Lect 45: 371-386.

Burger EH, Klein Nulend J, Veldhuijzen JP (1991). Modulation of osteogenesis in fetal bone rudiments by mechanical stress *in vitro*. J Biomech 24: 101-109.

Bushby AJ, Ferguson VL, Boyde A (2004). Nanoindentation of bone: Comparison of specimens tested in liquid and embedded in polymethylmethacrylate. J Mat Res 19: 249-259.

Cadet ER, Gafni RI, McCarthy EF, McCray DR, Bacher JD, Barnes KM, Baron J (2003). Mechanisms responsible for longitudinal growth of the cortex: Coalescence of trabecular bone into cortical bone. J Bone Joint Surg Am 85: 1739-1748.

Camacho DL, Hopper RH, Lin GM, Myers BS (1997). An improved method for finite element mesh generation of geometrically complex structures with application to the skullbase. J Biomech 30: 1067-1070.

Cann CE (1988). Quantitative CT for determination of bone mineral density: A review. Radiology 166: 509-522.

Carter DR, Orr TE (1992). Skeletal development and bone functional adaptation. J Bone Miner Res 7: S389-S395.

Chen PS, Toribara TY, Warner H (1956). Microdetermination of phosphorus. Anal Biochem 28: 1755-1758.

Choi K, Kuhn JL, Ciarelli MJ, Goldstein SA (1990). The elastic moduli of human subchondral, trabecular, and cortical bone tissue and the size-dependency of cortical bone modulus. J Biomech 23: 1103-1113.

Christensen LV (1975). A review of the embryology of the human temporomandibular joint. J Dent Assoc S Afr 30: 849-852.

Ciarelli TE, Fyhrie DP, Parfitt AM (2003). Effects of vertebral bone fragility and bone formation rate on the mineralization levels of cancellous bone from white females. Bone 32: 311-315.

Cooper C, Javaid MK, Taylor P, Walker-Bone K, Dennison E, Arden N (2002). The fetal origins of osteoporotic fracture. Calcif Tissue Int 70: 391-394.

Cooper DML, Matyas JR, Katzenberg MA, Hallgrimsson B (2004). Comparison of microcomputed tomographic and microradiographic measurements of cortical bone porosity. Calcif Tissue Int 74: 437-447.

Copray JCVM, Dibbets JMH, Kantomaa T (1988). The role of condylar cartilage in the development of the temporomandibular joint. Angle Orthod 58: 369-380.

Crane NJ, Popescu V, Morris MD, Steenhuis P, Ignelzi MA (2006). Raman spectroscopic evidence for octacalcium phosphate and other transient mineral species deposited during intramembranous ossification. Bone 39: 434-442.

Currey JD (1984). Effects of differences in mineralization on the mechanical properties of bone. Philos Trans R Soc Lond B Biol Sci 304: 509-518.

Currey JD (1988). The effect of porosity and mineral content on the Young's modulus of elasticity of compact bone. J Biomech 21:131-139.

Currey JD (1998). Mechanical properties of vertebrate hard tissues. Proc Inst Mech Eng [H] 212: 399-411.

Currey JD (1999). What determines the bending strength of compact bone? J Exp Biol 202: 2495-2503.

Currey JD (2003). The many adaptations of bone. J Biomech 36: 1487-1495.

de Vries JIP, Visser GHA, Prechtl HFR (1982). The emergence of fetal behaviour. I. Qualitative aspects. Early Hum Dev 7: 301-322.

de Vries JIP, Visser GHA, Prechtl HFR (1985). The emergence of fetal behaviour. II. Quantitative aspects. Early Hum Dev 12: 99-120.

Dickerson JWT (1962a). The effect of development on the composition of a long bone of the pig, rat and fowl. Biochem J 82: 47-55.

Dickerson JWT (1962b). Changes in the composition of the human femur during growth. Biochem J 82: 56-61.

Ding M (2000). Age variations in the properties of human tibial trabecular bone and cartilage. Acta Orthop Scand 71: 1-45.

Ding M, Odgaard A, Danielsen CC, Hvid I (2002). Mutual associations among microstructural, physical and mechanical properties of human cancellous bone. J Bone Joint Surg Br 84: 900-907.

Ding M, Odgaard A, Hvid I (1999). Accuracy of cancellous bone volume fraction measured by micro-CT scanning. J Biomech 32: 323-326.

Doskocil M (1989). Mechanisms of the reduction of Meckel's cartilage in man. Folia Morphol 37: 113-118.

Driessens FC, Schaafsma G, van Beresteijn EC, Rotgans J (1986). Maturation of mammalian bone minerals. A new method for determining bone metabolism. Z Orthop Ihre Grenzgeb 124: 599-602.

Dufresne TE (1998). Segmentation techniques for analysis of bone by three-dimensional computed tomographic imaging. Technol Health Care 6: 351-359.

Durkin JF, Irving JT (1973). The cartilage of the mandibular condyle. Oral Sci Rev 2: 29-99.

Dyson ED, Whitehouse WJ (1968). Composition of trabecular bone in children and its relation to radiation dosimetry. Nature 217: 576-578.

Dziedzic-Goclawska A, Emerich J, Grzesik W, Stachowicz W, Michalik J, Ostrowski K (1988). Differences in the kinetics of the mineralization process in endochondral and intramembranous osteogenesis in human fetal development. J Bone Miner Res 3: 533-539.

Evans HE, Sack WO (1973). Prenatal development of domestic and laboratory mammals: Growth curves, external features and selected references. Zentralbl Veterinarmed [C] 2: 11-45.

Fan Z, Rho JY (2003). Effects of viscoelasticity and time-dependent plasticity on nanoindentation measurements of human cortical bone. J Biomed Mater Res 67: 208-214.

Fan Z, Swadener JG, Rho JY, Roy ME, Pharr GM (2002). Anisotropic properties of human tibial cortical bone as measured by nanoindentation. J Orthop Res 20: 806-810.

Feldkamp LA, Goldstein SA, Parfitt AM, Jesion G, Kleerekoper M (1989). The direct examination of three-dimensional bone architecture in vitro by computed tomography. J Bone Miner Res 4: 3-11.

Ferguson C, Alpern E, Miclau T, Helms JA (1999). Does adult fracture repair recapitulate embryonic skeletal formation? Mech Dev 87: 57-66.

Follet H, Boivin G, Rumelhart C, Meunier PJ (2004). The degree of mineralization is a determinant of bone strength: a study on human calcanei. Bone 34: 783-789.

Fratzl P, Gupta HS, Paschalis EP, Roschger P (2004). Structure and mechanical quality of the collagen-mineral nano-composition in bone. J Mater Chem 14: 2115-2123.

Friant M (1968). Le cartilage de Meckel du porc (sus domesticus Gray). Les premiers stades de son evolution. Folia Morphol 16: 209-214.

Frommer J, Margolies MR (1971). Contribution of Meckel's cartilage to ossification of the mandible in mice. J Dent Res 50: 1260-1267.

Fyhrie DP, Schaffler MB (1994). Failure mechanisms in human vertebral cancellous bone. Bone 15: 105-109.

Giesen EBW, Ding M, Dalstra M, van Eijden TMGJ (2001). Mechanical properties of cancellous bone in the human mandibular condyle are anisotropic. J Biomech 34: 799-803.

Giesen EBW, Ding M, Dalstra M, van Eijden TMGJ (2003). Architectural measures of the cancellous bone of the mandibular condyle identified by principal components analysis. Calcif Tissue Int 73: 225-231.

Giesen EBW, van Eijden TMGJ (2000). The three-dimensional cancellous bone architecture of the human mandibular condyle. J Dent Res 79: 957-963.

Glimcher MJ (1987). The nature of the mineral component of bone and the mechanism of calcification. Instr Course Lect 36: 49-69.

Gong JK, Arnold JS, Cohn SH (1964). Composition of trabecular and cortical bone. Anat Rec 149: 325-331.

Goret-Nicaise M (1981). Influence des insertions des muscles masticateurs sur la structure mandibulaire du nouveau-né. Bull Assoc Anat 65: 287-296.

Goret-Nicaise M, Dhem A (1982). Presence of chondroid tissue in the symphyseal region of the growing human mandible. Acta Anat 113: 189-195.

Goret-Nicaise M, Dhem A (1984). The mandibular body of the human fetus. Histologic analysis of the basilar part. Anat Embryol 169: 231-236.

Grynpas MD (1993). Age and disease-related changes in the mineral of bone. Calcif Tissue Int 53: S57-S64.

Grynpas MD, Bonar LC, Glimcher MJ (1984). Failure to detect an amorphous calcium-phosphate solid phase in bone mineral: a radial distribution function study. Calcif Tissue Int 36: 291-301.

Grynpas MD, Holmyard D (1988). Changes in quality of bone mineral on aging and in disease. Scanning Microsc 2: 1045-1054.

Guldberg RE, Hollister SJ, Charras GT (1998). The accuracy of digital image-based finite element models. J Biomech Eng 120: 289-295.

Guo XE, Goldstein SA (2000). Vertebral trabecular bone microscopic tissue elastic modulus and hardness do not change in ovariectomized rats. J Orthop Res 18: 333-336.

Hall BK (1982). Mandibular morphogenesis and craniofacial malformations. J Craniofac Genet Dev Biol 2: 309-322.

Hall BK (1987). Earliest evidence of cartilage and bone development in embryonic life. Clin Orthop 225: 255-272.

Hall BK (1998). The embryonic development of bone. Am Sci 76: 174-181.

Hammersberg P, Mångård M (1998). Correction for beam hardening artefacts in computerized tomography. J X-Ray Sci Technol 8: 75-93.

Hara T, Tanck E, Homminga J, Huiskes R (2002). The influence of microcomputed tomography threshold variations on the assessment of structural and mechanical trabecular bone properties. Bone 31: 107-109.

Harrigan TP, Jasty M, Mann RW, Harris WH (1988). Limitations of the continuum assumption in cancellous bone. J Biomech 21: 269-275.

Harrigan TP, Mann RW (1984). Characterization of microstructural anisotropy in orthotropic materials using a second rank tensor. J Mater Sci 19: 761-767.

Hengsberger S, Ammann P, Legros B, Rizzoli R, Zysset P (2005). Intrinsic bone tissue properties in adult rat vertebrae: modulation by dietary protein. Bone 36: 134-141.

Hengsberger S, Boivin G, Zysset PK (2002). Morphological and mechanical properties of bone structural units: A two-case study. JSME Int J C-Mech Sy 45: 936-943.

Hildebrand T, Laib A, Müller R, Dequeker J, Rüegsegger P (1999). Direct three-dimensional morphometric analysis of human cancellous bone: microstructural data from spine, femur, iliac crest, and calcaneus. J Bone Miner Res 14: 1167-1174.

Hildebrand T, Rüegsegger P (1997a). A new method for the model-independent assessment of thickness in three-dimensional images. J Microsc 185: 67-75.

Hildebrand T, Rüegsegger P (1997b). Quantification of bone microarchitecture with the structure model index. Comput Methods Biomech Biomed Engin 1: 15-23.

Hoc T, Henry L, Verdier M, Aubry D, Sedel L, Meunier A (2006). Effect of microstructure on the mechanical properties of Haversian cortical bone. Bone 38: 466-474.

Hodges PC (1953). Ossification in the fetal pig; a radiographic study. Anat Rec 116: 315-325.

Homminga J, van Rietbergen B, Lochmüller EM, Weinans H, Eckstein F, Huiskes R (2004). The osteoporotic vertebral structure is well adapted to the loads of daily life, but not to infrequent “error” loads. Bone 34: 510-516.

Hounsfield GN (1973). Computerized transverse axial scanning (tomography): Part I. Description of the system. Br J Radiol 46: 1016-1022.

Hounsfield GN (1977). The E.M.I. scanner. Proc R Soc Lond 195: 281-289.

Humphrey T (1968). The development of mouth opening and related reflexes involving the oral area of human fetuses. Ala J Med Sci 5: 126-157.

Jaasma MJ, Bayraktar HH, Niebur GL, Keaveny TM (2002). Biomechanical effects of intraspecimen variation in tissue modulus for trabecular bone. J Biomech 35: 237-246.

Javaid MK, Cooper C (2002). Prenatal and childhood influences on osteoporosis. Best Pract Res Clin Endocrinol Metab 16: 349-367.

Jee WSS (2001). Integrated bone tissue physiology: anatomy and physiology. In: Cowin SC. Bone mechanics handbook. CRC Press, Boca Raton, USA, pp.1-68.

Kabel J, van Rietbergen B, Dalstra M, Odgaard A, Huiskes R (1999a). The role of an effective isotropic tissue modulus in the elastic properties of cancellous bone. J Biomech 32: 673-680.

Kabel J, van Rietbergen B, Odgaard A, Huiskes R (1999b). Constitutive relationships of fabric, density, and elastic properties in cancellous bone architecture. Bone 25: 481-486.

Kalender WA (2006). X-ray computed tomography. Phys Med Biol 51: R29-R43.

Keaveny TM, Guo XE, Wachtel EF, McMahon TA, Hayes WC (1994). Trabecular bone exhibits fully linear elastic behaviour and yields at low strains. J Biomech 27: 1127-1136.

Kinney JH, Ladd AJC (1998). The relationship between three-dimensional connectivity and the elastic properties of trabecular bone. J Bone Miner Res 13: 839-845.

Kriewall TJ, McPherson GK, Tsai AC (1981). Bending properties and ash content of fetal cranial bone. J Biomech 14: 73-79.

Kumar U, Ramakrishna GS, Pendharkar AS, Singh G (2002). Behaviour of reconstructed attenuation values with X-ray tube voltage in an experimental third-generation industrial CT system using *Xscan* linear detector array. Nucl Instrum Meth A 490: 379-391.

Laib A, Barou O, Vico L, Lafage-Proust MH, Alexandre C, Rüegsegger P (2000). 3D micro-computed tomography of trabecular and cortical architecture with application to a rat model of immobilization osteoporosis. Med Biol Eng Comput 38: 326-332.

Laib A, Hauselmann HJ, Rüegsegger P (1998). In vivo high resolution 3D-QCT of the human forearm. Technol Health Care 6: 329-337.

Landis WJ (1995). The strength of a calcified tissue depends in part on the molecular structure and organization of its constituent mineral crystals in their organic matrix. Bone 16: 533-544.

Langenbach GEJ, van Eijden TMGJ (2001). Mammalian feeding motor patterns. Am Zool 41: 1338-1351.

Lee SK, Kim YS, Oh HS, Yang KH, Kim EC, Chi JG (2001). Prenatal development of the human mandible. Anat Rec 263: 314-325.

Leeson TS, Leeson CR (1970). Histology. 2nd edition, Saunders, Philadelphia.

Lerner AL, Kuhn JL (1997). Characterization of regional and age-related variations in the growth of the rabbit distal femur. J Orthop Res 15: 353-361.

Linde F (1994). Elastic and viscoelastic properties of trabecular bone by a compression testing approach. Dan Med Bull 41: 119-138.

Low A (1909). Further observations on the ossification of the human lower jaw. J Anat 44: 83-95.

Maki K, Miller AJ, Okano T, Shibasaki Y (2001). A three-dimensional, quantitative computed tomographic study of changes in distribution of bone mineralization in the developing human mandible. Arch Oral Biol 46: 667-678.

Malzbender J, den Toonder JMJ, Balkenende AR, de With G (2002). Measuring mechanical properties of coatings: a methodology applied to nano-particle-filled sol-gel coatings on glass. Mater Sci Eng R 36: 47-103.

McCalden RW, McGeough JA, Court-Brown CM (1997). Age-related changes in the compressive strength of cancellous bone. The relative importance of changes in density and trabecular architecture. J Bone Joint Surg Am 79: 421-427.

McCullough EC (1975). Photon attenuation in computed tomography. Med Phys 2: 307-320.

Meneghini C, Dalconi MC, Nuzzo S, Mobilio S, Wenk RH (2003). Rietveld refinement on X-ray diffraction patterns of bioapatite in human fetal bones. Biophys J 84: 2021-2029.

Mérida-Velasco JA, Sánchez-Montesinos I, Espín-Ferra J, Garcia-Garcia JD, Roldan-Schilling V (1993). Developmental differences in the ossification process of the human corpus and ramus mandibulae. Anat Rec 235: 319-324.

Mérida-Velasco JR, Rodríguez-Vázquez JF, Mérida-Velasco JA, Sánchez-Montesinos I, Espín-Ferra J, Jiménez-Collado J (1999). Development of the human temporomandibular joint. Anat Rec 255: 20-33.

Meunier PJ, Boivin G (1997). Bone mineral density reflects bone mass but also the degree of mineralization of bone: Therapeutic implications. Bone 21: 373-377.

Mittra E, Akella S, Qin YX (2006). The effects of embedding material, loading rate and magnitude, and penetration depth in nanoindentation of trabecular bone. J Biomed Mater Res A 79: 86-93.

Morgan TG, van der Meulen MCH, Bourne BC (2002). Density versus depth from trabecular surface measured by quantitative micro-CT. Trans Orthop Res Soc 27: 110.

Mori S, Harruf R, Ambrosius W, Burr DB (1997). Trabecular bone volume and microdamage accumulation in the femoral heads of women with and without femoral neck fractures. Bone 21: 521-526.

Mulder L, Koolstra JH, den Toonder JMJ, van Eijden TMGJ (2006a). Relationship between tissue stiffness and degree of mineralization of developing trabecular bone. Submitted for publication.

Mulder L, Koolstra JH, de Jonge HW, van Eijden TMGJ (2006b). Architecture and mineralization of developing cortical and trabecular bone of the mandible. Anat Embryol 211: 71-78.

Mulder L, Koolstra JH, van Eijden TMGJ (2004). Accuracy of microCT in the quantitative determination of the degree and distribution of mineralization in developing bone. Acta Radiol 45: 769-777.

Mulder L, Koolstra JH, Weijs WA, van Eijden TMGJ (2005). Architecture and mineralization of developing trabecular bone in the pig mandibular condyle. Anat Rec A Discov Mol Cell Evol Biol 285: 659-667.

Mulder L, van Groningen LB, Potgieser YA, Koolstra JH, van Eijden TMGJ (2006c). Regional differences in architecture and mineralization of developing mandibular bone. Anat Rec A Discov Mol Cell Evol Biol 288: 954-961.

Mulder L, van Ruijven LJ, Koolstra JH, van Eijden TMGJ (2006d). Biomechanical consequences of developmental changes in trabecular architecture and mineralization of the pig mandibular condyle. J Biomech. In press.

Mulder L, van Ruijven LJ, Koolstra JH, van Eijden TMGJ (2006e). The influence of mineralization on intratrabecular stress and strain distribution in developing trabecular bone. Submitted for publication.

Müller R (2003). Bone microarchitecture assessment: current and future trends. Osteoporosis Int 14: S89-S99.

Müller R, Hahn M, Vogel M, Delling G, Rüegsegger P (1996). Morphometric analysis of noninvasively assessed bone biopsies: comparison of high-resolution computed tomography and histologic sections. Bone 18: 215-220.

Müller R, van Campenhout H, van Damme B, van der Perre G, Dequeker J, Hildebrand T, Rüegsegger P (1998). Morphometric analysis of human bone biopsies: a quantitative structural comparison of histological sections and micro-computed tomography. Bone 23: 59-66.

Nafei A, Danielsen CC, Linde F, Hvid I (2000a). Properties of growing trabecular ovine bone. Part I: Mechanical and physical properties. J Bone Joint Surg Br 82: 910-920.

Nafei A, Kabel J, Odgaard A, Linde F, Hvid I (2000b). Properties of growing trabecular ovine bone. Part II: Architectural and mechanical properties. J Bone Joint Surg Br 82: 921-927.

Nuzzo S, Meneghini C, Braillon P, Bouvier R, Mobilio S, Peyrin F (2003). Microarchitectural and physical changes during fetal growth in human vertebral bone. J Bone Miner Res 18: 760-768.

Nuzzo S, Peyrin F, Cloetens P, Baruchel J, Boivin G (2002). Quantification of the degree of mineralization of bone in three dimensions using synchrotron radiation microtomography. Med Phys 29: 2672-2681.

Odgaard A, Gundersen HJG (1993). Quantification of connectivity in cancellous bone, with special emphasis on 3-D reconstructions. Bone 14: 173-182.

Odgaard A, Kabel J, van Rietbergen B, Dalstra M, Huiskes R (1997). Fabric and elastic principal directions of cancellous bone are closely related. J Biomech 30: 487-495.

Oliver WC, Pharr GM (1992). An improved technique for determining hardness and elastic modulus using load and displacement sensing indentation experiments. J Mater Res 7: 1564-1583.

Opperman LA (2000). Cranial sutures as intramembranous bone growth sites. Dev Dyn 219: 472-485.

Orliaguet T, Darcha C, Déchelotte P, Vanneuville G (1994). Meckel's cartilage in the human embryo and fetus. Anat Rec 238: 491-497.

Orliaguet T, Déchelotte P, Scheye T, Vanneuville G (1993). The relationship between Meckel's cartilage and the development of the human fetal mandible. Surg Radiol Anat 15: 113-118.

Ouyang J, Yang GT, Wu WZ, Zhu QA, Zhong SZ (1997). Biomechanical characteristics of human trabecular bone. Clin Biomech 12: 522-524.

Oyedepo AC, Henshaw DL (1997). Calcification of the lumbar vertebrae during human fetal development. Calcif Tissue Int 61: 179-182.

Panattoni GL, D'Amelio P, Di Stefano M, Sciolla A, Isaia GC (1999). Densitometric study of developing femur. Calcif Tissue Int 64: 133-136.

Panattoni GL, Sciolla A, Isaia GC (1995). Densitometric studies of developing vertebral bodies. Calcif Tissue Int 57: 74-77.

Parfitt AM, Mathews CHE, Villanueva AR, Kleerekoper M, Frame B, Rao DS (1983). Relationships between surface, volume, and thickness of iliac trabecular bone in aging and in osteoporosis. Implications for the microanatomic and cellular mechanisms of bone loss. J Clin Invest 72: 1396-1409.

Paschalis EP, Betts F, DiCarlo E, Mendelsohn R, Boskey AL (1997). FTIR microspectroscopic analysis of normal human cortical and trabecular bone. Calcif Tissue Int 61: 480-486.

Perry HT, Xu Y, Forbes DP (1985). The embryology of the temporomandibular joint. Cranio 3: 125-132.

Pidaparti RM, Turner CH (1997). Cancellous bone architecture: advantages of nonorthogonal trabecular alignment under multidirectional joint loading. J Biomech 26: 111-119.

Pistoia W, van Rietbergen B, Lochmüller EM, Lill CA, Eckstein F, Rüegsegger P (2002). Estimation of distal radius failure load with micro-finite element analysis models based on three-dimensional peripheral quantitative computed tomography images. Bone 30: 842-848.

Postnov AA, Vinogradov AV, van Dijck D, Saveliev SV, de Clerck NM (2003). Quantitative analysis of bone mineral content by x-ray microtomography. Physiol Meas 24: 165-178.

Pugliarello MC, Vittur F, de Bernard B, Bonucci E, Ascenzi A (1973). Analysis of bone composition at the microscopic level. Calcif Tissue Res 12: 209-216.

Radlanski RJ (2003). Prenatal craniofacial morphogenesis: four-dimensional visualization of morphogenetic processes. Orthod Craniofac Res 6: 89-94.

Radlanski RJ, Renz H, Müller U, Schneider RS, Marcucio RS, Helms JA (2002). Prenatal morphogenesis of the human mental foramen. Eur J Oral Sci 110: 452-459.

Radlanski RJ, Renz H, Klarkowski MC (2003). Prenatal development of the human mandible. 3D reconstructions, morphometry and bone remodelling pattern, sizes 12-117 mm CRL. Anat Embryol 207: 221-232.

Rho JY, Currey JD, Zioupos P, Pharr GM (2001). The anisotropic Young's modulus of equine secondary osteones and interstitial bone determined by nanoindentation. J Exp Biol 204: 1775-1781.

Rho JY, Hobatho MC, Ashman RB (1995). Relations of mechanical properties to density and CT numbers in human bone. Med Eng Phys 17: 347-355.

Rho JY, Roy ME, Tsui TY, Pharr GM (1999). Elastic properties of microstructural components of human bone tissue as measured by nanoindentation. J Biomed Mater Res 45: 48-54.

Rho JY, Tsui TY, Pharr GM (1997). Elastic properties of human cortical and trabecular lamellar bone measured by nanoindentation. Biomaterials 18: 1325-1330.

Rho JY, Zioupos P, Currey JD, Pharr GM (2002). Microstructural elasticity and regional heterogeneity in human femoral bone of various ages examined by nanoindentation. J Biomech 35: 189-198.

Roschger P, Grabner BM, Rinnerthaler S, Tesch W, Kneissel M, Berzlanovich A, Klaushofer K, Fratzl P (2001). Structural development of the mineralized tissue in the human L4 vertebral body. J Struct Biol 136: 126-136.

Roy ME, Rho JY, Tsui TY, Evans ND, Pharr GM (1999). Mechanical and morphological variation of the human lumbar vertebral cortical and trabecular bone. J Biomed Mater Res 44: 191-197.

Rüegsegger P, Elsasser U, Anliker M, Gnehm H, Kind H, Prader A (1976). Quantification of bone mineralization using computed tomography. Radiology 121: 93-97.

Rüegsegger P, Koller B, Müller R (1996). A microtomographic system for the nondestructive evaluation of bone architecture. Calcif Tissue Int 58: 24-29.

Salle BL, Braillon PM, Glorieux FH, Brunet J, Cavero E, Meunier PJ (1992). Lumbar bone mineral content measured by dual energy X-ray absorptiometry in newborns and infants. Acta Paediatr 81: 953-958.

Salle BL, Rauch F, Travers R, Bouvier R, Glorieux FH (2002). Human fetal bone development: Histomorphometric evaluation of the proximal femoral metaphysis. Bone 30: 823-828.

Scott JH (1951). The development of joints concerned with early jaw movements in the sheep. J Anat 85: 36-43.

Shibata S, Suzuki S, Tengan T, Ishii M, Kuroda T (1996). A histological study of the developing condylar cartilage of the fetal mouse mandible using coronal sections. Arch Oral Biol 41: 47-54.

Silva MJ, Brodt MD, Fan Z, Rho JY (2004). Nanoindentation and whole-bone bending estimates of material properties in bone from the senescence accelerated mouse SAMP6. J Biomech 37: 1639-1646.

Skedros JG, Bloebaum RD, Bachus KN, Boyce TM, Constantz B (1993). Influence of mineral content and composition on graylevels in backscattered electron images of bone. J Biomed Mater Res 27: 57-64.

Sneddon IN (1965). The relationship between load and penetrations in the axisymmetric Boussinesq problem for a punch of arbitrary profile. Int J Eng Sci 3: 47-57.

Spyropoulos MN (1977). The morphogenetic relationship of the temporal muscle to the coronoid process in human embryos and fetuses. Am J Anat 150: 395-410.

Stauber M, Rapillard L, van Lenthe GH, Zysset P, Müller R (2006). Importance of individual rods and plates in the assessment of bone quality and their contribution to bone stiffness. J Bone Miner Res 21: 586-595.

Steiger JH (1980). Tests for comparing elements of a correlation matrix. Psychol Bull 87: 245-251.

Stover SM, Pool RR, Martin RB, Morgan JP (1992). Histological features of the dorsal cortex of the third metacarpal bone mid-diaphysis during postnatal growth in thoroughbred horses. J Anat 181: 455-469.

Su XW, Feng QL, Cui FZ, Zhu XD (1997). Microstructural and micromechanical properties of the mid-diaphyses of human fetal femurs. Connect Tissue Res 36: 271-286.

Su XW, Sun K, Cui FZ, Landis WJ (2003). Organization of apatite crystals in human woven bone. Bone 32: 150-162.

Swadener JG, Rho JY, Pharr GM (2001). Effects of anisotropy on elastic moduli measured by nanoindentation in human tibial cortical bone. J Biomed Mater Res 57: 108-112.

Tanck E, Homminga J, van Lenthe GH, Huiskes R (2001). Increase in bone volume fraction precedes architectural adaptation in growing bone. Bone 28: 650-654.

Tanck E, Hannink G, Ruimerman R, Buma P, Burger EH, Huiskes R (2004). Cortical bone development under the growth plate is regulated by mechanical load transfer. Proceedings of ESB 2004, ‘s-Hertogenbosch, the Netherlands.

Teng S, Herring SW (1995). A stereological study of trabecular architecture in the mandibular condyle of the pig. Archs Oral Biol 40: 299-310.

Teng S, Herring SW (1996). Anatomic and directional variation in the mechanical properties of the mandibular condyle in pigs. J Dent Res 75: 1842-1850.

Tomo S, Ogita M, Tomo I (1997). Development of mandibular cartilages in the rat. Anat Rec 249: 233-239.

Turner CH, Cowin SC, Rho JY, Ashman RB, Rice JC (1990). The fabric dependence of the orthotropic elastic constants of cancellous bone. J Biomech 23: 549-561.

Ulrich D, van Rietbergen B, Laib A, Rüegsegger P (1999). The ability of three-dimensional structural indices to reflect mechanical aspects of trabecular bone. Bone 25: 55-60.

Uchiyama T, Tanizawa T, Muramatsu H, Endo N, Takahashi HE, Hara T (1997). A morphometric comparison of trabecular structure of human ilium between microcomputed tomography and conventional histomorphometry. Calcif Tissue Int 61: 493-498.

van der Harst MR, Brama PA, van de Lest CH, Kiers GH, deGroot J, van Weeren PR (2004). An integral biochemical analysis of the main constituents of articular cartilage, subchondral and trabecular bone. Osteoarthritis Cartilage 12: 752-761.

van der Linden JC, Birkenhäger-Frenkel DH, Verhaar JAN, Weinans H (2001). Trabecular bone's mechanical properties are affected by its non-uniform mineral distribution. J Biomech 34: 1573-1580.

van Eijden TMGJ (2000). Biomechanics of the mandible. Crit Rev Oral Biol Med 11: 123-136.

van Eijden TMGJ, van Ruijven LJ, Giesen EBW (2004). Bone tissue stiffness in the mandibular condyle is dependent on the direction and density of the cancellous structure. Calcif Tissue Int 75: 502-508.

van Eijden TMGJ, van der Helm PN, van Ruijven LJ, Mulder L (2006). Structural and mechanical properties of mandibular condylar bone. J Dent Res 85: 33-37.

van Rietbergen B, Huiskes R, Eckstein F, Rüegsegger P (2003). Trabecular bone tissue strains in healthy and osteoporotic human femur. J Bone Miner Res 18: 1781-1788.

van Rietbergen B, Müller R, Ulrich D, Rüegsegger P, Huiskes R (1999). Tissue stresses and strain in trabeculae of a canine proximal femur can be quantified from computer reconstructions. J Biomech 32: 165-173.

van Rietbergen B, Odgaard A, Kabel J, Huiskes R (1998). Relationship between bone morphology and bone elastic properties can be accurately quantified using high-resolution computer reconstructions. J Orthop Res 16: 23-28.

van Rietbergen B, Weinans H, Huiskes R, Odgaard A (1995). A new method to determine trabecular bone elastic properties and loading using micromechanical finite-element models. J Biomech 28: 69-81.

van Ruijven LJ, Giesen EBW, Mulder L, Farella M, van Eijden TMGJ (2005). The effect of bone loss on rod-like and plate-like trabeculae in the cancellous bone of the mandibular condyle. Bone 36: 1078-1085.

van Ruijven LJ, Giesen EBW, van Eijden TMGJ (2002). Mechanical significance of the trabecular microstructure of the human mandibular condyle. J Dent Res 81: 706-710.

van Ruijven LJ, Giesen EBW, Farella M, van Eijden TMGJ (2003). Prediction of mechanical properties of the cancellous bone of the mandibular condyle. J Dent Res 82: 819-823.

van Ruijven LJ, Mulder L, van Eijden TMGJ (2006). Variations in mineralization affect the stress and strain distributions in cortical and trabecular bone. J Biomech doi:10.1016/j.jbiomech.2006.06.004.

Verhulp E, van Rietbergen B, Huiskes R (2005). Comparison of micro-level and continuum-level voxel models of the proximal femur. J Biomech doi:10.1016/j.jbiomech.2005.10.027.

Wachter NJ, Augat P, Krischak GD, Mentzel M, Kinzl L, Claes L (2001). Prediction of cortical bone porosity *in vitro* by microcomputed tomography. Calcif Tissue Int 68: 38-42.

Wissmer A (1927). Le développement et l'organisation statique le la mandibule foetale chez l'homme. Arch Anat 7: 335-425.

Wolff J (1892). Das Gesetz der Transformation der Knochen. (Translated as: The law of bone remodeling.) Maquet P, Furlong R. Berlin, Springer Verlag, 1986.

Wolschrijn CF, Weijs WA (2004). Development of the trabecular structure within the ulnar medial coronoid process of young dogs. Anat Rec A Discov Mol Cell Evol Biol 278: 514-519.

Wong M, Carter DR (1990). A theoretical model of endochondral ossification and bone architectural construction in long bone ontogeny. Anat Embryol 181: 523-532.

Wong SY, Kariks J, Evans RA, Dunstan CR, Hills E (1985). The effect of age on bone composition and viability in the femoral head. J Bone Joint Surg Am 67: 274-283.

Xu J, Rho JY, Mishra SR, Fan Z (2003). Atomic force microscopy and nanoindentation characterization of human lamellar bone prepared by microtome sectioning and mechanical polishing technique. J Biomed Mater Res 67: 719-726.

Zioupos P, Currey JD (1994). The extent of microcracking and the morphology of microcracks in damaged bone. J Mater Sci 29: 978-986.

Ziv V, Wagner HD, Weiner S (1996). Microstructure-microhardness relations in parallel-fibered and lamellar bone. Bone 18: 417-428.

Zysset PK, Guo XE, Hoffler CE, Moore KE, Goldstein SA (1998). Mechanical properties of human trabecular bone lamellae quantified by nanoindentation. Technol Health Care 6: 429-432.

Zysset PK, Guo XE, Hoffler CE, Moore KE, Goldstein SA (1999). Elastic modulus and hardness of cortical and trabecular bone lamellae measured by nanoindentation in the human femur. J Biomech 32: 1005-1012.

DANKWOORD

Aan een mooie en zeer leerzame periode bij Functionele Anatomie is een einde gekomen. Promoveren is natuurlijk een individuele prestatie van de promovendus, maar aan de andere kant ook zeker een teamprestatie. Gelukkig werd ik tijdens de afgelopen vier jaar gesteund door een geweldig team! Mede dankzij hen kon dit proefschrift, waar ik erg trots op ben, tot stand komen. Een klein groepje, maar o zo divers en daardoor erg complementair, waardoor het onderzoek vaak vlot verliep en ik nooit het gevoel had dat ik er alleen voor stond. Het kleine aantal personen in de groep, die daadwerkelijk altijd beschikbaar waren, gaf ook altijd de mogelijkheid voor "wandelgangen wetenschap".

Theo, jouw nimmer aflatende enthousiasme voor het onderzoek werkt erg aanstekelijk op de afdeling en inspireerde me enorm. Een voorbeeld hiervan is dat je om de haverklap weer de afdeling opgestormd kwam met de diep inhoudelijke, maar erg duidelijke vraag: "en?". Jouw beste kwaliteiten, namelijk focus en balans, hebben me erg geholpen bij het schrijven van de manuscripten en vaak verbaasde me het hoe simpel een oplossing voor tekstuele problemen soms kan zijn. Ik heb zeer veel van je geleerd!

Jan Harm, jouw inzicht in de biomechanica was onontbeerlijk en heeft het me makkelijker gemaakt om resultaten van het betreffende onderzoek te analyseren. Ook jouw suggesties voor de manuscripten waren altijd van nut. Dankzij jouw heldere gedachtegang tijdens discussies zijn vele onbelangrijke zijwegen door ons overgeslagen.

Leo, de onbetwiste flipperkampioen van de afdeling (alleen in de pauze!). Ik heb samen met jou heel wat uurtjes gediscussieerd over de microCT en daardoor zijn we erachter gekomen wat er nu eigenlijk in die blauwe doos gebeurt en konden we zelfs nieuwe toepassingen uitvogelen. Tijdens onze tripjes naar Zwitserland was ik altijd blij dat jij (en ook Liesbeth) erbij was.

Hans en Peter, een onofficiële stelling, behorende bij dit proefschrift: Functionele Anatomie zonder Hans en Peter is als een trein zonder locomotief. Zonder jullie bijdrage zou de rijdende trein die Functionele Anatomie heet al snel tot stilstand komen.

Tim, ik heb altijd prettig met je samengewerkt en het was maar goed dat we vaak met z'n tweeën op de kamer zaten, anders waren er misschien een paar mensen gek geworden op de afdeling. Het slappe geouwehoer hebben we tot kunst verheven en tijdens het TGIF (Thank God It's Friday) gevoel kwam dit tot een hoogtepunt. Het is maar goed dat de ramen in het AMC versterkt zijn anders hadden ze het nooit gehouden als wij weer eens onze zangkwaliteiten met die van de artiest op de radio aan het vergelijken waren.

Geerling en Thorsten, bedankt voor de vele discussies over experimenten en manuscripten en voor de gezelligheid op de afdeling.

Nu Tim en ik weg zijn, is het stokje aan de volgende lichting aanstormend talent overgedragen. Nop en Wilco, veel succes met jullie promotieonderzoek. Met een groep mensen achter jullie zoals die hierboven staat opgesomd is dat vast een makkelijkere taak.

Bachelorstudenten van Tandheelkunde zijn er toch wel een aantal geweest: Peter van der Helm, Tajana Bersma, Maartje Dam, Ruud "sport is voor apen" Sips, Figen Ay, Linde van Groningen, Yvonne Potgieser en natuurlijk Greetje "bonzo" Renders. Jullie zorgden voor heel wat vertier op de afdeling. Regelmatig werd de chaos ook met serieuze zaken afgewisseld, maar dat duurde gelukkig nooit lang. Vooral tijdens de pauzes bereikte dit een hoogtepunt en vlogen voornamelijk de jongleerballen door de ruimte (Linde, sorry nog hè van die oorbel). Ik heb er een paar goede vrienden aan overgehouden en op die hamburger-eet-wedstrijd komen we nog wel eens terug.

I would like to thank people at Scanco Medical and in particular Andres Laib for his answers to uncountable emails regarding the use of microCT software. Bert van Rietbergen wil ik bedanken voor zijn hulp bij het vervaardigen en het debuggen van de FE modellen.

Ik wil de mensen die mij geholpen hebben bij de nanoindentatie-experimenten uiteraard ook bedanken. Jaap den Toonder, Kees Meesters en Marc van Maris bedankt dat ik zoveel van jullie tijd en faciliteiten op de TU/e gebruik heb mogen maken.

Rob Exterkate en Arie Werner van ACTA, bedankt voor de mogelijkheid om bij jullie een belangrijk deel van de preparatie van mijn samples uit te mogen voeren.

Ik mag ook de mensen van de faculteit Diergeneeskunde van de Universiteit van Utrecht niet vergeten. Jet de Jonge, Wim Weijs en Henk van Dijk, bedankt voor jullie hulp bij het verzamelen van de varkentjes en van oude en dus vaak onvindbare literatuur over de ontwikkeling van de onderkaak. Ik zal ons tripje naar het slachthuis in Eindhoven niet snel vergeten.

Nu we het toch over Eindhoven hebben: alle vrienden en vriendinnen, van oudsher BMT-genoten, maar onderhand heel wat uitgebreid met aanhang gaven de nodige afwisseling,

ondanks dat iedereen nu zo ongeveer over het gehele land is verspreid. De jaarlijksterugkerendealiasexcuusomveeltedrinkenuitkleineglaasjesBMTweekendjes en bijbehorende commissie moeten absoluut in stand blijven. Om van de mannenstapavonden maar niet te spreken. Jullie zijn heel belangrijk voor me. Ik zie jullie snel!

Pa, Ma en Lucia, bedankt voor jullie steun en onvoorwaardelijke liefde. Bedankt dat jullie mij de vrijheid en mogelijkheid gaven om te gaan studeren wat ik wilde. Ik hou van jullie!

Mar, zonder jou was dit allemaal niet gelukt. Ik had aan het eind van de dag altijd zin om richting huis te gaan en jou in de trein alweer te zien. En nu gaan we trouwen! Dat zegt genoeg lijkt me zo.

CURRICULUM VITAE

Lars Mulder werd geboren op 7 november 1978 in Oss. Na het behalen van zijn VWO diploma aan het Titus Brandsmalyceum in 1997, ging hij Biomedische Technologie studeren aan de Technische Universiteit te Eindhoven. Tijdens de laatste twee jaren van de studie werd zijn interesse voor wetenschappelijk onderzoek gewekt. Zijn afstudeerstage bij de vakgroep Materials Technology betrof het modificeren van een hydrogel en het in kaart brengen van enkele belangrijke eigenschappen van deze hydrogel, welke mogelijk toegepast zou kunnen worden als dragermateriaal bij het kweken van hartkleppen met patiënteneigen lichaamsweefsel. In november 2002 studeerde hij af en in januari 2003 begon hij als assistent in opleiding bij de sectie Functionele Anatomie van het Academisch Centrum Tandheelkunde Amsterdam (ACTA). Zijn onderzoeksproject ging over de verandering van de botstructuur en mineralisatie van de onderkaak van het varken tijdens de prenatale ontwikkeling en over de biomechanische consequenties hiervan.

List of publications

Mulder L, Koolstra JH, van Eijden TMGJ (2004). Accuracy of microCT in the quantitative determination of the degree and distribution of mineralization in developing bone. Acta Radiol 45: 769-777.

Mulder L, Koolstra JH, Weijs WA, van Eijden TMGJ (2005). Architecture and mineralization of developing trabecular bone in the pig mandibular condyle. Anat Rec A Discov Mol Cell Evol Biol 285: 659-667.

Mulder L, Koolstra JH, de Jonge HW, van Eijden TMGJ (2006). Architecture and mineralization of developing cortical and trabecular bone of the mandible. Anat Embryol 211: 71-78.

Mulder L, van Groningen LB, Potgieser YA, Koolstra JH, van Eijden TMGJ (2006). Regional differences in architecture and mineralization of developing mandibular bone. Anat Rec A Discov Mol Cell Evol Biol 288: 954-961.

Mulder L, Koolstra JH, van Eijden TMGJ (2006). Accuracy of microCT in the quantitative determination of the degree and distribution of mineralization in developing bone. Acta Radiol 47: 882-883.

Mulder L, van Ruijven LJ, Koolstra JH, van Eijden TMGJ (2006). Biomechanical consequences of developmental changes in trabecular architecture and mineralization of the pig mandibular condyle. J Biomech. In press.

Mulder L, van Ruijven LJ, Koolstra JH, van Eijden TMGJ (2006). The influence of mineralization on intratrabecular stress and strain distribution in developing trabecular bone. Submitted for publication.

Mulder L, Koolstra JH, den Toonder JMJ, van Eijden TMGJ (2006). Relationship between tissue stiffness and degree of mineralization of developing trabecular bone. Submitted for publication.

Mulder L, Koolstra JH, den Toonder JMJ, van Eijden TMGJ (2006). Intratrabecular distribution of tissue stiffness in developing trabecular bone. J Struct Biol. Conditionally accepted for publication.

Renders GAP, Mulder L, van Ruijven LJ, van Eijden TMGJ (2006). Degree and distribution of mineralization in the human mandibular condyle. Calcif Tissue Int 79: 190-196.

Renders GAP, Mulder L, van Ruijven LJ, van Eijden TMGJ (2006). Porosity of human mandibular condylar bone. J Anat. Accepted for publication.

Sips RJA, Mulder L, Koolstra JH, van Eijden TMGJ (2006). Development of the micro-architecture and mineralization of the basilar part of the pig occipital bone. Submitted for publication.

van Eijden TMGJ, van der Helm PN, van Ruijven LJ, Mulder L (2006). Structural and mechanical properties of mandibular condylar bone. J Dent Res 85: 33-37.

van Ruijven LJ, Giesen EBW, Mulder L, Farella M, van Eijden TMGJ (2005). The effect of bone loss on rod-like and plate-like trabeculae in the cancellous bone of the mandibular condyle. Bone 36: 1078-1085.

van Ruijven LJ, Mulder L, van Eijden TMGJ (2006). Variations in mineralization affect the stress and strain distributions in cortical and trabecular bone. J Biomech. In press.

Willems NMBK, Mulder L, Langenbach GEJ, Grünheid T, Zentner A, van Eijden TMGJ (2006). Age-related changes in microarchitecture and mineralization of cancellous bone in the porcine mandibular condyle. J Struct Biol. Conditionally accepted for publication.